

T-3087

DELINEATING PIERRE FORMATION FRACTURE RESERVOIRS  
USING COMPRESSIONAL AND  
HORIZONTAL SHEAR WAVE SEISMIC DATA  
NEAR FLORENCE, FREMONT COUNTY, COLORADO

by

Douglas M. Gable

ARTHUR LAKES LIBRARY  
COLORADO SCHOOL OF MINES  
GOLDEN, COLORADO 80401

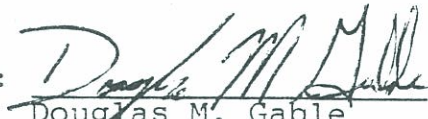
T-3087

A thesis submitted to the Faculty and the Board of Trustees of the Colorado School of Mines, in partial fulfillment of the requirements for the degree of Master of Science in Geophysical Engineering.

Golden, Colorado

Date Oct. 27 1986

Signed:

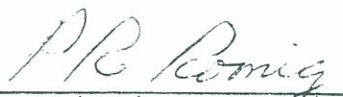
  
Douglas M. Gable

Approved:

  
Dr. Thomas L. Davis  
Thesis Advisor

Golden, Colorado

Date 28 October 1986

  
Dr. Phillip R. Romig  
Department Head  
Department of Geophysics

ABSTRACT

The Florence field in the Cañon City graben, Colorado, is the second oldest oil field in the United States (Mallory, 1977). Oil is found in fractured zones within the Pierre Formation. A seven mile compressional (P)- and horizontal shear (SH)-wave seismic survey was analyzed to investigate the possibility of detecting fractured zones in the Pierre Formation.

The SH-wave reprocessed preserved amplitude section shows an amplitude increase throughout the Pierre and along the Niobrara horizon within the Florence field's limits. Zones which show an amplitude increase result from SH-wave velocities being lower in fractured intervals. Section above Niobrara Formation may be fractured throughout, not just in specific production intervals. Specific production intervals are evidence of open fractures.

$V_s/V_p$  ratios decrease within areas of preferential fracturing. Both P- and SH-wave amplitudes increase in fractured zones, causing the  $A_s/A_p$  ratio to show a slight increase in zones with fracturing. SH-wave velocity information is more definitive than P-wave velocity information of fractured areas. Northeastern end of both seismic lines indicates an area of fractures and a structural flexure which warrants this area for future exploration.

TABLE OF CONTENTS

	<u>Page</u>
ABSTRACT. . . . .	iii
TABLE OF CONTENTS . . . . .	iv
LIST OF FIGURES . . . . .	vi
LIST OF TABLES. . . . .	x
LIST OF PLATES. . . . .	xi
ACKNOWLEDGMENTS . . . . .	xii
INTRODUCTION. . . . .	1
Previous Work. . . . .	1
Density . . . . .	4
Attenuation (Q) . . . . .	4
Velocity. . . . .	6
Bulk Modulus (Incompressibility). . . . .	8
Shear Modulus (Rigidity). . . . .	10
Temperature . . . . .	11
Pressure. . . . .	12
Poisson Ratio . . . . .	13
Anisotropy. . . . .	15
Summary . . . . .	18
GEOLOGY . . . . .	23
Stratigraphy . . . . .	23
Structure. . . . .	29
Production . . . . .	30
SEISMIC DATA. . . . .	38
Data Acquisition . . . . .	38
Recording Information. . . . .	41
Data Processing. . . . .	41
Polarity Conventions . . . . .	46
WELL LOG DATA . . . . .	47

	<u>Page</u>
INTERPRETATION. . . . .	63
P- and SH-Wave Calculations. . . . .	70
Velocities. . . . .	71
$V_s/V_p$ Calculations. . . . .	75
Travel Times. . . . .	86
$T_p/T_s$ Calculations. . . . .	88
Amplitudes. . . . .	92
Modeling . . . . .	98
$A_s/A_p$ Calculations. . . . .	104
FUTURE WORK . . . . .	113
ALTERNATE INTERPRETATION. . . . .	118
CONCLUSIONS . . . . .	119
REFERENCES CITED. . . . .	121
APPENDIX. . . . .	129

LIST OF FIGURES

<u>Figure</u>	<u>Page</u>
1 Study area location map . . . . .	2
2 Stratigraphic column in study area. . . . .	3
3 Structural cross section of Cañon City area	24
4 Pierre Formation stratigraphic zoning . . . . .	27
5 Syslap method . . . . .	39
6 Florence field area wells. Production information includes initial production and/or sustained production (from Petroleum Information). . . . .	48
7 Florence field area wells, from Washborne (1908). . . . .	49
8 Synthetic seismogram generated from a sonic log (Continental Oil, Huffman #1, SW NW sec 30, T19S, R68W) . . . . .	50
9 Synthetic seismogram generated from a resistivity log using Faust's formula ( $V = 1948 * Z^{1/6} * R_t^{1/6}$ ) (Continental Oil, Huffman #1, SW NW sec 30, T19S, R68W) . . . . .	52
10 Wells used in calculation of "A" coefficients. . . . .	55
11 Synthetic seismogram generated from a resistivity log using Faust's formula with a varying "A" coefficient; $V = A * Z^{1/6} * R_t^{1/6}$ (Continental Oil, Huffman #1, SW NW sec 30, T19S, R68W) . . . . .	56
12 Synthetic seismogram generated from a resistivity log using Faust's formula ( $V = 1948 * Z^{1/6} * R_t^{1/6}$ ) (Brehm-Anderson #1 Scheel, NE SW sec 27, T19S, R69W) . . . . .	58

<u>Figure</u>	<u>Page</u>
13 Synthetic seismogram generated from a resistivity log using Faust's formula with a varying "A" coefficient; $V = A * Z^{1/6} * R_t^{1/6}$ (Brehm-Anderson #1 Scheel, NE SW sec 27, T19S, R69W) . . . . .	59
14 P-wave seismic section correlation with Brehm-Anderson #1 Scheel (resistivity) pseudo synthetic seismogram (reverse polarity) and Continental Oil Huffman #1 (sonic) synthetic seismogram (reverse polarity) . . . . .	60
15 SH-wave seismic section correlation with Brehm-Anderson #1 Scheel (resistivity) pseudo synthetic seismogram (reverse polarity) and Continental Oil Huffman #1 (sonic) synthetic seismogram (reverse polarity) . . . . .	61
16 Wells along seismic line. . . . .	64
17 SH-wave stacking velocities for horizons 1 and 3 with production information for the Pierre and Niobrara Formations. . . . .	78
18 SH-wave stacking velocities for horizons 2 and 4 with production information for the Pierre and Niobrara Formations. . . . .	79
19 P-wave stacking velocities for horizons 1 and 3 with production information for the Pierre and Niobrara Formations. . . . .	80
20 P-wave stacking velocities for horizons 2 and 4 with production information for the Pierre and Niobrara Formations. . . . .	81
21 SH-wave interval velocities between horizons 1 to 2 and 2 to 3, with production information for the Pierre and Niobrara Formations. . . . .	83

<u>Figure</u>	<u>Page</u>
22 P-wave interval velocities between horizons 1 to 2 and 2 to 3, with production information for the Pierre and Niobrara Formations. . . . .	84
23 $V_s/V_p$ ratio for intervals between horizons 1 <sup>s</sup> to 3 <sup>p</sup> and 2 to 3, with production information for the Pierre and Niobrara Formations. . . . .	85
24 $V_s/V_p$ ratio for intervals between horizons 2 <sup>s</sup> to 3 <sup>p</sup> and 2 to 4, with production information for the Pierre and Niobrara Formations. . . . .	87
25 SH-wave two-way interval travel times between horizons 1 and 3, with production information for the Pierre and Niobrara Formations. . . . .	90
26 SH-wave two-way interval travel times between horizons 3 and 4, with production information for the Pierre and Niobrara Formations. . . . .	91
27 P-wave two-way interval travel times between horizons 1 and 3, with production information for the Pierre and Niobrara Formations. . . . .	93
28 $T_p/T_s$ ratios for interval travel times between horizons 1 to 2, with production information for the Pierre and Niobrara Formations. . . . .	94
29 $T_p/T_s$ ratios for interval travel times between horizons 2 to 3 and 2 to 4, with production information for the Pierre and Niobrara Formations . . . . .	95
30 General seismic model for varying Poisson's ratio . . . . .	99

<u>Figure</u>	<u>Page</u>
31 Lateral varying Poisson's ratio for interval horizon 3, accounting for losses due to transmission effects and reflection coefficients . . . . .	102
32 Lateral varying Poisson's ratio for interval horizon 4, accounting for losses due to transmission effects and reflection coefficients . . . . .	103
33 SH-wave amplitudes along horizons 2 and 3, with production information for the Pierre and Niobrara Formations. . . .	106
34 SH-wave amplitudes along horizons 1 and 4, with production information for the Pierre and Niobrara Formations. . . .	107
35 SH-wave amplitudes along horizons 2 and 4, with production information for the Pierre and Niobrara Formations. . . .	108
36 P-wave amplitudes along horizons 1 and 3, with production information for the Pierre and Niobrara Formations. . . . .	109
37 $A_s/A_p$ ratio for horizons 2 and 3, with production information for the Pierre and Niobrara Formations . . . . .	111
38 $A_s/A_p$ ratio for horizons 3 and 4, with production information for the Pierre and Niobrara Formations . . . . .	112
39 Amplitude spectrum of P- and SH-wave preserved amplitude seismic traces. . . .	114

LIST OF TABLES

<u>Table</u>		<u>Page</u>
1	P-wave recording parameters . . . . .	130
2	SH-wave recording parameters. . . . .	131
3	Standard preserved amplitude P-wave processing. . . . .	132
4	SSC preserved amplitude P-wave processing	133
5	PI completion record information (T19S R69W) . . . . .	134
6	PI completion record information (T20S R69W) . . . . .	136
7	Completion information after Washborne (1908); USGS Bulletin 381 (T19S R69W) . .	139
8	Completion information after Washborne (1908); USGS Bulletin 381 (T20S R69W) . .	148
9	"A" parameters used for smoothing Faust's formula . . . . .	151

LIST OF PLATES

Plate

- 1 CGG P-wave final stack normal polarity (1979)
- 2 CGG P-wave preserved amplitude stack normal polarity (1979)
- 3 CGG SH-wave final stack reverse polarity (1979)
- 4 CGG SH-wave preserved amplitude stack reverse polarity (1984)
- 5 UNOCAL P-wave final stack normal polarity (1986)
- 6 UNOCAL P-wave preserved amplitude stack normal polarity (1985)
- 7 UNOCAL SH-wave final stack reverse polarity (1986)
- 8 UNOCAL SH-wave preserved amplitude stack reverse polarity (1986)
- 9 UNOCAL SH-wave final stack normal polarity (1986)
- 10 UNOCAL SH-wave preserved amplitude stack normal polarity (1986)
- 11 UNOCAL P-wave preserved amplitude stack normal polarity: SH-wave frequencies (1985)

ACKNOWLEDGMENTS

I am indebted to Compagnie Generale De Geophysique (CGG) of Denver, Colorado, who provided the seismic data. Also, without the use of the computer facilities at CGG, the initial reprocessing of the SH-wave data would have been impossible.

A special note of thanks goes to Gildas Omnes of CGG, whose comments and advice helped the initial progress of this study.

I am also indebted to Union Oil Company of California who supplied the computer resources for the final reprocessing of the SH- and P-wave data, along with all modeling attempted in this thesis.

Appreciation is also expressed to Daniel Lessar of Seismograph Service Companies (SSC), whose time and assistance was greatly appreciated in the seismic re-processing sequence.

I wish to express my special thanks to Dr. Thomas L. Davis for his time and help in acting as my thesis advisor. I wish also to express my gratitude to Drs. Schneider and Weimer for their suggestions and guidance while serving on my committee.

I also wish to express gratitude to my parents and friends who supplied eternal support throughout the extend of this thesis.

## INTRODUCTION

Compressional (P) and horizontal shear (SH) wave seismic surveys were conducted by CGG in the Florence field area of Colorado in 1978 (Figure 1). The Florence field is located in the central part of the Cañon City graben. The field's main producing zone is related to fracturing within the Lower Pierre Formation, Late Cretaceous age (Figure 2). The first well to recover oil in the area was drilled by A.M. Cassidy in 1862, along Fourmile creek, 9 miles north of Florence, which only found oil in the strata near the surface. It was not until 1876, that A.M. Cassidy and Isaac Canfield struck oil, which marked the first production in Florence Field. Since this time, over 600 wells have been drilled with cumulative production from the Florence-Cañon City field in excess of 15 million barrels (PI, 1985). Currently the Florence-Cañon City field has production from approximately 34 oil wells and one gas well.

### Previous Work

With our knowledge today, the seismic reflection response is mainly attributed to three factors: bulk density, attenuation, and velocity. Several

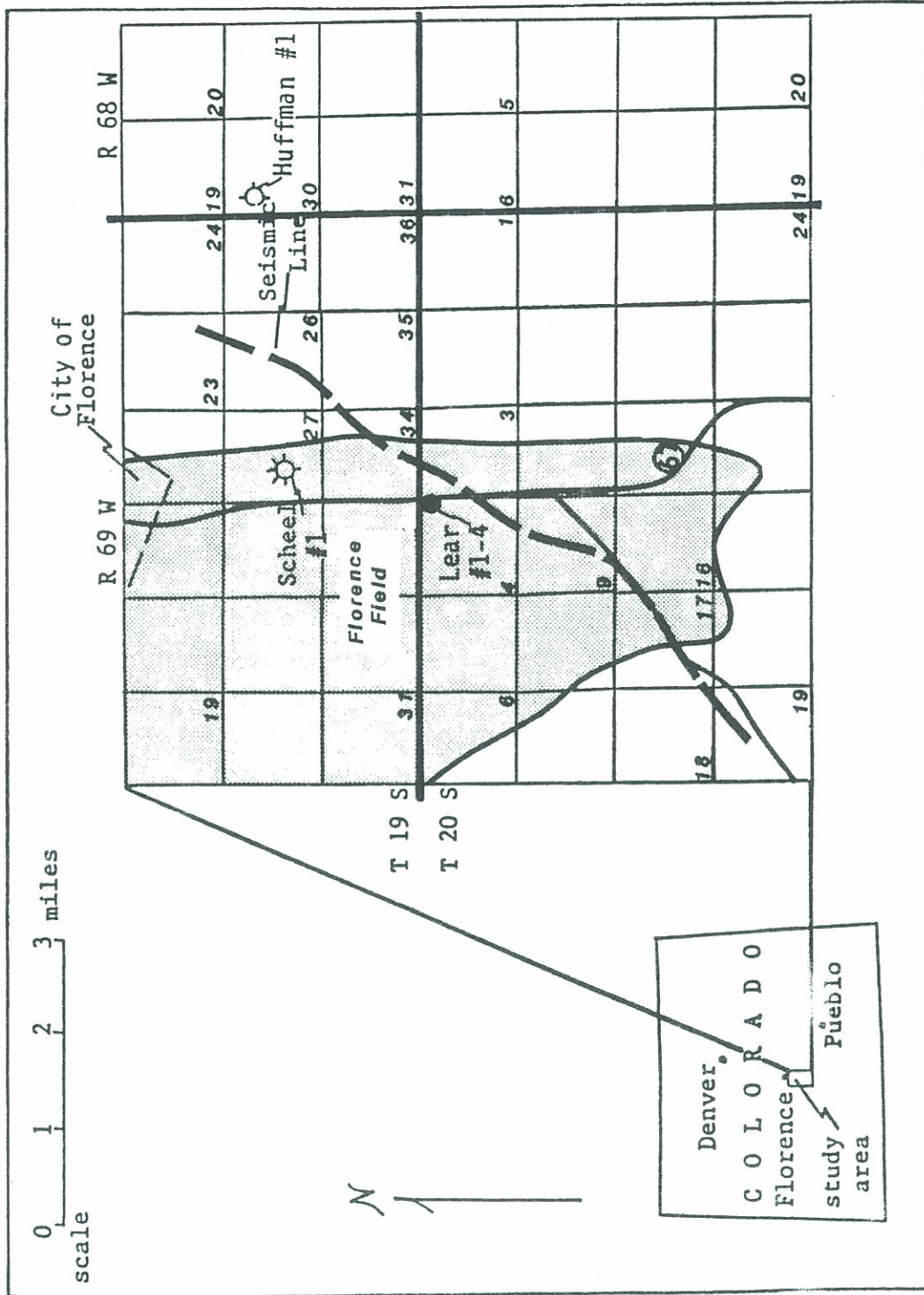


Figure 1: Study area location map.

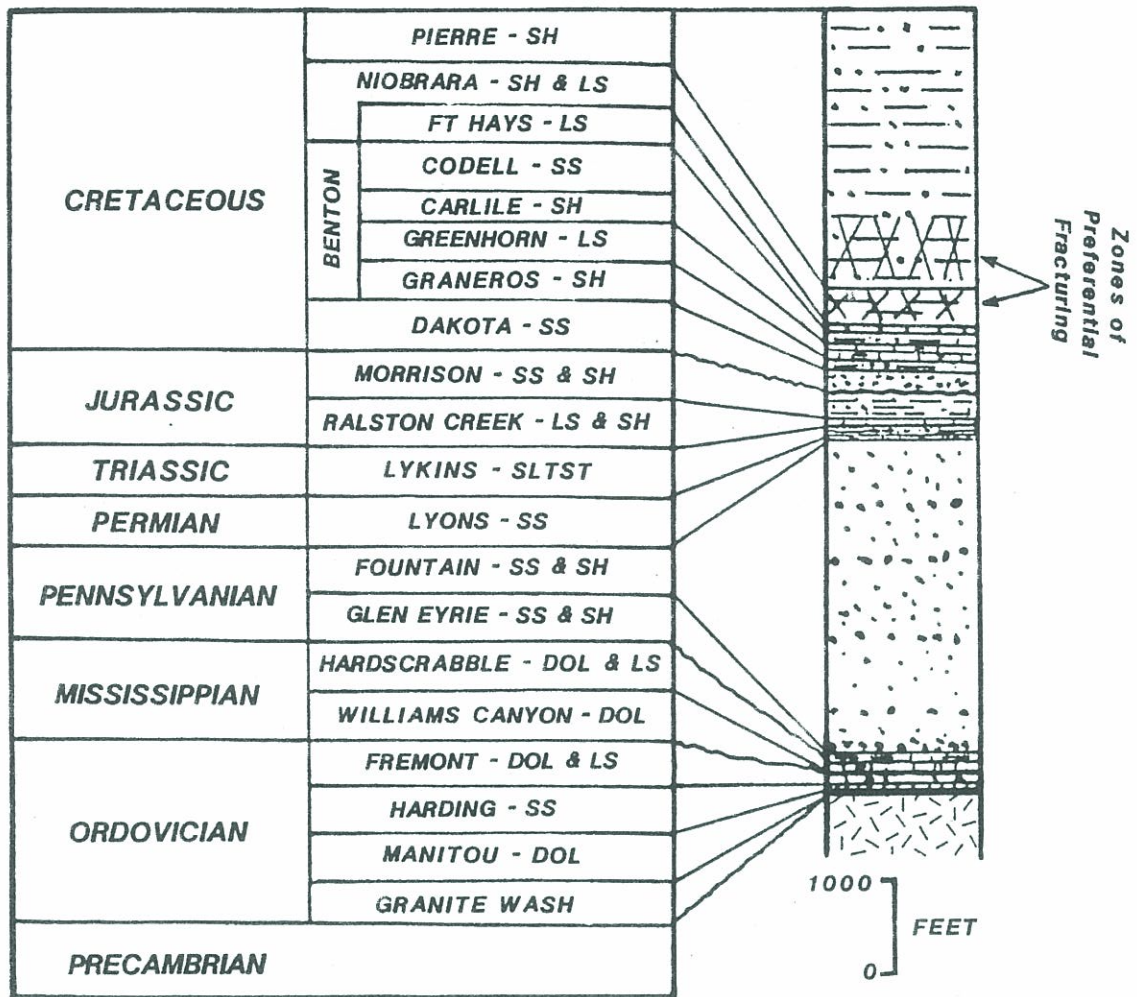


Figure 2: Stratigraphic column in study area. Section from Brehm-Anderson #1 Scheel, NE SW sec 27, T19S, R69W(Amstrat, 1963).

properties which influence the above three factors are; porosity, mineral composition, overburden pressure, formation pressure, temperature, micro-cracks (fractures), frequency, and age. An understanding of how these properties influence the seismic character visible on the P- and SH-wave sections, possibly will aid in the delineation of fractured systems.

#### Density

Although this paper concentrates on velocity variations, it is important to mention several properties of a rock's density. Statistical distributions of P- and S-wave velocities versus density show when the velocities increase so do the densities (Nafe and Drake, 1957).

Experimentally, Gregory (1976) showed that as porosity increases the bulk density linearly decreases; however, with an increase in fluid saturation the bulk density linearly increases.

#### Attenuation (Q)

Another factor that will be mentioned in this report is attenuation. Attenuation is important in elastic wave propagation. Solid and viscous friction losses

are the two most commonly documented attenuation mechanisms. The primary solid friction loss mechanism is documented in low permeability rocks (Gregory, 1977). Unlike solid friction, viscous losses caused by the relative motion between pore fluid and solid material in porous and permeable rocks can be calculated from theory (Biot, 1956).

Attenuation in highly consolidated rocks is lower than in poorly cemented or unconsolidated rocks. An increase in attenuation usually occurs with the addition of pore fluids and/or a decrease in fluid viscosity. These results imply the Pierre Formation's fracture zones should exhibit an increase in attenuation.

Since the S-wave decrement exceeds the P-wave decrement by a factor usually larger than two, S-wave amplitudes should decrease more rapidly than P-wave amplitudes.

Increasing the static pressure on the frame of a rock reduces  $Q$  for the P-wave but  $Q$  for the S-wave is not affected (Gregory, 1977). Therefore, because fractures release pressures stored within rocks, producing intervals within the Pierre Formation should exhibit larger P-wave

amplitude attenuations than non-fractured intervals. However, for a change in pressure, S-waves will show no change through fractured or non-fractured zones.

Although attenuation was not heavily studied in this report, measurable differences between P- and S-wave attenuations should be measurable when the signal to noise ratio is high.

#### Velocity

This study is concerned with changes in P- and SH-wave velocities and how these changes could help indicate fractured intervals.

S-waves travel in the earth with a velocity that depends on the modulus of rigidity and density;

$$V_s = (\mu/\rho)^{\frac{1}{2}}.$$

$V_s$  : Velocity in m/s.

$\mu$  : Rigidity (shear) modulus in  $N/m^2$ .

$\rho$  : Density in  $kg/m^3$ .

As these S-waves pass through a medium, that medium will undergo a torsional deformation.

S-waves are subdivided into two types, SV-wave and SH-wave. If the particle motion is parallel to the wave's plane of incidence, then the wave is designated as a SH-wave. However, a wave whose particle motion is perpendicular to the plane of incidence, is designated as a SV-wave.

An SV-wave incident on a boundary will generate both SV- and P-reflections and refractions. Since SV- and P-waves travel at different velocities and conversion from one to both types occurs at every boundary (Cherry and Waters, 1968), the resulting record could be very complex. Unlike SV-waves, SH-waves in parallel layered beds are reflected and refracted as only SH-waves.

A source for SH-waves is any force system that does not have a spherical symmetry in a homogeneous medium. The force system used to produce both P- and SH-waves for this project was Primacord.

Like the S-wave, the P-wave propagates with a velocity that depends on rigidity and density; however, the P-wave velocity also is dependent on incompressibility;

$$V_p = ((k+4\mu/3)/\rho)^{1/2}.$$

k: Incompressibility (bulk) modulus in  $N/m^2$ .

$\mu$ : Rigidity (shear) modulus in  $N/m^2$ .

$\rho$ : Density in  $kg/m^3$ .

As a P-wave passes through a medium, that medium will undergo volume variations.

A shear (S-wave) wave is a disturbance which moves through an infinite medium, such that the point's displacement is parallel to the wavefront, unlike the compressional (P-wave) wave's point displacement, which is perpendicular to the wavefront. Velocities of the two wave types are different and are controlled by the density and two different medium elastic moduli; bulk and shear moduli (Cherry and Waters, 1968). For most rocks the moduli effects for gas and crude-oil saturations are similar to those for gas and water.

#### Bulk Modulus (Incompressibility)

Compaction, which causes a sediment volume reduction has less effect on increasing rigidity, than on increasing the bulk modulus (Walsh, 1965), therefore compaction should increase P-wave velocities more than S-wave

velocities. Further, Walsh shows the bulk modulus is strongly affected by the presence of a few long cracks and that the bulk modulus of a material with cracks is less than the original solid material. When density increases, so must the bulk modulus since an increase in density has been shown to increase both P- and S-wave velocities.

Dynamic measurements of rocks show the bulk modulus varies with porosity, pressure, temperature, and fluid saturation. Usually, the bulk modulus increases as liquid saturation increases. Replacing pore liquids with gas reduces the rock's bulk modulus and the effect is enhanced by decreasing pressure. Bulk modulus will also decrease as porosity increases. If pressure decreases and both porosity and gas content increase, then significant reductions in the bulk modulus occur. A reduction in the bulk modulus occurs when temperature increases.

Lowest values for bulk modulus are obtained for high porosity rocks containing large amounts of gas. Generally an increase in confining pressure causes the bulk modulus to increase. Low pressure rocks exhibit a noticeable change in the bulk modulus when water saturation is replaced by gas. Medium porosity rocks show a definite change in the bulk modulus for an addition of gas to a water saturated rock.

### Shear Modulus (Rigidity)

Rigidity links particles to each other and therefore affects both P- and S-waves. When cementation fills the pores with solid material, the filled pores increase the rocks rigidity, which should cause the P- and S-wave velocities to increase. Where cementation is not important, as with recent sediments, clays, or shales, lower S-wave velocities should be expected. Because of evidence which shows that as density increases so do both the P- and S-wave velocities, the rigidity modulus must therefore increase.

Jointing and fracturing should cause a considerable decrease of the macroscopic rigidity modulus. Fracturing causes a decrease in both the rigidity and bulk moduli, with theory showing changes in the rigidity modulus having a larger affect on S-waves than P-waves.

The rigidity modulus decreases with either a temperature or porosity increase. Replacing pore liquids with gas reduces the rock's shear modulus and the effect is enhanced by decreasing pressure. Low and medium porosity rocks at constant pressure with an increase in fluid saturation exhibit a minimal effect on the rigidity modulus, which is probably a result of the changes in

bulk density. High porosity rocks, however, are very sensitive to small amounts of pore liquid. Large increases in the rigidity modulus occur when water is withdrawn from the vicinity of grain contacts, which is not totally accounted for by density.

Usually an increase in confining pressure will cause the rigidity modulus to increase. In low pressure rocks the effects on the rigidity modulus differ when water saturation is replaced by gas. Significant reductions in the rigidity modulus occur as pressure decreases and as porosity and gas content increase.

#### Temperature

Both P-wave and S-wave velocities decrease with an increase in temperature (Gregory, 1977). In most sedimentary rocks, the rigidity and bulk modulus and Poisson's ratio will all decrease with an increase in temperature.

An increased temperature is believed to increase the number of microcracks, which may contribute to permeability at low pressures.  $T_{\max}$  (temperatures at which maximum yield occurs during pyrolysis) values for the Sharon Springs Member are within the petroleum generation window, which provides the best evidence of thermal maturity for initial stages of oil generation in the Florence field (Gauthier,

et al, 1984). A larger than normal thermal gradient in the Florence field should influence changes in velocity.

### Pressure

Velocity increases as pressure on the rock frame increases. The increase in velocity with pressure is attributed to the presence of microcracks at low pressure, which are diminished at higher pressures.

Overburden pressure is usually defined as the vertical stress caused by all the solid and fluid material above the formation. An average value is one pound per square inch (psi) for each foot of burial (0.23 kg per square cm per m of burial).

Fluid pressure is usually defined as the pressure exerted by a column of free solution that would be in equilibrium with the formation. The normal fluid pressure gradient is frequently assumed to be 0.465 psi for each foot of burial (1.07 kg per square cm per m of burial).

The effective overburden pressure on a reservoir is usually defined as the difference of the formation fluid from the total overburden pressure. Changes in the effective overburden pressure could result in velocity variations.

The influence of pressure on velocity becomes small at pressures corresponding to deeper sediments in situ

(Wyllie, et al, 1956). Pore fluid has relatively little influence on velocity at depths greater than approximately 6000 feet (1,830m) (Gregory, 1977). Within the study area, Pierre Formation producing interval's depth of burial is under 4000 feet. In deeper sediments, the velocity is determined primarily by porosity and mineral composition.

#### Poisson Ratio

Since Poisson's ratio is a function of  $V_s$  and  $V_p$ ;

$$\sigma = \frac{1}{2} \frac{\left(\frac{V_p}{V_s}\right)^2 - 2}{\left(\frac{V_p}{V_s}\right)^2 - 1}$$

either  $V_s/V_p$  or Poisson's ratio maybe used as an indicator of lithologic changes, pore fluids, and fractures. For a homogeneous medium, the higher the medium's Poisson ratio, that medium will more readily generate S-waves (Hazelbroek, 1966). As a function of  $V_s/V_p$ , Poisson's ratio rapidly increases for larger values of  $V_s/V_p$ ,  $V_s/V_p$  values greater than .75, and asymptotically approaches .5 for smaller values of  $V_s/V_p$ .

For isotropic materials, Poisson's ratio is limited to values less than 0.5 because of theoretical reasons explained by Love (1927) and usually varies from 0.25

to 0.33 (Gregory, 1976). Most rocks exhibit anisotropic behavior, causing Poisson's ratio to be stress dependent. Because of anisotropy Poisson's ratio can vary over a wide range of possible values and may even be negative. Negative values of Poisson's ratio are not excluded by theory, but are found only in anisotropic rocks (Love, 1927).

Poisson's ratio is also influenced by fluid saturation, temperature, and porosity. An increase in temperature will cause Poisson's ratio to decrease. Poisson's ratio tends to slightly increase over normal values as porosity increases at a constant pressure. As a function of pressure, however, Poisson's ratio may increase, remain constant, or even decrease as porosity increases. Replacing pore liquids with gas reduces the rocks Poisson's ratio and the effect is enhanced by decreasing pressure. When gas is added to a water saturated rock at low pressure, Poisson's ratio will definitely change. Medium porosity rocks show Poisson's ratio has a definite relationship to the type of pore fluid. Poisson's ratio is also useful for distinguishing between gas and water saturated rocks at higher porosities. Along with anisotropic rocks, negative values for Poisson's ratio could mean that the rock is under low pressure and contains gas.

Largely because of cementation and compaction, older rocks will have a lower Poisson ratio. Because of attenuation, fractures do not obey Hooke's law and therefore depending on the seismic energies angle of incidence, fractures could change Poisson's ratio.

### Anisotropy

The assumption of elastic isotropy for materials in the earth's crust has been valuable in the past for studies of seismic-wave propagation. Anisotropy, of which transverse isotropy is a special case, maybe a more realistic condition for many crustal materials, especially in sedimentary rocks. Unlike isotropic rocks, anisotropic rocks cause both P- and S-wave velocities to differ from predicted values of Biot's theory. The velocity with which an elastic wave travels in an isotropic solid is independent of direction, whereas the velocity for travel in an anisotropic solid changes as the direction of travel changes.

A homogeneous sandstone is not expected to be anisotropic, because fine, randomly oriented quartz grains are the same to seismic waves propagating through them in any direction. Shales of uniformly oriented clay

particles are anisotropic. Therefore, a rock's anisotropy provides information about that rock's properties.

Velocity anisotropy can be caused by layering of isotropic media as well as by microscopic rock properties (Backus, 1962; Levin, 1979). This horizontal layering causes a type of anisotropy called transverse isotropy.

Commonly, beds are thin compared to a wavelength. If the interfaces between beds are parallel, theory indicates the most likely type of anisotropy for a layered earth section made up of thin beds is transverse isotropy. A transversely isotropic solid is defined as having properties exhibiting a symmetry around a vertical axis, these properties can then differ with angle from vertical but not with azimuth or within a bedding plane.

An investigation of anisotropy provides important information about the in situ interval structure of a layer, with the interval structure possibly caused by the overall alignments of cracks, pores, minerals, crystals or laminations. Anisotropy is largely a function of the percentage of clay in rocks, independent of layering effects, even where fine layering and large variability in velocity from layer to layer is obvious in P-wave sonic logs (Winterstein, 1986). Anisotropy is also affected by the jointing in limestones and sandstones (Garotta, et al, 1977).

This study is hampered because shales are generally more acoustically anisotropic than limestones or sandstones (Omnes, 1978), which could produce unrelatable velocities in the production interval. The amount of anisotropy could also be a measure of fractures.

SH-waves are more strongly affected by the anisotropy of layered media than P-waves. Anisotropic rocks even cause the S-wave velocities to increase for low confining pressures (under 4000 psi) when the pore space is filled with hydrocarbons. The degree of anisotropy decreases significantly as confining pressure is increased and at high confining pressures, velocities are found to approach the behavior predicted by Biot's theory. Therefore, at higher confining pressures the S-wave velocity decreases and eventually the S-wave velocity for hydrocarbon saturated rocks becomes less than the unsaturated rocks velocity. The anomalous behavior of the S-wave velocity for the saturated rock at low confining pressures, these conditions are present in study area, is probably caused by relaxation behavior of liquid contained in the fractures.

If vertically oriented fractures are present in a medium, that medium will be anisotropic to the transmission of horizontal shear waves. Horizontal shear wave energy

will be split between particle motion parallel and perpendicular to the fractures. Those two modes of horizontal shear wave propagation will separate and travel at velocities that are dependent upon the degree of anisotropy. The individual components can be determined by suitably recording both these phases, then the fracture direction and anisotropic factor can be calculated. If seismic acquisition is parallel to the orientation of fractures the SH-wave velocity will be faster and when acquisition is perpendicular to the fracture orientation the SH-wave velocity will be the slowest. Knowing these different velocities will help define the direction of micro-fractures. When interval velocity measurements are good enough, the SH-wave anisotropy can be estimated, therefore velocity anisotropy offers another potential exploration tool.

#### Summary

Omnes (1978) showed that S-waves travel only through the rock's matrix and are not influenced to the same degree as P-waves by fluids in the pore space, as fluids reportedly have no shear strength. Theory and experimentation have shown that S-wave velocities are always smaller than

corresponding P-wave velocities. Theoretically and experimentally Tatham and Stoffa also show that the S-wave velocity of a porous rock is less sensitive to fluid saturants, than the P-wave velocity. For isotropic rock's King's data shows that a rock's S-wave velocity behaves in agreement with that predicted by Biot's theory.

The theory of Biot (1956), based on the assumption that microcracks are negligible, concludes that the S-wave velocity of dry rocks should always exceed the velocity of the same rocks when fully saturated with liquid.

As with S-wave velocities, King's data shows for isotropic rocks that a rock's P-wave velocity behaves in agreement with that predicted by Biot's theory. Vertically oriented micro-fractures affect P-wave velocities since these micro-fractures are fluid filled. Gregory (1976) produced results that agree with Tatham and Stoffa (1976) and King (1966) in that P-waves significantly depend on the fluid type filling the pore space. An increase in P-wave velocity occurs when the rock is saturated with a liquid, with the P-wave velocity of an aqueous saturated rock being higher than a rock saturated with hydrocarbons. Also, fluid saturation effects on P-wave velocities are larger in low porosity than in high porosity rocks.

At low porosities, less than 17% porosity, a large reduction effect of P-wave velocities is apparent when gas is added to the pore space. For higher porosity rocks, the addition of gas to the pore space has less of an effect on the P-wave velocities (Gregory, 1976). P-wave velocity was shown by Gregory (1976) to increase with an increasing confining pressure. This relation between P-wave velocity and confining pressure is parabolic with a rapid increase of P-wave velocity associated with an increase at lower confining pressures.

For P-waves, when the effective overburden pressure is increased, the velocity increases; when the effective overburden pressure is constant, the velocity remains constant except at low values of total overburden pressure. For confining pressures less than about 9000 psi ( $633 \text{ kg/cm}^2$ ), small increases in the confining pressure will dramatically increase the P-wave velocity.

Gregory (1977) shows that for pressures greater than 9000 psi ( $633 \text{ kg/cm}^2$ ) S-wave velocities follow Biot's theory for all porosities. However, for pressures lower than 9000 psi, S-wave velocities for low porosity rocks begin to depart from Biot's theory. Because these results are pressure dependent, Gregory (1977) suggests that

microcracks of low porosity rocks may account for these discrepancies with Biot's theory. For normal confining pressures within the bounded zone of the Pierre Formation, pressures of about 1000-3000 psi (70-232 kg/cm<sup>2</sup>), Gregory (1976) showed for porosities less than about 15% the S-wave velocity will disagree with Biot's theory.

Regional and lithologic variations in P-wave velocities, may even be greater than the already discussed anomalies. Therefore, P-wave data alone may not be sufficient to identify fracture zones. Since gases are more compressible than liquids, a P-wave velocity in a gas-filled rock is usually lower than the velocity in a liquid-filled rock (Gregory, 1977).

Fractures within the Pierre Formation should cause attenuations to increase on P-wave seismic sections, while SH-wave seismic sections should reflect even larger attenuations.

Field behavior by Domenico (1977) supports  $V_p$  decreasing with an increasing porosity, however  $V_s$  results exhibit even a larger decrease with porosity. Domenico's work contradicts results obtained by Tatham and Stoffa, Garotta, and Gregory.

Although fluids reportedly have no shear strength, King's results show that S-wave velocities are lower when a rock is saturated with a liquid. Water saturation causes a greater reduction in S-wave velocity than does hydrocarbon saturation. While adding hydrocarbons to the pore space causes a large reduction in P-wave velocities, Gregory (1976) also shows that S-wave velocities slightly increase. Since S-wave velocities are less sensitive to fluid saturants, the S-wave's velocities should work as a normalizing quantity, when compared to the P-wave velocities.

If P- and SH-wave seismic data are of high quality, then a detailed study of the properties mentioned in this chapter can be applied to identify fractured intervals.

For future reference, a Department file contains materials (logs, sepias, processing output, etc.) used in this study. Contact Colorado School of Mines, Department of Geophysics for further information.

### GEOLOGY

Structure in the Florence field area is dominated by a horst block and graben (Figure 3). A thicker, more complete geologic section occurs in the graben. The Florence field is located within the Cañon City graben, with the oil-bearing section occurring in the Pierre and Niobrara Formations.

Recurrent movement occurred along old fault trends during the Paleozoic, with the present structural configuration of the fault blocks being the result of Late Cretaceous and Tertiary fault movement (Weimer, 1980).

### Stratigraphy

Coarse granites with associated pegmatites make-up the Precambrian basement in the Florence field area. During Late Precambrian, one or more orogenic periods occurred causing diverse, fault blocks bounded by nearly vertical shear zones (Weimer, 1980). Regionally these faults trend northeast and northwest.

The Brehm-Anderson #1 Scheel well, NE SW sec 27, T19S, R69W was drilled to a total depth of 8815 feet (2687m) (Figures 1 and 2). American Stratigraphic Company,

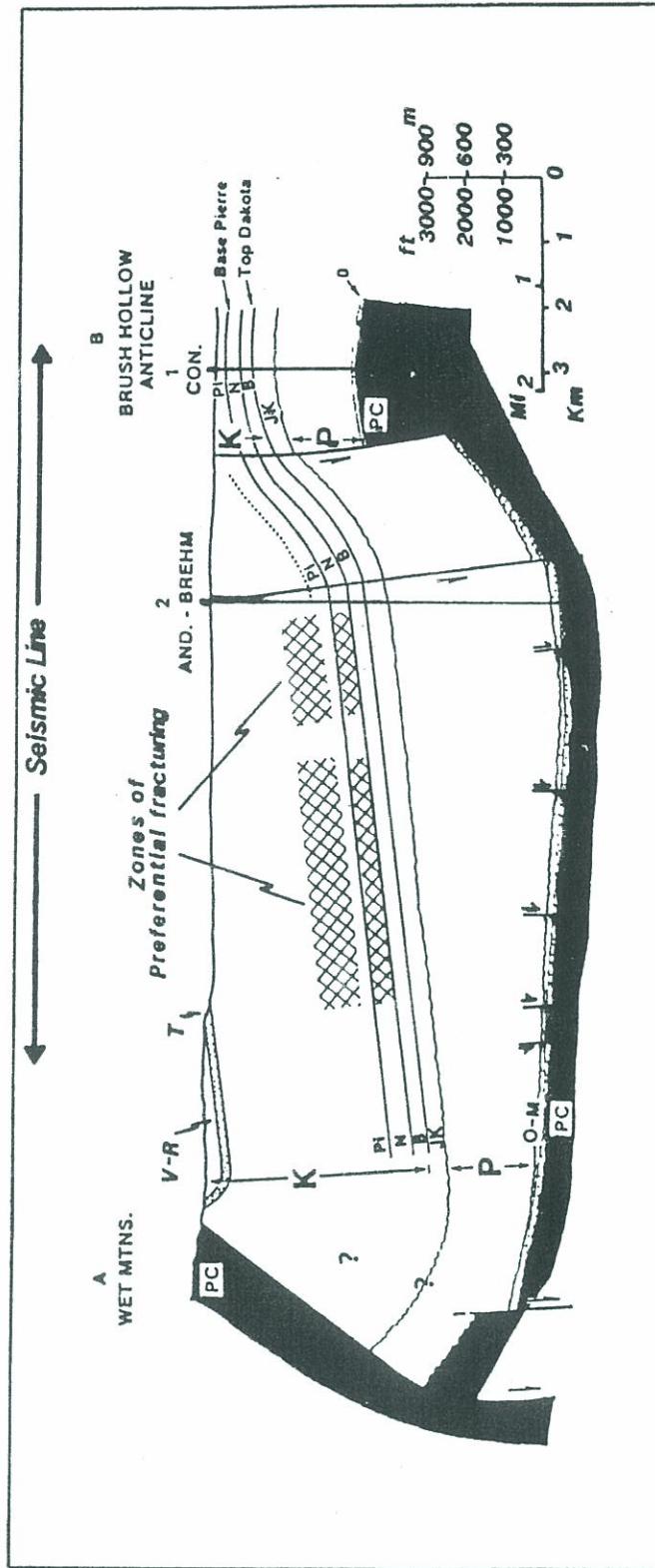


Figure 3: Structural cross section of Cañon City area. Symbols are as follows: PC=Precambrian; O-M=Ordovician and Mississippian; P=Pennsylvanian and Permian; JK=Jurassic and Lower Cretaceous; K=Upper Cretaceous with the following rock units: B=Benton; N=Niobrara; PI=Pierre; T=Trinidad; V=Vermejo; R=Raton(adapted from Weimer, 1980).

along with the author, state the Brehm-Anderson #1 Scheel well's total depth is within the Ordovician Harding Formation; estimated to be less than 100 feet (30m) above the Precambrian contact. The well exhibits a 215 feet (66m) thick section for the Ordovician dolomites and sandstones with interbedded shales (Fremont and Harding Formations), 145 feet (44m) of Mississippian dolomite and limestone (Hardscrabble and Williams Canyon Formations), and 3,835 feet (1169m) of Pennsylvanian and Permian red arkoses, sandstones and shales (Glen Eyrie, Fountain and Lyons-Lykins Formations). Above the Permian section is the 402 feet (122m) Jurassic siltstone and vari-colored shales, sandstone with several thin limestone intervals. From the Jurassic to the surface, Brehm-Anderson #1 Scheel well shows 4218 feet (1286m) of Cretaceous rocks, with 3105 feet (946m) being the Pierre Formation. The thicknesses of Cretaceous Formations in the well are as follows (in ascending order): 216 feet (66m) of Dakota Sandstone and shale; 92 feet (28m) of Graneros Shale; 170 feet (52m) of Greenhorn Limestone; 150 feet (46m) of Carlile shale which grades into the overlying Codell sandstone (0-30 feet; 0-9m); 45 feet (14m) of Ft. Hays limestone; remaining 440 feet (134m) of Niobrara limestone and shale; and, the oil-producing Pierre shale

shale (production is absent in this well), 3105 feet (946m) thick, which has interbeds of limestone and sandy, clayey zones.

Although the Brehm-Anderson #1 Scheel well encountered the Pierre Formation at the surface, the Cañon City graben also includes the Cretaceous age Trinidad sandstone with several interbedded shale zones. Above the Trinidad Formation is the Vermejo Formation, which contains sandstones, lignitic shales, claystones, and several mineable coal beds. Some areas include slightly consolidated gravels and silts, which are Pleistocene or Late Tertiary age.

The Pierre Formation may be divided into seven units in the Florence area (Figure 4), with fossil ammonites providing the key for stratigraphic zonation (Cobban and Scott, 1975). The Lower Transition Member contains mostly calcareous non-concretionary shale, with thin bentonite layers and is 295-430 feet (90-130m) thick.

In the Florence area the Apache Creek Member is a sandy to silty shale that ranges in thickness from 10 feet (3m) at the basin's northern end to 135 feet (40m) at the southern end. Bentonite beds occur within this member.

The Sharon Springs Member consists of a silty, hard, organic rich shale, that ranges in thickness from 35 to

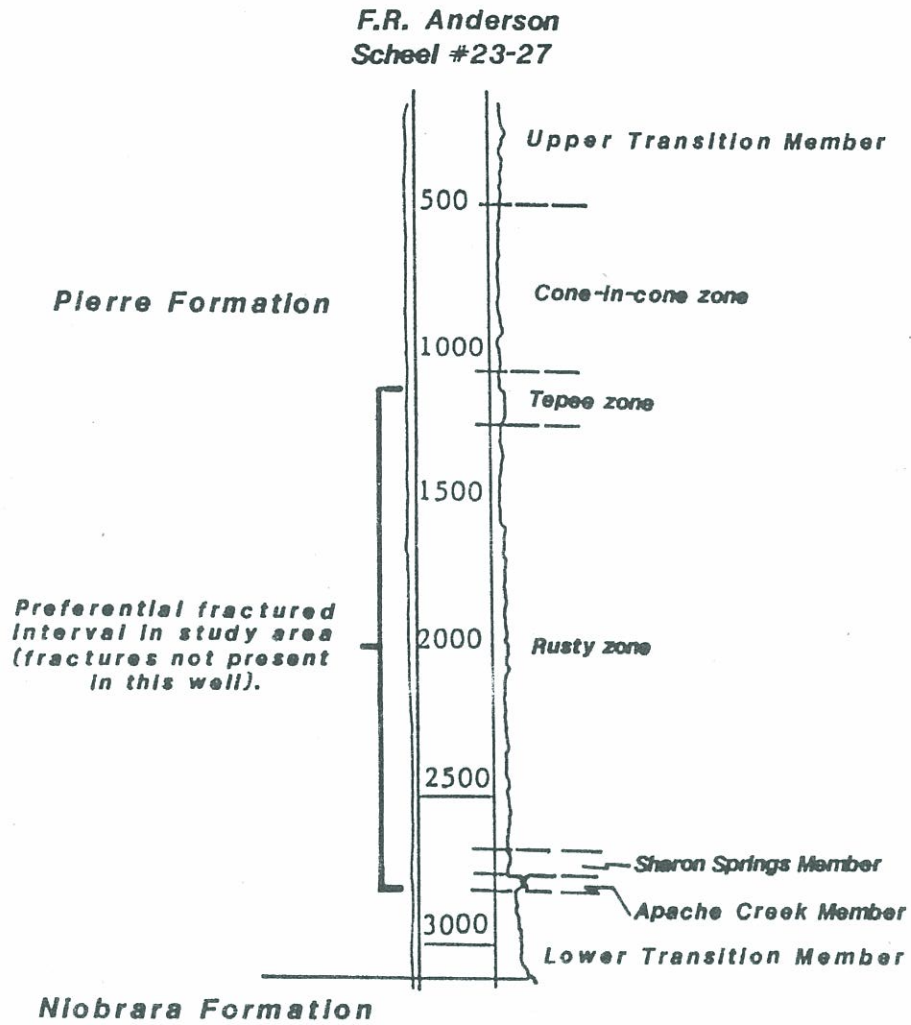


**Figure 4: Pierre Formation stratigraphic zoning (modified from Cobban and Scott, 1975).**

nearly 90 feet (11-27m). The organic content is high enough for the Member to be considered a source bed for petroleum (Gautier, et al, 1984). Also included in the Sharon Springs Member are many limestone concretions, phosphatic nodules, gypsum, and bentonite beds.

Composition of the Rusty Member is a blocky to fissile shale that contains concretions and thin beds of white bentonite. This Member is about 1,450 feet (442m) thick.

Thickness for the Tepee Member is 200 feet (61m) and contains silty, micaceous, and bentonitic shales, with bentonite beds being common. The Tepee Member also contains locally small erosional masses of crystalline limestone that form cores for the features called Tepee Buttes.

Cone-in-Cone Member is 600 feet (180m) thick and contains clayey or silty shale, limestone concretions, bentonite beds, and cone-in-cone concretion structures.

Upper Transition Member consists of sandstone, shaley sandstone, and sandy shale with a total thickness of about 500 feet (152m).

This author believes the producing members within the Pierre Formation are the clayey and silty zones of Apache Creek, Sharon Springs, Rusty, and Tepee Butte Members. These members contain intermittently opened fractures to form the

oil reservoirs. While the Cone-in-Cone Member forms the vertical migration seal over these clayey and silty zones, the Lower Transition Member effectively prevents the invasion of water from the underlying sediments. This Cone-in-Cone Member also inhibits influx of water from above the production interval and since there is no formation water, older wells do not become water wet.

Additional reservoir rocks may be present in Cretaceous formations below the Pierre Formation in the Cañon City graben. Production in these horizons would probably be related to both structural and stratigraphic traps which would have required more sophisticated geophysical techniques to define than were in use during the early development of the Pierre Formation. Production might be anticipated from the Dakota, Codell, and Niobrara Formations in the Florence-Cañon City area, since these horizons have had only limited exploration.

### Structure

Previous work done by Brown (1978) indicates a complex structural development in the Cañon City embayment area. Two periods of tectonic activity are documented. The first

period resulted in the development of the horst and graben structure present within the study area. Second period, Laramide in age, renewed activity on existing faults and produced small basement faults.

Basement faulting interpreted on P-wave sections (Plates 5 and 6) shows flexures at the Niobrara level between shot points 75 to 130 and 170 to 250. These flexures correspond to areas of preferential fracturing within the Pierre Formation. SH-wave sections (Plates 7 and 8) do not exhibit similar structural flexures at the Niobrara level.

#### Production

Fractured reservoirs are common along the Front Range. In addition to Florence, other fractured reservoirs that have been developed include Berthoud, Loveland, and Boulder fields in the Denver basin.

The Florence field is the oldest, continuous producing area in the United States. Initial production was from oil seeps along Fourmile Creek, nine miles northwest of Florence. A.M. Cassidy drilled six wells into the Holocene gravels and lower Morrison Formation along the creek in 1862. Four of the wells ranged in depth from 20 to 90 feet, while the other two wells went as deep as 400 feet. Oil was found only in the strata near the surface. This production marked the

first commercial oil production west of the Mississippi and the second in the country. After two water wells, drilled in the southern portion of the Cañon City graben, encountered oil along with water, Isaac Canfield was persuaded to help drill a well about 12 miles south-southeast to the Cassidy oil spring area, just south of the present town of Coal Creek. In 1876, he struck oil at 1187 feet. This well marked the first production in Florence field.

The Cañon City field was discovered in 1926 and is the smaller of the two accumulations. Although the reservoir rock is the same Pierre Formation, this reservoir is structurally unrelated to the Florence field. The Cañon City field occurs within the Oil Creek anticline.

To date, about 1,500 wells have been drilled in the area, primarily with cable tools and primitive completion techniques. Although the area has been traditionally characterized by shallow, low-potential wells, production has continued to the present day. Some wells in the field are over 80 years old and still average four to seven barrels of oil per day. Wells are economic despite their relatively low daily production, since the wells are long lived.

The Florence-Cañon City field area produced 23,305 barrels of oil during 1985 from 39 active wells. Almost all

of the just over 15 million barrels of oil produced has been from the Upper Cretaceous Pierre Formation, with minor production from the Niobrara Formation.

Production from the Niobrara Formation will not be covered in this paper. However, fracturing in the Niobrara will be assumed to coincide with fracturing in the overlying Pierre Formation.

Oil reportedly does not follow any bed or series of beds in the Pierre Formation. As shown by the outcrop, the oil zone does not contain any continuous sandstones or other porous beds capable of acting as reservoirs. When a well is drilled, the oil's initial rise can vary from 300 to 1,500 feet, with a maximum of 2,500 feet, therefore different pressure cells exist indicating a discontinuous, heterogeneous reservoir (Washborne, 1908).

Completion reports indicate Florence field reservoir is composed of producing zones at 1200 feet (366m) and between 1,900 and 3,200 feet (579-975m) below the surface. Lower limit of production within the Pierre is just above the Niobrara Formation. Presumably, the producing zones occur within the Tepee Butte, Rusty, Sharon Springs and Apache Creek Members of the Pierre Formation. Carpenter (1961) states that most Florence-Cañon City production is

from the Tepee Butte Member, fractures within soft thin sandy shales being the reservoir. Production reports, however, show the Florence field's production is largely from the lower Rusty, Sharon Springs, and Apache Creek Members of the Pierre Formation.

Zones of strata which have yielded oil along the vicinity of the seismic line are from approximately 1,200 feet (366m), 1,900-2,200 feet (579-670m), 2,300-2,600 feet (701-792m), and a rich zone between 2,800 and 3,200 feet (853 and 975m). Producing intervals probably contain numerous beds of fine-grained sandy shale which occur either as a succession of layers or as lenticular masses which lack continuity to provide a reservoir, except for fracturing (Darton, 1905).

Previously cited evidence shows that oil occurs in the Pierre Formation's joints and fractures. This evidence was summarized by DeFord (1929).

- 1) Interfering wells surface alignment corresponds with the rocks major joint direction.
- 2) Wells drilled within a few feet of each other, do not encounter oil at the same depth.
- 3) A shallow gas well often immediately ruins an adjacent well, which is several hundred feet deeper by tapping its pressure source.

- 4) Many wells draw adjacent wells that are much shallower.
- 5) Adjacent, same depth wells having dissimilar pressures.

The extent of some of the fractures is indicated by the extremely long lives and the slow production decline curves of the better wells. There is no formation water, so instead of going to water, depleted wells simply quit producing oil.

The oil seeps on Fourmile Creek, which led to the discovery of Florence and Cañon City fields, are updip from the main field area. Only minor production was obtained from the Cassidy wells in area of the oil seeps. Actually, these seeps are in the Jurassic Morrison Formation, which is 1000 feet stratigraphically lower than the Pierre Formation.

Oil characteristics for the Pierre Formation in Florence field are (Carpenter, 1961):

Gravity	- 30.9 <sup>o</sup> API.
Sulphur	- .34%.
Pourpoint	- 51 <sup>o</sup> F.
Paraffin Base	

Tests have shown that the field's oil has a high paraffin base. Therefore, as a well was produced, paraffin precipitated out of the oil and deposited in the pores of the rocks and fissures of the fractured system, eventually choking off the flow of oil to the well bore.

A geochemical study of Cretaceous oils in the Denver basin by Clayton and Swetland (1980) supports an indigenous source for oils produced from fractured shale reservoirs at the Florence field.

No established drilling patterns are apparent when all the old wells are analyzed and there is often no record of why a well was abandoned. Most wells drilled in the area were drilled on speculation, with less than a dozen wells logged. Few wells were drilled below the Pierre Formation. Drilling often stopped when they hit oil or the Niobrara or both. Very few of the old wells were cased; therefore, many wells that are reported as dry and abandoned were probably plugged because the hole had caved.

Florence field fractures postdate rock burial, compaction and lithification, but probably predate or occurred concurrently with hydrocarbon generation. Oil entry in these fractures probably occurred during a relatively short time period. As previously stated, presumably the primary

production lies within the lower Rusty, Sharon Springs and Apache Creek members, which are sandy, organic rich shales, with thin interbedded limestone, clays, and bentonite beds. Because shales have low permeability, the generated petroleum did not escape or migrate any great distance, other than possibly into the more permeable beds within the lower Rusty, Sharon Springs, and Apache Creek Members, which might have provided oil and gas retention in the Pierre Formation prior to development of any fracture system. Beds within the lower Rusty, Sharon Springs, and Apache Creek Members were the Pierre Formation's limited primary permeable intervals, until natural fracturing imparted secondary permeability.

DeFord (1929) discussed the following idea for the cause of accumulation. When the Trinidad and Vermejo sandstones were eroded away from the graben's eastern half, the strains stored in the Pierre Formation were released, which possibly opened already existing joints or possibly opened newly formed fractures within the Pierre Formation's lower interval. However, since oil has been found beneath areas where the Trinidad and Vermejo sandstones are present, DeFord's theory appears invalid or is secondary in nature at best.

Another cause for accumulation might be associated with the drape folding over the Brush Hollow anticline. The drape folding possibly progressed to the extent that elongation normal to the fold's trend exceeded the ability of the rocks to deform elastically, resulting in the development of extensional open fractures.

Another proposed cause might be associated with horst and graben structures, which could have caused compression of the beds. Following the areas compression, relaxation might have resulted in extension and opening fractures within the less ductile parts of the lower Pierre Formation.

Whichever case occurred, commercial production is from these fractures.

SEISMIC DATAData Acquisition

The seismic data involved were supplied by CGG (Figure 1). Sources were 100 feet (30m) strands of 200 grain per foot Primacord buried in three parallel trenches, separated by three feet (1m) intervals. In some locations, boulders caused the strands to be buried less than two or three feet. Since horizontal receivers are much more sensitive to ambient noise than vertical receivers, the orientation of horizontal receivers must be maintained. The seismic data were shot and recorded using the Syslap\* technique. The Syslap method was designed to increase the fraction of energy transmitted as SH-waves. The strand fired in the central trench was designed as the P-wave source and the two fired straddling trenches are SH-wave sources (Figure 5). Vertical axes compressional wave geophones were used for recording when the central strand was fired and horizontal axes shear wave geophones were used when both the straddling strands were fired.

\*Trademark of CGG (Compagnie Generale De Geophysique).

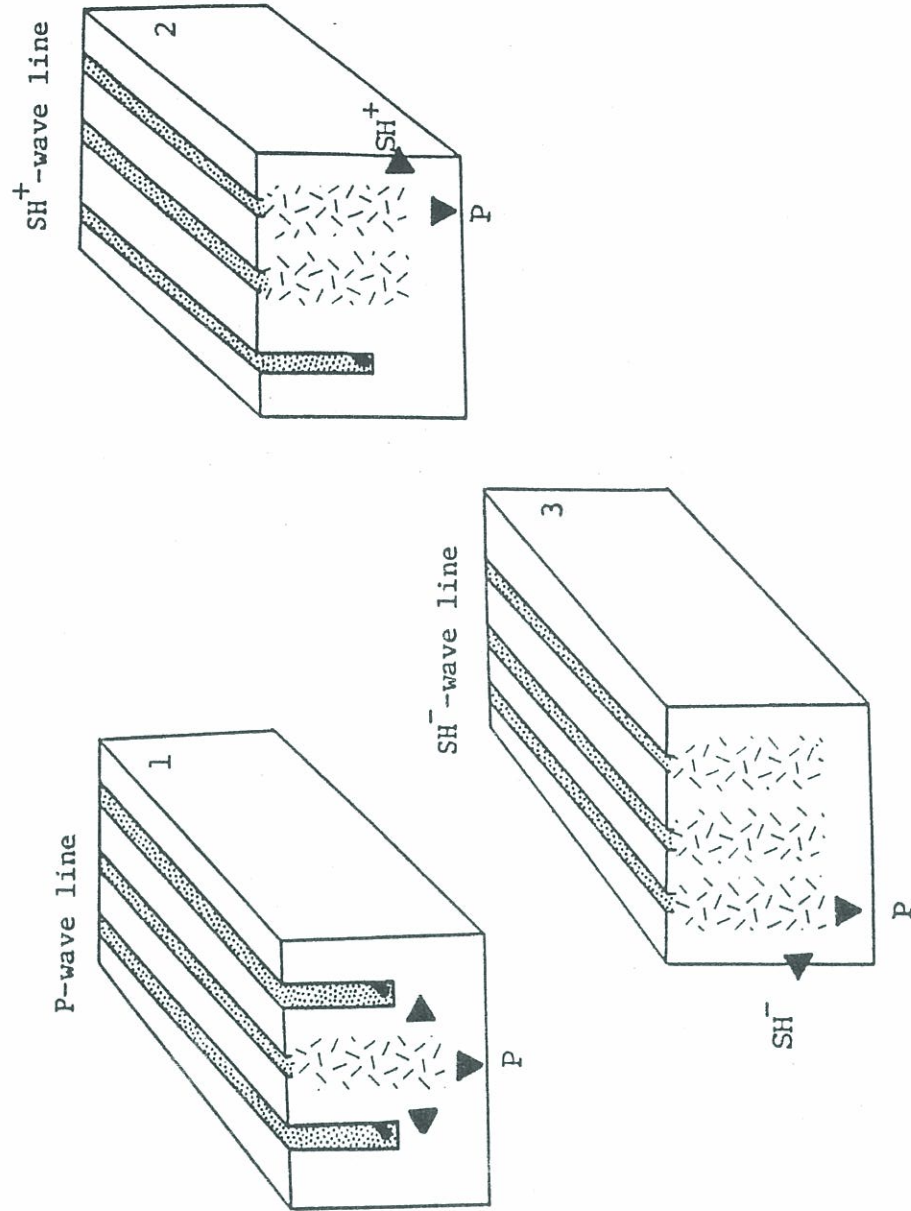


**Figure 5: Syslap Method( Omnes, 1976). Dominant compressional(P) and/or shear(SH) wave energy generated when each primacord source is fired.**

Because the earth is inhomogeneous the line explosive actually generates some S-wave energy along with the dominate P-wave energy. The P-wave spread records a P-wave signal along with a SV-wave signal. After the middle trench is fired the material around this middle trench is unconsolidated, presumably causing some of the explosive generated pressure waves to be absorbed in the loose material.

Next, one sideline is fired. Absorption causes the sideline explosions to be a non-spherical center of expansion, creating SH-waves by the unbalanced pressure on the side opposite to the middle trench. Each S-wave spread then records a SH-wave signal along with the P-wave signal.

Finally the other sideline is fired. Because this trench is located along the plane of symmetry of the other two line sources, the corresponding SH-wave signals received at a given station location along the receiver trends have mirror image polarities. Polarity is not reversed for the P-wave signals.

When subtracting one of the two identical SH-wave shot point records obtained on opposite sides of the central trench, the SH-wave signals will add up, while the P-wave

signals will cancel out. Actually, because the amplitude of the P-wave signals are not equal, the subtraction is optimized by minimizing the average amplitude ratio (average amplitude in the P-wave domain)/(average amplitude in the SH-wave domain). The P-wave domain is defined as the part of the record between the P- and SH-wave first breaks, while the SH-wave domain is any time interval where there are strong SH-wave events. After this optimized subtraction, very little energy is supposedly left in the P-wave domain, leaving visible SH-wave first breaks and reflections.

#### Recording Information

Approximately seven miles of P- and SH-wave seismic information were recorded in 1978. Author was not involved in the acquisition of either the P- nor SH-wave seismic data. The recording parameters for the P-wave section are shown in Table 1, while the SH-wave section's recording parameters are shown in Table 2.

#### Data Processing

The initial processing was performed by CGG in 1978. P- and SH-wave data followed almost identical processing

sequences to minimize differences between the CGG presented P- and SH-wave final stacks (Plates 1 and 3). CGG also followed a standard preserved amplitude processing sequence (Table 3) for the P-wave data and a preserved amplitude section was generated (Plate 2).

The SH-wave processing sequence begins with a weighted subtraction of the two corresponding opposite polarity SH-wave records. Subtraction was performed in order to eliminate P- and SV-signals following demultiplexing. After subtraction, the SH-wave processing followed the P-wave preserved amplitude processing sequence.

S-wave static corrections are much more difficult to define and to adjust for than are P-wave static corrections. A stabilizing effect of the water table exists only for P-waves. Automatic residual statics are also more difficult, because the velocity ratio  $V_s/V_p$  of the near surface may reach five to ten, whereas the frequency ratio of P- to S-waves is generally not more than two or three (Garotta, et al, 1977). Laterally varying conditions in the near-surface caused large S-wave statics problems. Due to the large S-wave statics and a relatively low signal to noise ratio (S/N) before stack, careful statics and velocity analysis were imperative in processing these S-wave data.

Therefore, during acquisition shorter arrays should be used to preserve accurate statics information, even though source-generated noise attenuation will probably increase.

Following the SH-wave preserved amplitude stack, a F-K (frequency-wave number) filter was applied to the SH-wave stack. The F-K filter eliminated strong criss-crossing line-ups visible on the SH-stacks. These unwanted line-ups correspond to SH-wave repeated first breaks with a velocity of about 5900 ft/s (1798m/s) and a dominant wavelength of 540 feet (164m) (CGG, 1980). Similar line-ups with an apparent velocity of about 5400 ft/s (1646m/s) and a 540 feet (164m) wavelength could be observed on the P-wave records (CGG, 1980). These lineups could be interpreted as SV-first arrivals, but predictive deconvolution effectively removed these events. Trying to filter these line-ups in the field with geophone arrays would have reduced the data quality.

Signal to noise ratio (S/N) on the SH-wave's final preserved amplitude section is fairly low, with criss-crossing line-ups still visible. In an attempt to reduce these criss-crossing line-ups, the writer applied the F-K filter sequence to improve the S/N ratio before stack. The resulting final preserved amplitude stacked section shows

a slight reduction in signal quality of the section's upper 1.5 seconds, even to the extent of reducing correlative horizon amplitudes.

S-wave frequency domains of noise and signal generally overlap and are sometimes identical (Garotta, et al, 1977). Reduction of these signal amplitudes is attributed to the SH-wave's first break velocities being in the vicinity of the horizon's SH-wave velocities.

The author felt the section processed with the F-K filter applied after stack shows an increased S/N ratio over the F-K filter being applied before stack, so the F-K filter after stack SH-wave preserved amplitude section is included in this report (Plate 4).

CGG felt that the S/N ratio of the original processed P-wave preserved amplitude section was of good quality and their decision was that no further processing would improve the section significantly. After analyzing well log information, synthetic seismograms, and the SH-wave sections, the author believed that the P-wave sections processed by CGG did not exhibit necessary reflection quality and detail within the Pierre Formation. The author reprocessed the P-wave data to enhance the detail available in the fractured interval of the Pierre Formation. In

an attempt to gain a greater understanding of the SH-wave velocities along given reflectors the SH-wave data was again reprocessed as well.

Following the SH-wave pre-processing by CGG to perform a weighted subtraction of the two corresponding opposite polarity SH-wave records, both the P- and SH-wave data were processed at the Casper, Wyoming Seismograph Service Center (SSC). Both P- and SH-wave data were processed with similar sequences to minimize differences (Table 4). Carefully constructed F-K filters were applied to both P- and SH-wave data before deconvolution. Normal polarity sections were generated for both the P-wave final stack (Plate 5) and P-wave preserved amplitude stack (Plate 6). Reverse polarity sections were generated for both the SH-wave final stack (Plate 7) and SH-wave preserved amplitude stack (Plate 8).

Uninterpreted normal polarity sections for the SH-wave preserved amplitude stack (Plate 10) and final stack (Plate 9) are included with this study for completeness and the readers scrutiny. Since these SH-wave sections have a lower frequency content, a P-wave preserved amplitude section was also generated for correlation purposes using the SH-wave final filters (Plate 11).

### Polarity Conventions

SEG is the adopted convention (Thigpen, Dalby and Landrum, 1975). For P-waves, the upward movement of the geophone case corresponds to a negative number being written on the field tape. Which is to have an increase in acoustic impedance, equivalent to a positive reflection coefficient, corresponding to a trough on the resultant normal polarity seismic section.

Normal polarity P-wave sections are used for this report. For SH-waves, azimuthal orientation of the horizontal geophones were always pointed in the direction of the recording line's progression. Therefore, a horizontal geophone's movement from left to right will correspond to a vertical geophone's upward movement. Because Syslap processing first takes the shot points left side record and then subtracts the right side record, a reverse polarity SH-wave section is used for this report. This reverse polarity SH-wave section will then correspond to the conventions adopted for the P-wave section.

CGG reported their seismic sections also adhered to SEG polarity conventions.

WELL LOG DATA

Petroleum Information completion records show most wells along this seismic line were drilled before 1960, with several wells being drilled in 1925 (Tables 5 and 6). Along the seismic line, completion records show production from the Pierre Formation is between 1200 and 3200 feet (365-975m) below the surface (Figures 6 and 7).

The only sonic log in vicinity of the seismic line is Continental Oil Company Huffman #1 well (SW NW sec 30, T19S, R68W). From this sonic log, a synthetic seismogram was constructed (Figure 8). Along with the sonic log, the Continental Huffman #1 has a resistivity log.

Logs from two other wells along seismic line include Brehm-Anderson #1 Scheel (NE SW sec 27, T19S, R69W) resistivity suite, and the Florence #1-4 well, located in sec 4, T20S, R69W. Productive interval in the Lear well is 2780-3255 feet (847-892m). Although Seaboard Oil Co. of Delaware (Texaco) acquired a continuous log and standard velocity survey for the Brehm-Anderson #1 Scheel well, this writer was unable to obtain a copy.

Faust (1951) showed that velocity and resistivity logs have a similar form. Both velocity and resistivity logs change with fluid content, but the resistivity log

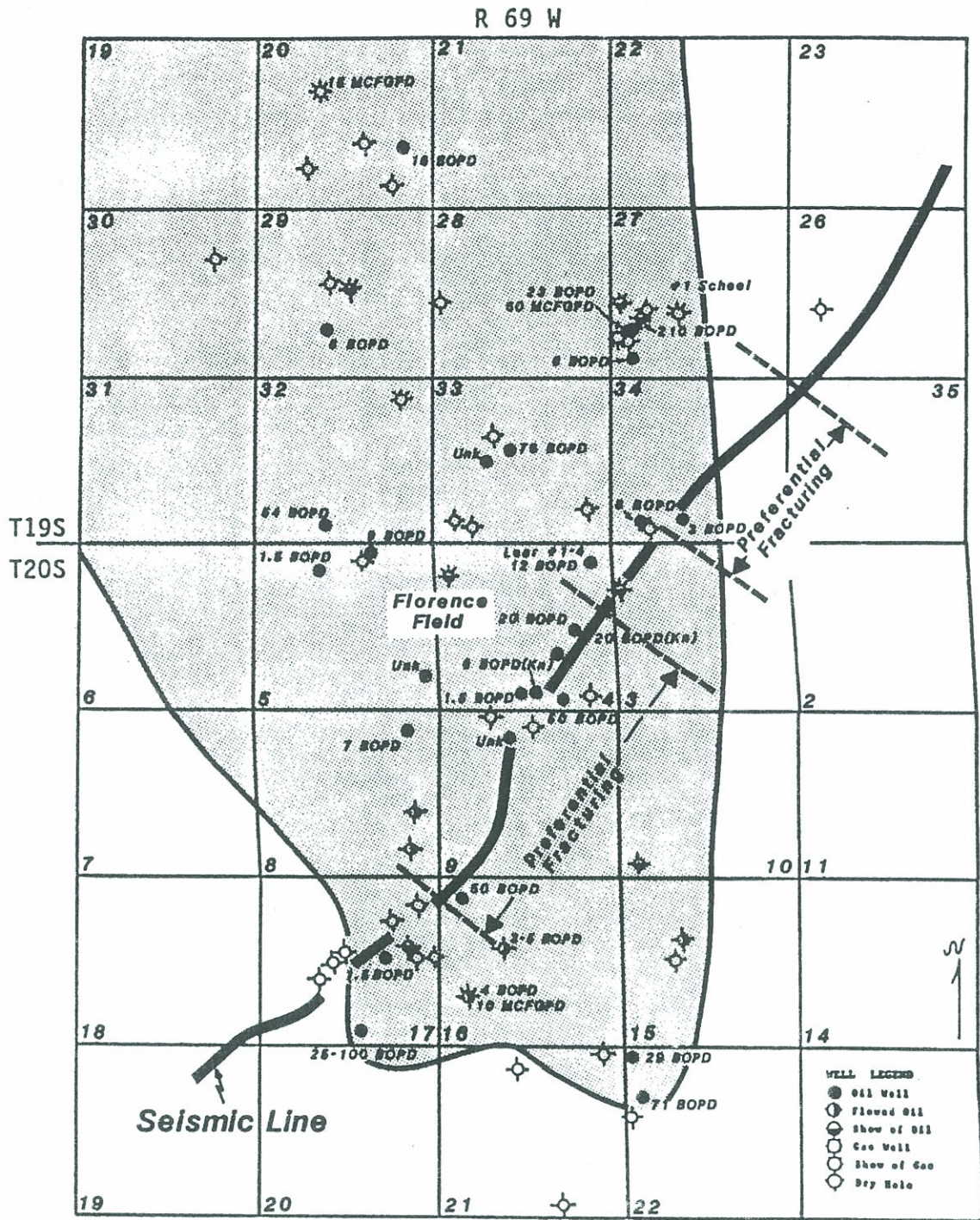


Figure 6: Florence field area wells. Production information includes initial production and/or sustained production (from Petroleum Information).

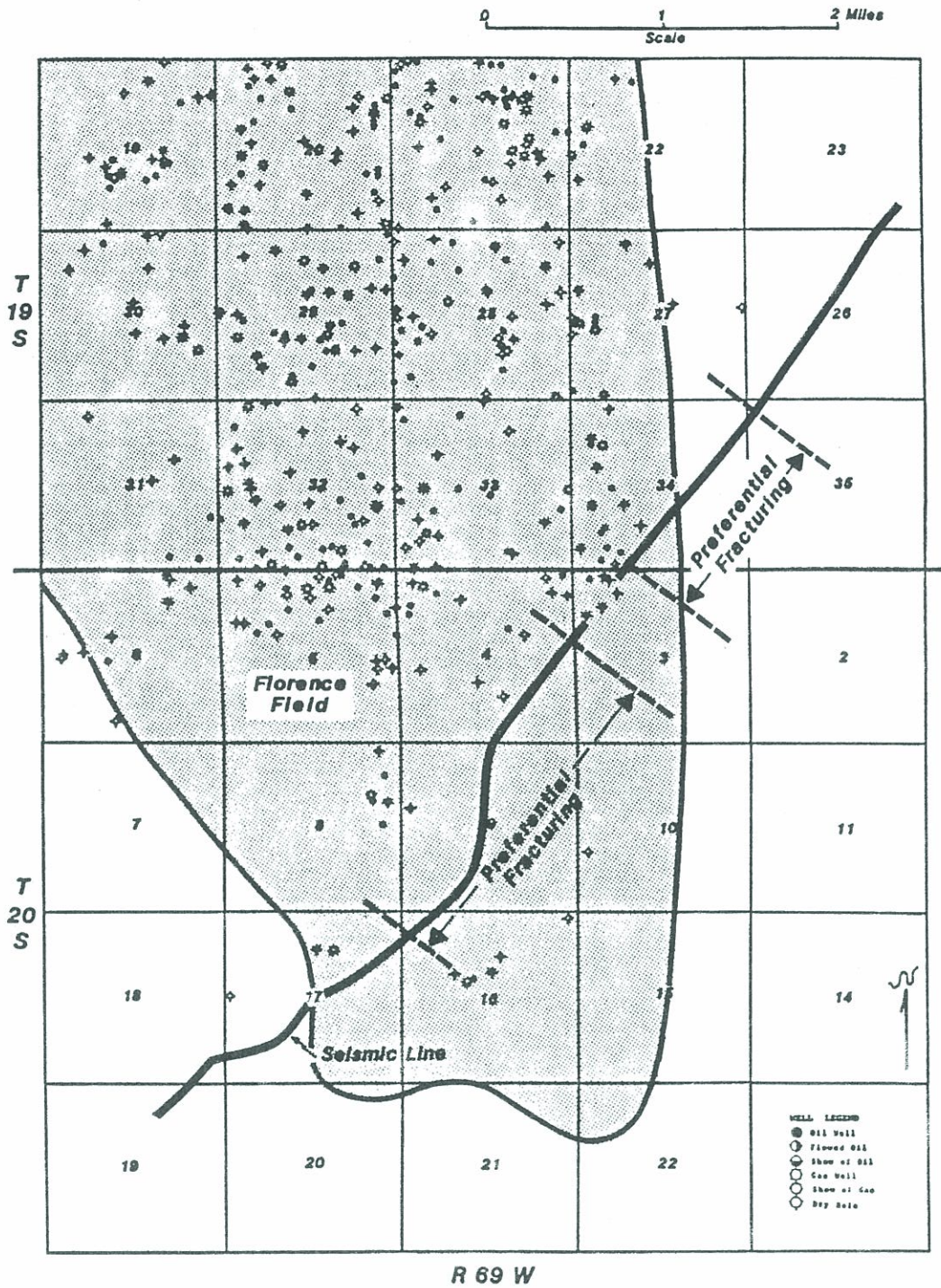


Figure 7: Florence field area wells, from Washborne(1908).



is less affected by borehole conditions. Assuming  $R_w$  values in the Florence area are the same for the different Pierre Formation intervals, Faust's formula will be used to convert the given resistivity values to usable velocity information. Faust statistically showed that for variations in  $R_w$ , which presumably average out for an interval, that resistivity is related to velocity by the following relation;

$$V = (1948) (Z * R_t)^{1/6}$$

where Z is depth (feet) and  $R_t$  is resistivity.

The author designed a computer program which calculated a velocity curve using Faust's formula. This estimated velocity log was then used to generate a synthetic seismogram (Figure 9).

Pseudo-velocities obtained by application of Faust's formula to the Continental Huffman #1 resistivity logs were compared to velocities measured by the Continental Huffman #1 sonic log (Figures 8 and 9). Although the correlations were good, the velocity contrasts are systematically too weak and too slow.

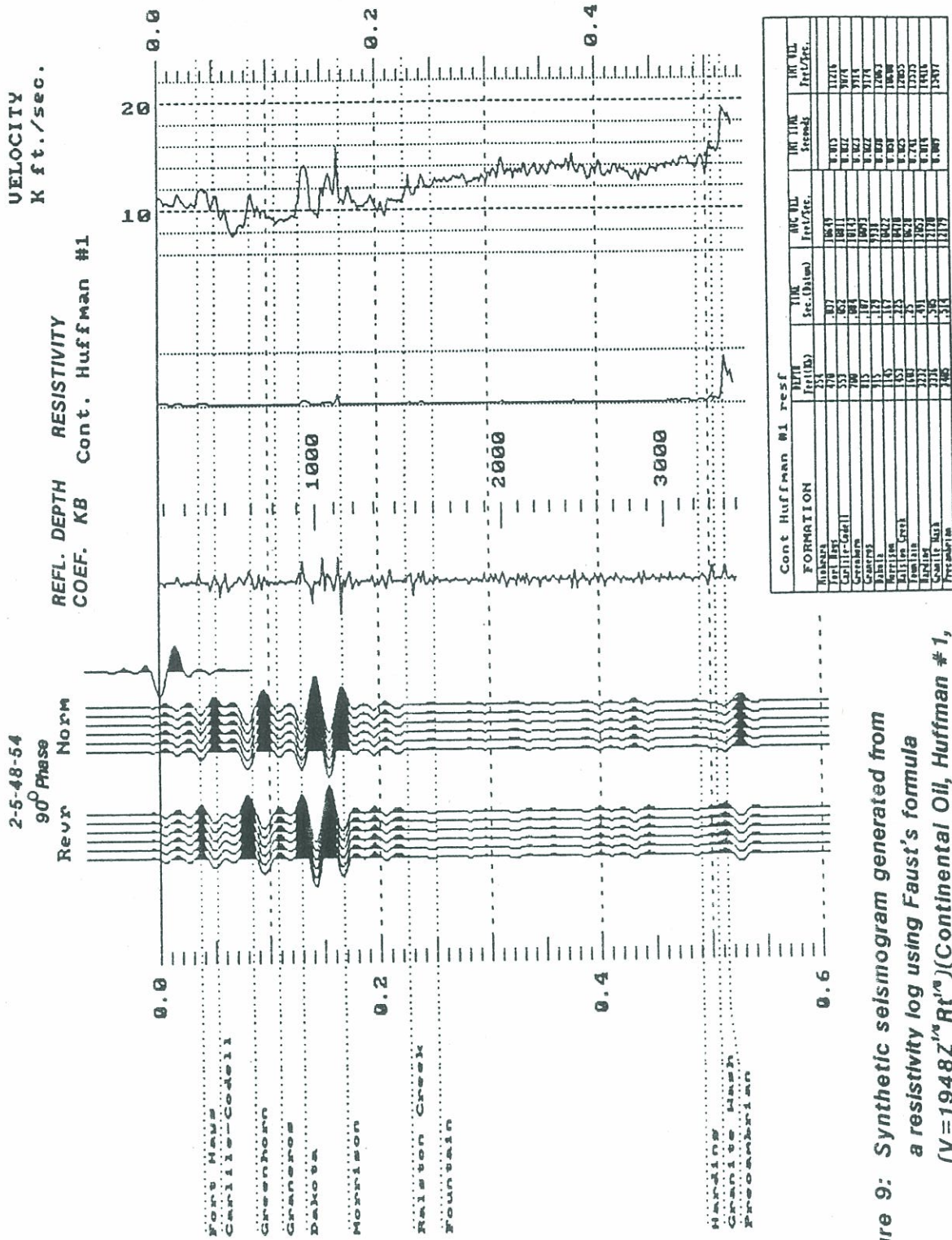


Figure 9: Synthetic seismogram generated from a resistivity log using Faust's formula ( $V = 1948Z^{.6} Rt^{.3}$ ) (Continental Oil, Huffman #1, SW NW sec 30, T19S, R68W).

An improvement was sought to Faust's formula. By using the Continental Huffman #1 sonic log as a velocity survey for calibration of the Continental Huffman #1 resistivity log, Faust's formula was modified by varying the coefficient "A";

$$V = A(Z \cdot Rt)^{1/6}$$

Coefficients for "A" were calculated by defining intervals on wells with both a resistivity and sonic log and then forcing the derived velocity for the defined resistivity interval to approximate that same interval's average velocity measured by the sonic log.

When a well had a density log without a sonic log the density was converted to velocity with Gardner's equation;

$$V = (D/.23)^4$$

This pseudo sonic log, derived from density, was then used for calibrating its corresponding resistivity log and the generation of that well's set of "A" coefficients. The following wells had either a sonic or density and

resistivity logs, from which a set of "A" coefficients were generated for each:

Continental Oil Huffman #1, 19S 68W Sec 30  
CSWNW(sonic).

Delhi-Taylor Oil Corp., #1-16 State, 18S  
69W Sec 16 SENW(sonic).

John C. Riggs, Gindro #1, 19S 70W Sec 27  
WCSWNESEW(density).

Forest Oil, McKinzie #1-3, 19S 69W Sec 3  
CSESEW(density).

Energetics, Inc., Continental #31-20, 19S  
69W Sec 20 WCNWNE(density).

Inca Oil & Gas, New England Ranch & Oil #1,  
20S 69W Sec 32 WCSWNE(density).

Inca Oil & Gas, New England Ranch & Oil #2,  
20S 69W Sec 32 WCSWNW(density).

"A" coefficients for the seven different wells (Figure 10) were averaged to provide a Florence basin data set (Table 9). Using the Continental Huffman #1 well logs, a pseudo synthetic seismogram was generated with these "A" coefficients (Figure 11) and this new synthetic seismogram showed a closer similarity when compared with the sonic generated Continental Huffman #1 synthetic seismogram (Figure 9).

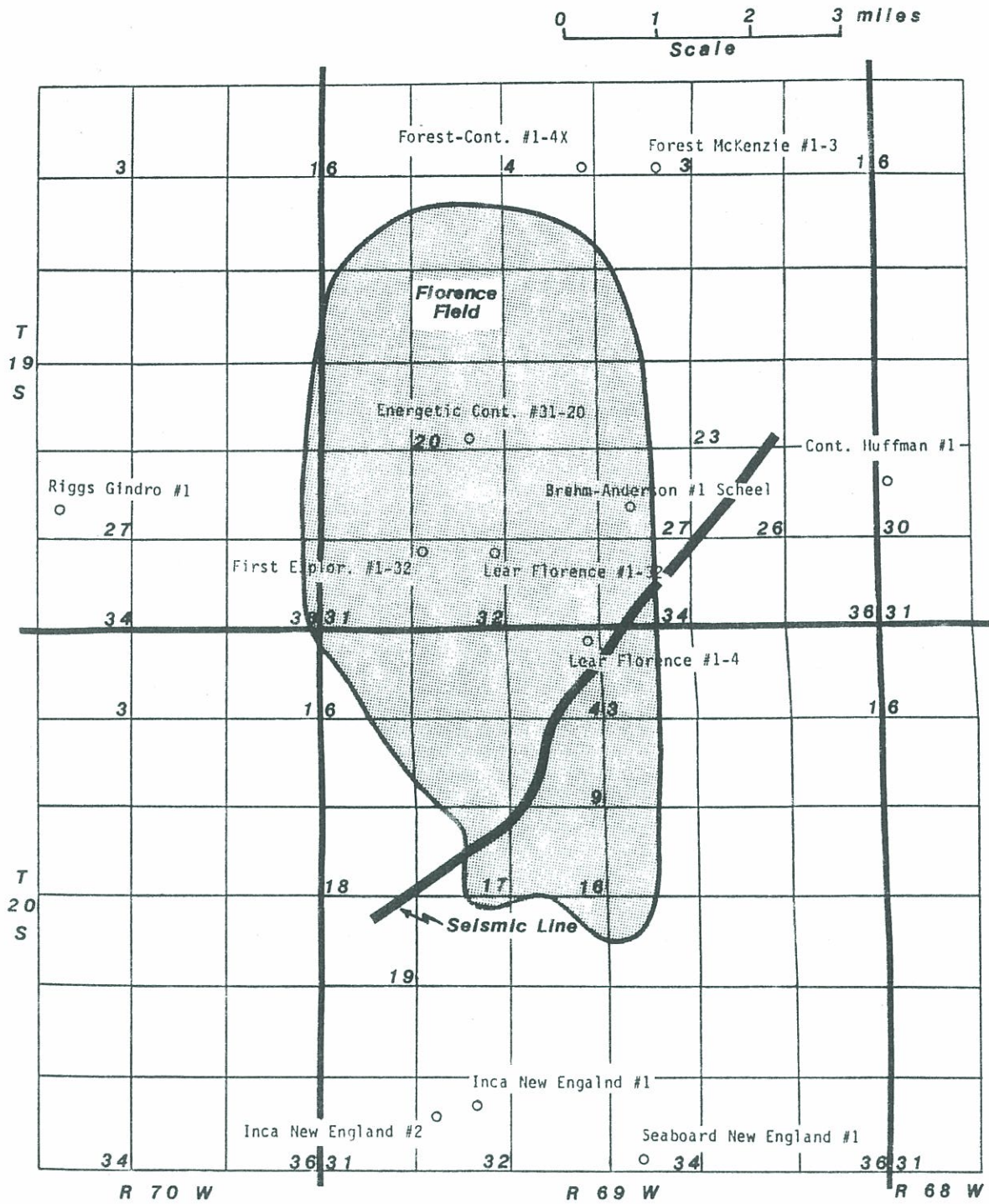


Figure 10: Wells used in calculation of "A" coefficients.

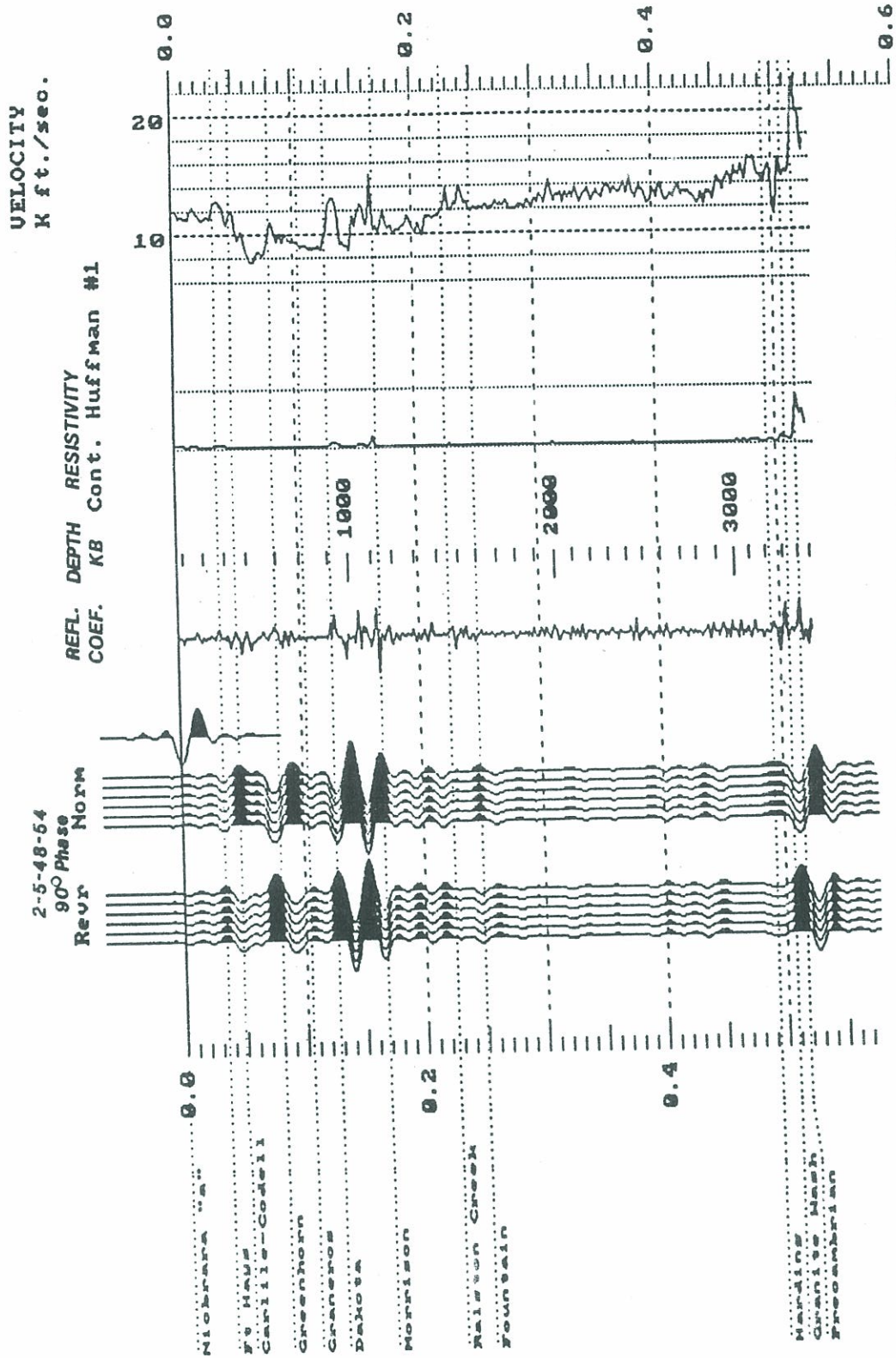


Figure 11: Synthetic seismogram generated from a resistivity log using Faust's formula with a varying "A" coefficient:  $V = AZ^{1/3} Rt^{1/6}$  (Continental Oil, Huffman #1, SW NW sec 30, T19S, R68W).

Because of these encouraging results the set of "A" coefficients was used to generate a synthetic seismogram for the Brehm-Anderson #1 Scheel well (Figure 12). For the readers comparison a synthetic seismogram was also generated from the Brehm-Anderson #1 Scheel resistivity log using Faust's original formula (Figure 13). After these "A" corrections were applied to Faust's formula, results were encouraging but still less accurate than a true velocity survey.

This Brehm-Anderson #1 Scheel pseudo synthetic seismogram (Figure 12) was helpful in identifying the seismic horizons within the Pierre Formation and for correlation of P-wave horizons through the entire section. Correlation of events within the Pierre Formation were not possible with the Continental Huffman #1 well, since the log was spudded in the Niobrara Formation. Correlation of P- and SH-wave data is shown with the Brehm-Anderson #1 Scheel pseudo-synthetic seismogram and the Continental Huffman #1 synthetic seismogram in Figures 14 and 15.

Comparison of synthetic seismograms against the seismic sections shows both P- and SH-wave seismic sections have a ninety degree phase shift. All synthetic seismograms presented in this study are shifted ninety

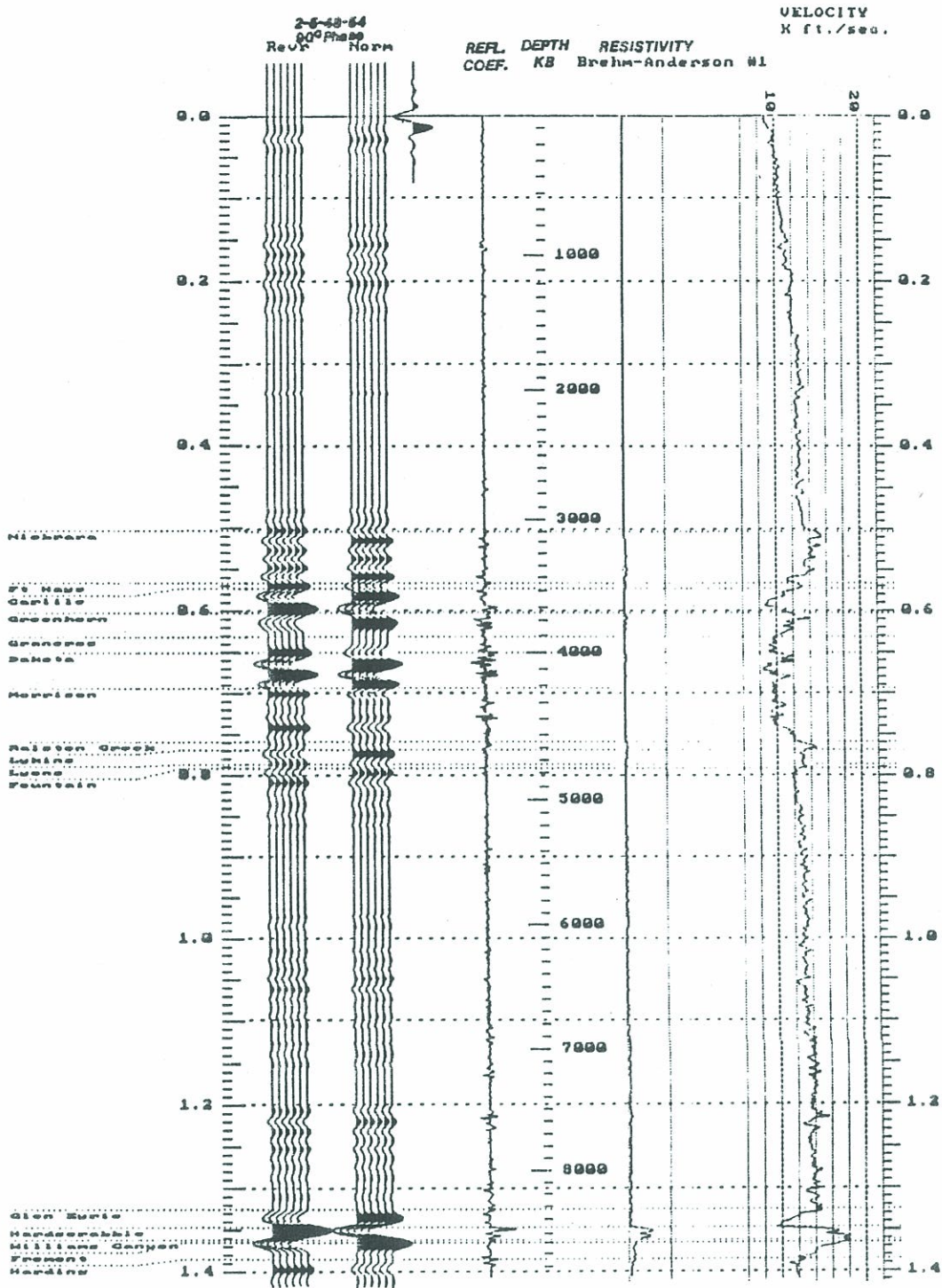


Figure 12: Synthetic seismogram generated from a resistivity log using Faust's formula with a varying "A" coefficient:  $V = AZ^{1/2} Rt^{1/8}$  (Brehm-Anderson #1 Scheel, NE SW sec 27, T19S, R69W).

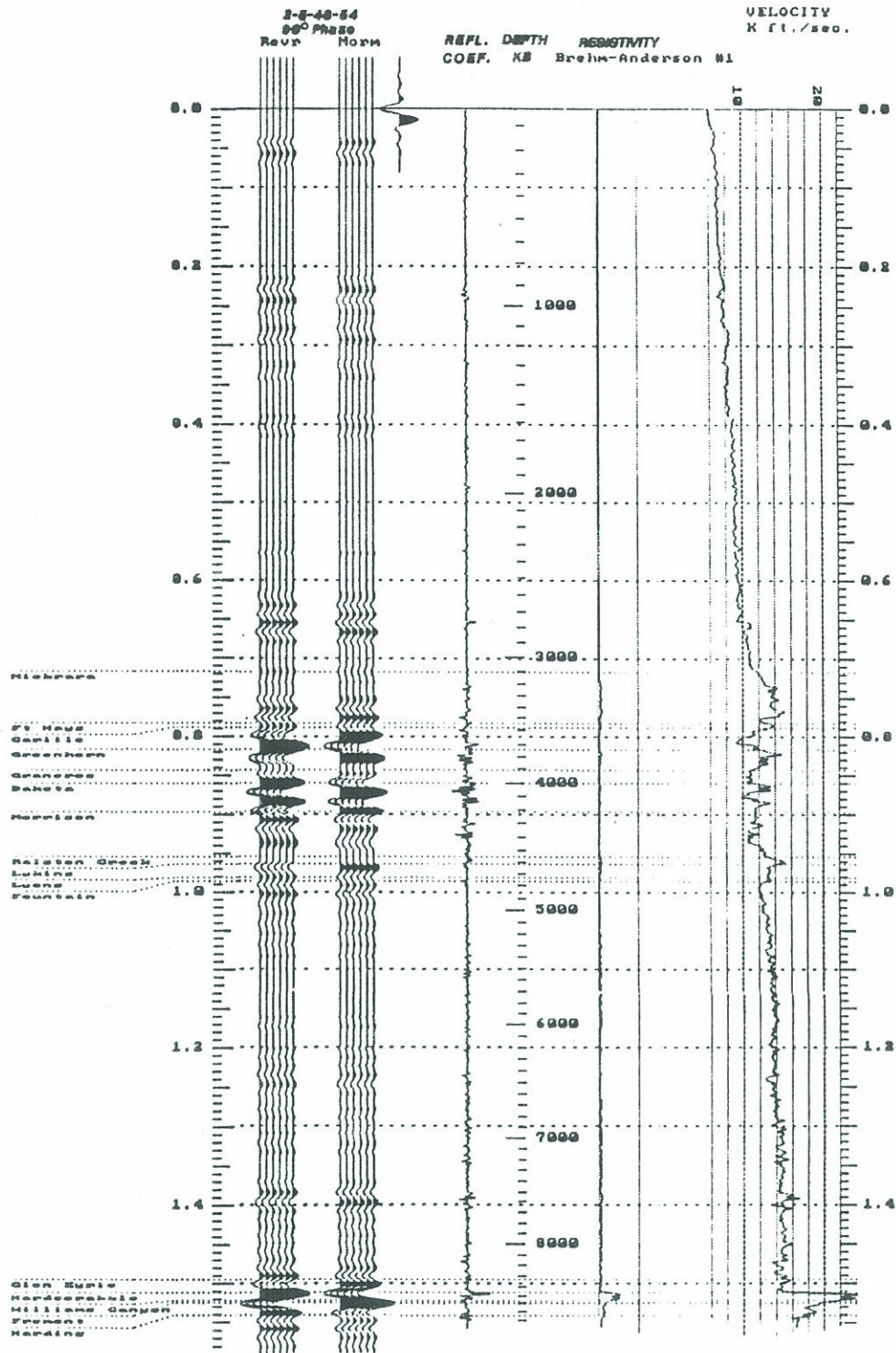


Figure 13: Synthetic seismogram generated from a resistivity log using Faust's formula:  $V = 1948Z^{-1/3}Rt^{1/3}$  (Brehm-Anderson #1 Scheel, NE SW sec 27, T19S, R69W).

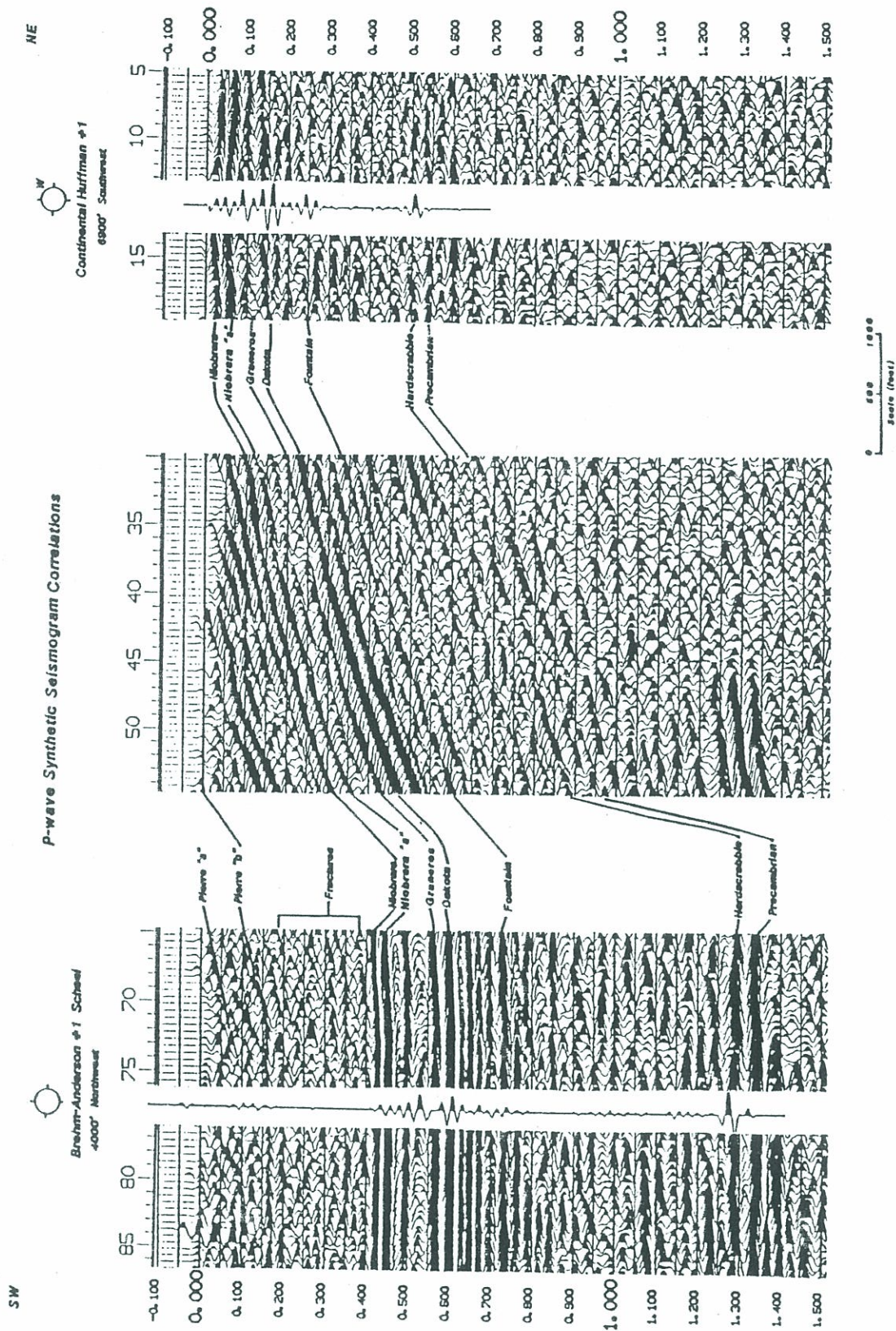


Figure 14: P-wave seismic section correlation with Brehm-Anderson #1 Scheel (resistivity) pseudo synthetic seismogram (reverse polarity) and Continental Oil Huffman #1 (sonic) synthetic seismogram (reverse polarity).

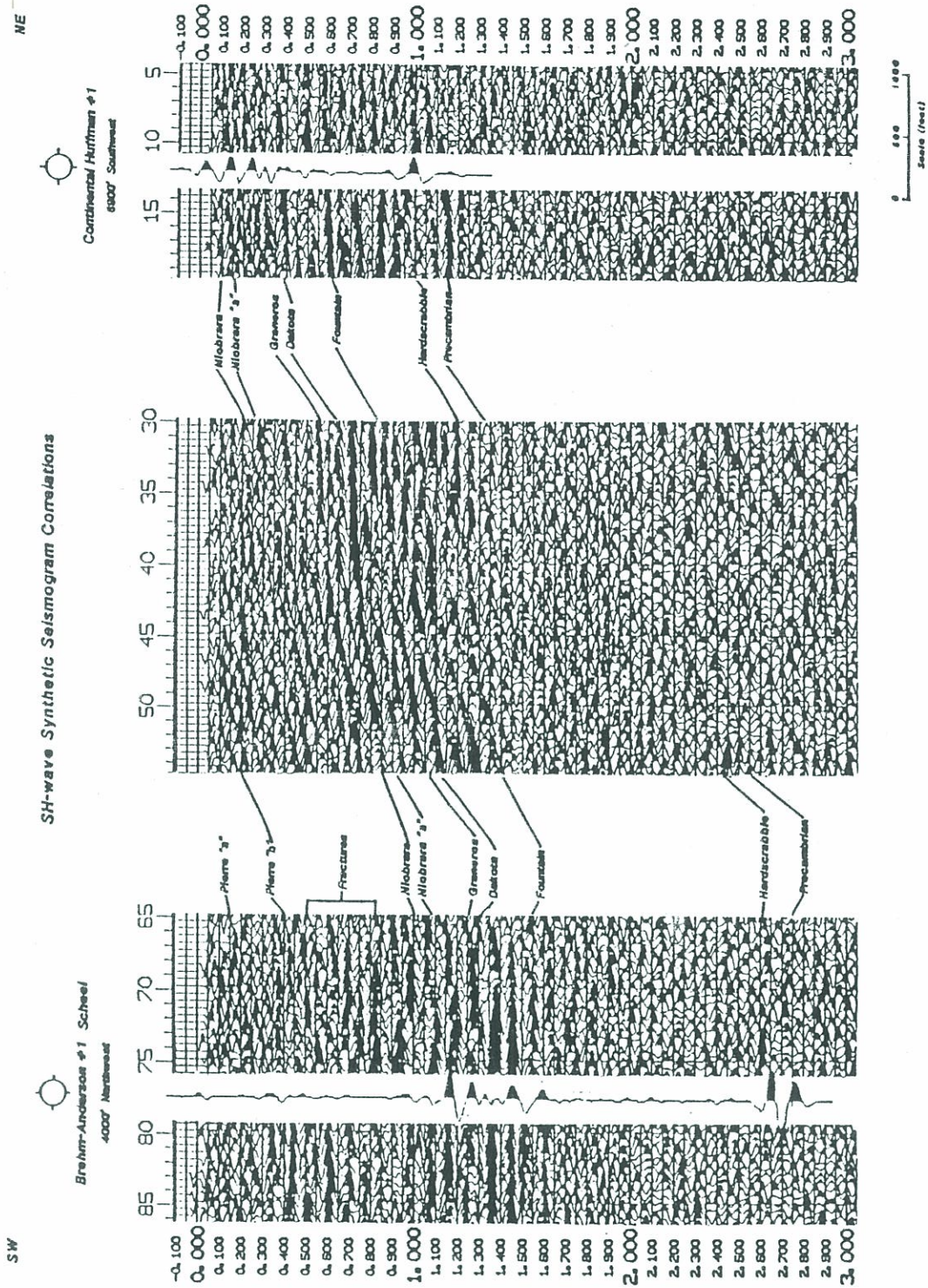


Figure 15: SH-wave seismic section correlation with Brehm-Anderson #1 Scheel(resistivity) pseudo synthetic seismicogram(reverse polarity) and Continental Oil Huffman #1(sonic) synthetic seismicogram(reverse polarity).

degrees. Frequency content of the P- and SH-wave seismic sections were determined. A 2-5-48-54 bandpass filter was applied to all P-wave synthetic seismograms, while a 2-5-30-36 bandpass filter was applied to all SH-wave synthetic seismograms.

### INTERPRETATION

Data processing resulted in a preserved amplitude stack generated for a normal polarity P-wave section and a reverse polarity SH-wave section.

In a horizontally layered medium, SH-waves are not affected by mode conversion as is the case for P- or SV-waves. Therefore, SH-wave sections are generally simpler than P-wave sections. Hazelbroek (1966) showed that for a homogeneous medium, the higher the medium's Poisson ratio the more conducive is that medium's ability to generate S-waves, except in a fluid medium S-waves do not propagate. Dominant wavelengths are shorter for SH-wave sections, as SH-wave velocities are always slower than P-wave velocities.

The Florence field's reservoir is due to fracturing of the Pierre Formation with existing and depleted oil wells along the seismic line being the basis for fracture confirmation (Figure 16). The writer assumes that the depleted wells still have oil remaining that could not be pumped out economically and, therefore, the fractures may not have closed entirely. From completion cards, most producing intervals are located within the 1900-3200 foot (579-975m) depth range. Since the Pierre Formation

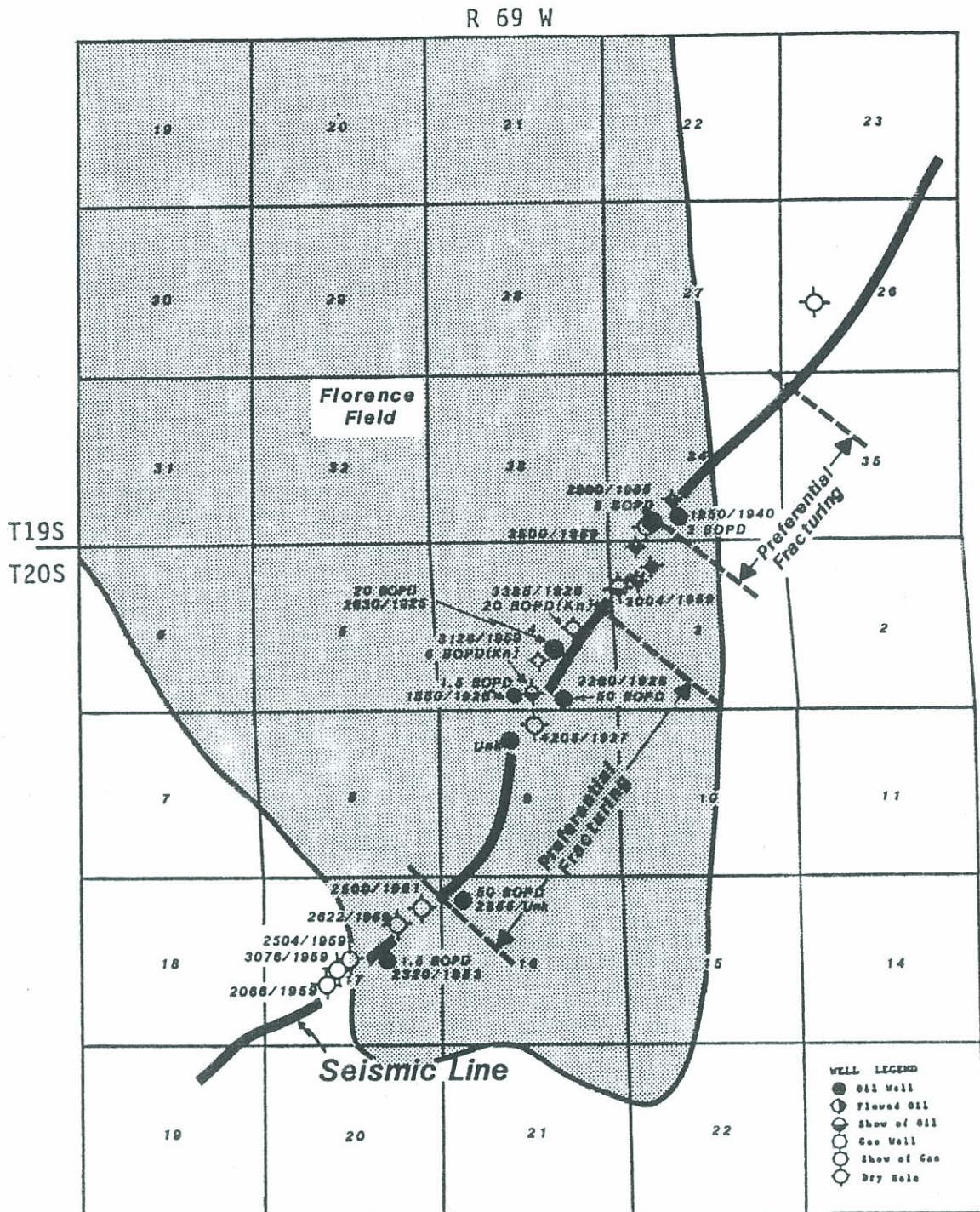


Figure 16: Wells along seismic line. Wells from Petroleum Information data are shown with a larger symbol than Washborne(1908) data.

outcrops at the surface, within the study area and the Pierre Formation's reported thickness is about 4000 feet (1219m), the producing interval lies just above the Niobrara Formation.

The P- and SH-wave sections were converted to a common vertical scale, to help in event correlation. A common vertical scale can be simulated by assuming a constant  $V_s/V_p$  earth ratio and adjusting the plotting scales accordingly. For this study,  $V_s/V_p$  is assumed to equal 0.5 and the SH-wave section was plotted at half the P-wave scale.

Correlation of events can be done with confidence, when both P- and SH-wave sections exhibit the same structural or stratigraphic features. In the writer's study area, the only significant structural features are the faulting and steep monocline on the eastern part of the section. A good stratigraphic aid for the interpreter is the peak associated with the top of the Niobrara Formation, because this horizon is continuous and lies directly below the producing Pierre interval.

Reflected events on the P-wave section were identified by comparing the traces with the synthetic seismograms generated from both sonic and resistivity well logs.

Formation tops were transferred from the P- to SH-wave preserved amplitude stacked section by visual similarity on the sections and by comparison between the sections and a known geologic cross-section constructed from well log information (Figure 3).

After correlation, the following reflectors were identified near shot point 80, where the Brehm-Anderson #1 Scheel well is projected into the seismic line. All reported seismic line reflector depths are measured against this Brehm-Anderson #1 Scheel well. Reported two-way times are from P- and SH-wave preserved amplitude sections (Figures 6 and 8) also in the vicinity of the Brehm-Anderson #1 Scheel well. The first time corresponds to the P-wave section and is followed by the SH-wave section's time. Eleven seismic events are identified on the sections and will be used in this study.

The first horizon identified on the sections is marked with the color reddish-orange and is labeled Pierre "a" (75ms,355ms). This event is approximately 500 feet (152m) below surface and possibly represents a siltstone interval at base of the upper transition interval or transition of upper transition interval's sandy shale to Cone-in-Cone Member's clayey-silty shale within the Pierre Formation.

The second identified horizon is marked with a silver color and is labeled Pierre "b" (165ms,515ms). This event is slightly deeper than 1100 feet (335m) below surface and is interpreted to be interbedded siltstones within the shale near the top of the Tepee Butte Member, Pierre Formation.

Both Pierre "a" and Pierre "b" reflectors are thought to occur above the fractured zone and can be used to upper bound the velocity and travel time interval calculations. Although the events are not continuous across the entire section, these reflectors will enable calculations over portions of the seismic lines.

Top of the Niobrara Formation is interpreted to be a peak (430ms,1030ms), identified as the third horizon with an aqua blue color. The Niobrara peak is 3100 feet (945m) below the surface. This continuous reflector results from the contrast between the lower Pierre Formation's silty shale changing to a calcareous shale at the top of the Niobrara Formation.

The fourth horizon is a continuous peak reflector (451ms,1080ms) within the Niobrara Formation at 3300 feet (1006m) below the surface. This event is labeled Niobrara "a" and is shown with a wine color.

Fifth horizon is a limestone series at the top of the Fort Hays Formation. The horizon is identified as a peak (485ms,1138ms) and is about 3550 feet (1082m) below the surface. A light green color marks this horizon.

Sixth horizon is a trough (505ms,1180ms) and reflects sands within the Carlile-Codell Formation at 3650 feet (1112m) below the surface. The Carlile-Codell Formation is shown with a lemon yellow color.

Seventh horizon is a peak (568ms,1300ms), the Graveros Formation. At about 4000 feet (1219m) below surface the horizon is shown with a true green color.

Eighth horizon is a peak (600ms,1355ms), the upper sands within the Dakota Formation. These sands are identified at about 4150 feet (1265m) below surface and are shown with a copenhagen blue color on the section.

Ninth horizon is a trough (740ms,1640ms) and reflects change from sandstones to siltstones at top of the Fountain Formation. This Fountain Formation is at about 4750 feet (1448m) below the surface and is represented by a lavender color.

Tenth identified horizon is a peak (1280ms,2630ms) and reflects limestone at top of the Hardscrabble Formation.

The Hardscrabble Formation is located at 8450 feet (2575m) below the surface and is shown with a copper color.

Eleventh horizon reflects top of the Precambrian (1330ms,2700ms) at approximately 8850 feet (2697m) below surface. Precambrian is shown with an orange color. Basement reflector lacks continuity and was picked on sections with difficulty.

Since the Florence field's reservoir is from fractured Pierre Formation, this study will mainly analyze reflectors that bound the fractured reservoir interval (reflectors 2 and 3). Since most Pierre Formation oil production ranges between approximately 1900 feet (579m) to 3200 feet (975m) below the surface, the writer will assume that both the Pierre "a" (reflector 1) and Pierre "b" (reflector 2) labeled reflectors are above the Pierre Formation's fractured zone.

Since the next correlative events below the fractured or producing interval are the intervals near the top of the Niobrara Formation (reflector 3) and the horizon labeled Niobrara "a" (reflector 4) at depths of approximately 3100 to 3300 feet (945-1006m) below the surface, reflectors 1, 2, 3, and 4 will then define the fractured

interval. This defined fractured interval is bounded by P-wave events with two-way travel times between 75ms and 450ms or when converted to depth, the fractures are bounded between 500 to 3300 feet (152-1006m) below the surface.

P-wave sections show two faults between the Brehm-Anderson #1 Scheel and the Huffman #1 wells which intersect all formations and appear to crop out at the surface. These faults show roughly 15ms of relief at the Niobrara Formation's level, while the eastern most fault block exhibits nearly 450ms of relief on the Precambrian.

#### P- and SH-Wave Calculations

Using both P- and SH-wave information, three different analyses of the data are utilized to delineate fractures and estimate fracture extent of the Pierre Formation along the seismic lines. These three approaches include;

- 1) Calculation of velocities along correlated P- and SH-wave reflectors ( $V_s/V_p$ ).
- 2) Calculation of  $T_p/T_s$  within intervals bounded by correlated P- and SH-wave reflectors.
- 3) Comparison of P- and SH-wave amplitudes.

Study includes four horizons which bound both the Pierre and Niobrara Formation's producing intervals. The first and second horizons used are respectively the events labeled Pierre "a" and Pierre "b". Both horizons one and two upper bound the Pierre Formation's producing interval. Third horizon is the peak event associated with the top of the Niobrara Formation. Fourth horizon is the event labeled Niobrara "a". Horizon's three and four are the lower bounds to the Pierre Formation's producing interval. Bounding the Niobrara's producing interval are horizon three (above) and horizon four (below).

It is important to remember that fractures do not always necessitate petroleum production. The author will only identify potential fractured areas.

#### Velocities

Tathan and Stoffa (1976) and Gregory (1977) indicate that the ratio of S- to P-wave velocities, the  $V_s/V_p$  ( $V_s$ : S-wave interval velocity;  $V_p$ : P-wave interval velocity) ratio is a potential hydrocarbon indicator. This  $V_s/V_p$  ratio represents a dynamic measurement of

the medium's elastic properties, which no longer has density as a variant and is only a function of the bulk and shear modulus, represented as;

$$V_s/V_p = ((k+4\mu/3)/\mu)^{\frac{1}{2}}$$

When both P-wave and S-wave velocity information is available, the  $V_s/V_p$  ratio may indicate whether the formations are consolidated or unconsolidated, if gas or oil is present, and possibly fracture extent.

Gardner and Harris (1968) showed  $V_s/V_p$  ratios greater than 0.5 represented water saturated unconsolidated sands, while  $V_s/V_p$  ratios less than 0.5 indicated either a consolidated rock or gas in an unconsolidated sandstone.

Results obtained by King (1966), Tatham and Stoffa (1976) and Gregory (1977) show that fractures should cause an observable increase in the  $V_s/V_p$  ratio and with the addition of hydrocarbons to the fractures, the  $V_s/V_p$  ratio should even increase further.

Since  $k$  is about  $2.5\mu$  to  $3.0\mu$ , most reflections have an average  $V_s/V_p$  ratio in the earth's first thousands of feet near 0.5 (Cherry and Waters, 1968). However,  $V_s/V_p$  has been shown to be as small as .17 in the earth's

low velocity zone (Erickson, Miller and Waters, 1968). This indicates that static problems are expected to be much more evident with S-waves than P-waves, because of the smaller S-wave velocities in this low velocity zone.

Although  $V_s/V_p$  is a constant for most isotropic materials, Walsh (1965) shows experimentally that  $V_s/V_p$  can have considerable range of values in rocks, especially depending on the confining pressure. Walsh attributes the range of values to the presence of microscopic cracks and voids. According to Tatham and Stoffa (1976) existing cracks in rocks cause P-wave velocities to decrease more than S-wave velocities, resulting in an observable increase in  $V_s/V_p$ .

Since P-waves are sensitive to fluid saturants, the  $V_s/V_p$  ratio is also sensitive to the type of fluid present within a rock's pore space. King's (1966) results agree,  $V_s/V_p$  may be sensitive to the presence of liquid hydrocarbons.

Since cementation tends to increase with age and burial depth,  $V_s/V_p$  should also be related to the age and depth of the geological formations.

$V_s/V_p$  ratio's at depths greater than about 6000 feet (1,830m) are relatively uninfluenced by the type of pore fluid, but the observed  $V_s/V_p$  differences may still

have practical significance (Gregory, 1977). An increase in formation fluid pressure will cause a decrease in both P- and S-wave velocities, while an increase in porosity causes both the P- and S-wave velocities to decrease, with the P-wave velocity decreasing at over twice the S-wave velocity's rate (Gregory, 1976). Therefore,  $V_s/V_p$  should increase with decreasing porosity.

The lowest P-wave velocities are recorded for gas-saturated rocks under low pressure, while the highest S-wave velocities are recorded for gas-saturated rocks under high pressure (Gregory, 1977). Pressure should increase  $V_s/V_p$  slightly, but the effect is not always consistent or predictable over a wide range of porosities. The ratio  $V_s/V_p$  is affected by changes in the lithology and when  $V_s/V_p$  is calculated for an interval between two reflections,  $V_s/V_p$  may indicate lateral facies changes.

Gregory's (1976) results show for a porous rock, as the pore system is filled with oil at a pressure between 1000 to 5000 psi the P-wave velocity slightly increases, while the S-wave velocity slightly decreases. Therefore, a porous rock being filled with oil would reflect a decreasing  $V_s/V_p$  ratio.

For Poisson ratio values less than 0.4 there is a slight decrease in  $V_s/V_p$  with a slight increase in Poisson's ratio. However, when Poisson's ratio becomes larger than about 0.4 the  $V_s/V_p$  ratio rapidly decreases.

#### $V_s/V_p$ Calculations

P-wave preserved amplitude section exhibits an overall reduction in stacking velocities between shot points 75 and 240. This decrease in velocity provides a general outline of the Florence field's limits. A quality check of the data shows a velocity problem between shot points 150 and 181, within these limits the stacking velocities used were too slow. Since no production occurs between 150 and 181, the author believes this area is outside the field's limits.

SH-wave sections show a similar effect, a reduction in stacking velocities is evident between shot points 75 to 130 and another zone between shot points 155 to 250. Similar to P-wave velocity problem, a velocity problem occurs on the SH-wave sections between shot points 122 to 165. An attempt to correct this velocity problem was done by increasing this area's stacking velocities. Results presented on SH-wave sections show these velocity problems were still not totally corrected.

Even though the P-wave stacking velocities are not as definitive as the SH-wave stacking velocities, the P-wave results indicate stacking velocities decrease within the Florence field.

After correlating P- and SH-wave events, velocity information can be derived along defined velocity horizons, using a moveout relation. For a transversely isotropic medium, SH-wave stacking velocities are a function of only the horizontal velocity, while P-wave stacking velocities are a function of only the medium's vertical velocity in the zero-offset approximation. Reasonable estimates of horizontal SH-wave interval velocities can be obtained from the stacking velocities if the offset range is limited (Levin, 1978). Therefore, SH-wave moveout curves in transversely isotropic media will have exactly the same functional form as P-wave moveout curves in isotropic media.

Event times were picked from the P-wave (Plate 6) and SH-wave (Plate 8) preserved amplitude time sections. Low S/N ratios on the P- and SH-wave seismic sections, largely limits the computed velocity's accuracy.

Velocity analyses based on moveout curves were done in the usual way, although with considerably more care

and in considerably greater detail than for normal exploration work. To fully utilize the velocity information inherent in moveout curves and minimize irregularities, the velocity analysis was computed at every common depth point.

SH-wave velocities are plotted in Figures 17 (horizons 1 and 3) and 18 (horizons 2 and 4). SH-wave velocities are lower for an area between SP's (shot points) 155 and 250, which the author believes outlines the Florence field in the study area. An anomalous large velocity zone occurs between SP's 130 and 155. This large velocity zone could be a lithologic change, but is more likely a processing problem. Between SP's 75 and 130 the SH-wave velocity again decreases, potential limits of a separate field, however the northeastern area's velocity is 750 ft/s faster than the western area's velocity.

P-wave velocities are shown in Figures 19 (horizons 1 and 3) and 20 (horizons 2 and 4). Lithologic and/or processing problems visible on the SH-wave velocities do not influence the P-wave velocities. Both Figures 19 and 20 show areas southwest of SP 160 where the P-wave stacking velocities decrease.

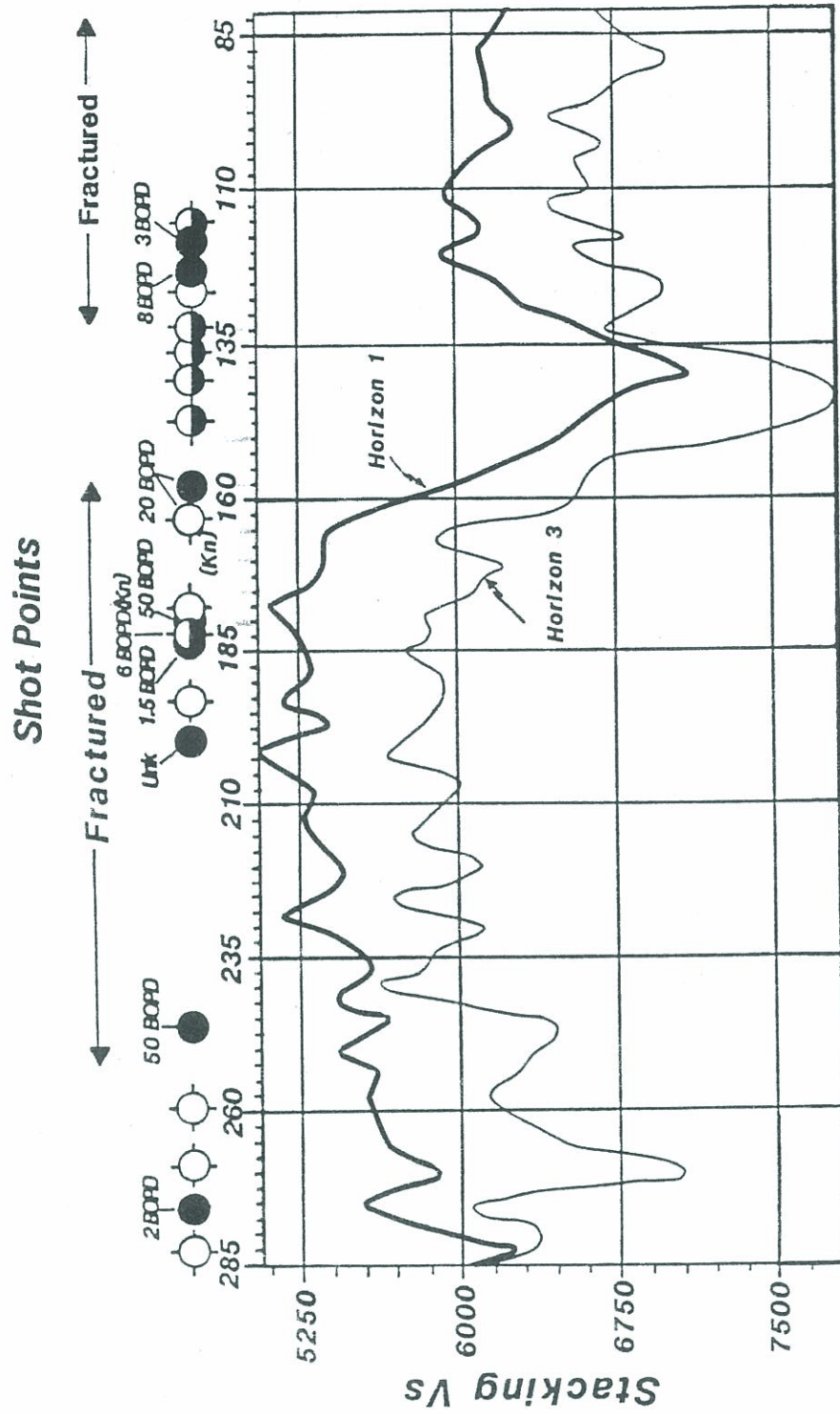


Figure 17: SH-wave stacking velocities for horizons 1 and 3 with production information for both Pierre and Niobrara Formations.

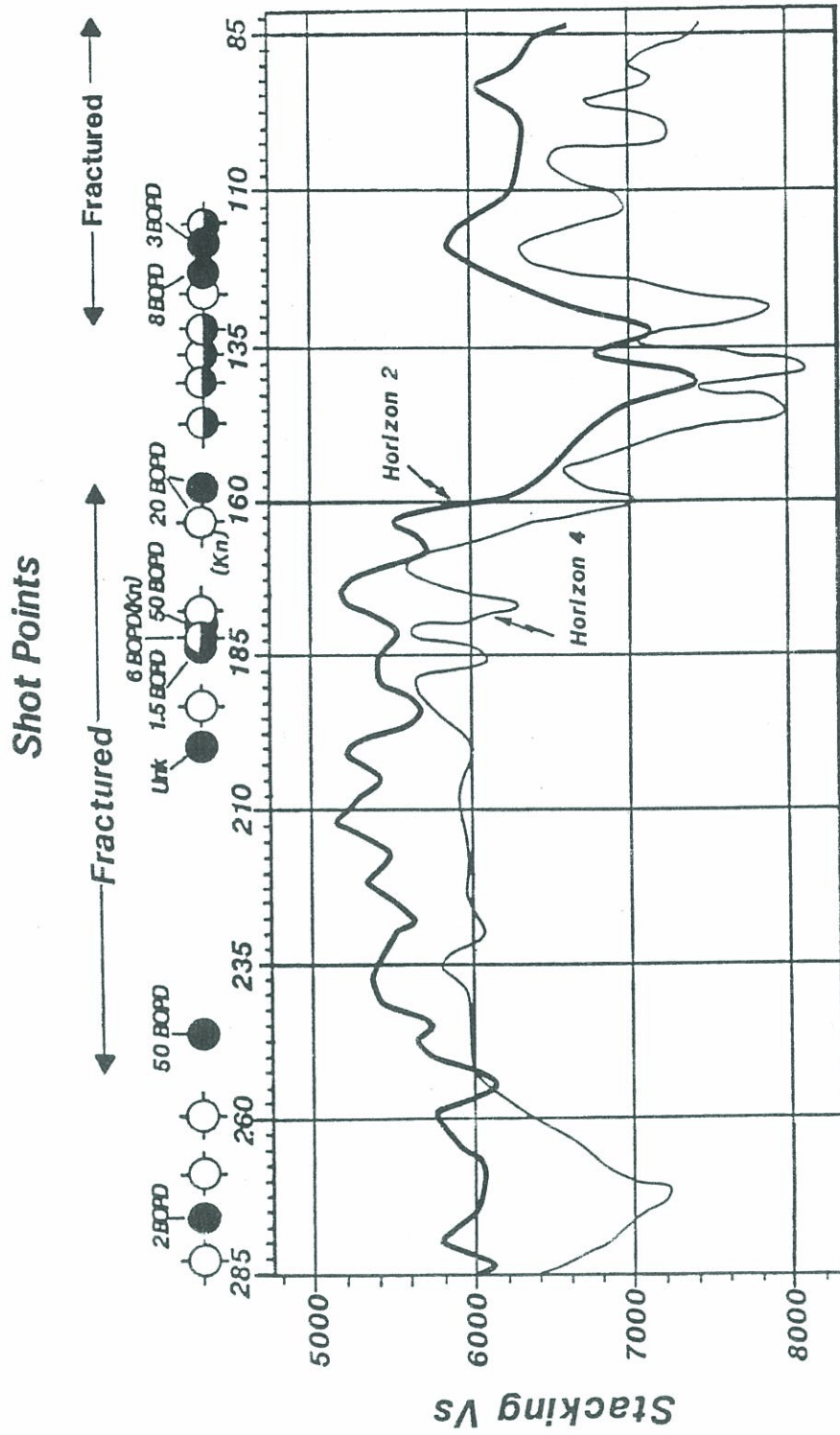


Figure 18: SH-wave stacking velocities for horizons 2 and 4 with production information for both Pierre and Niobrara Formations.

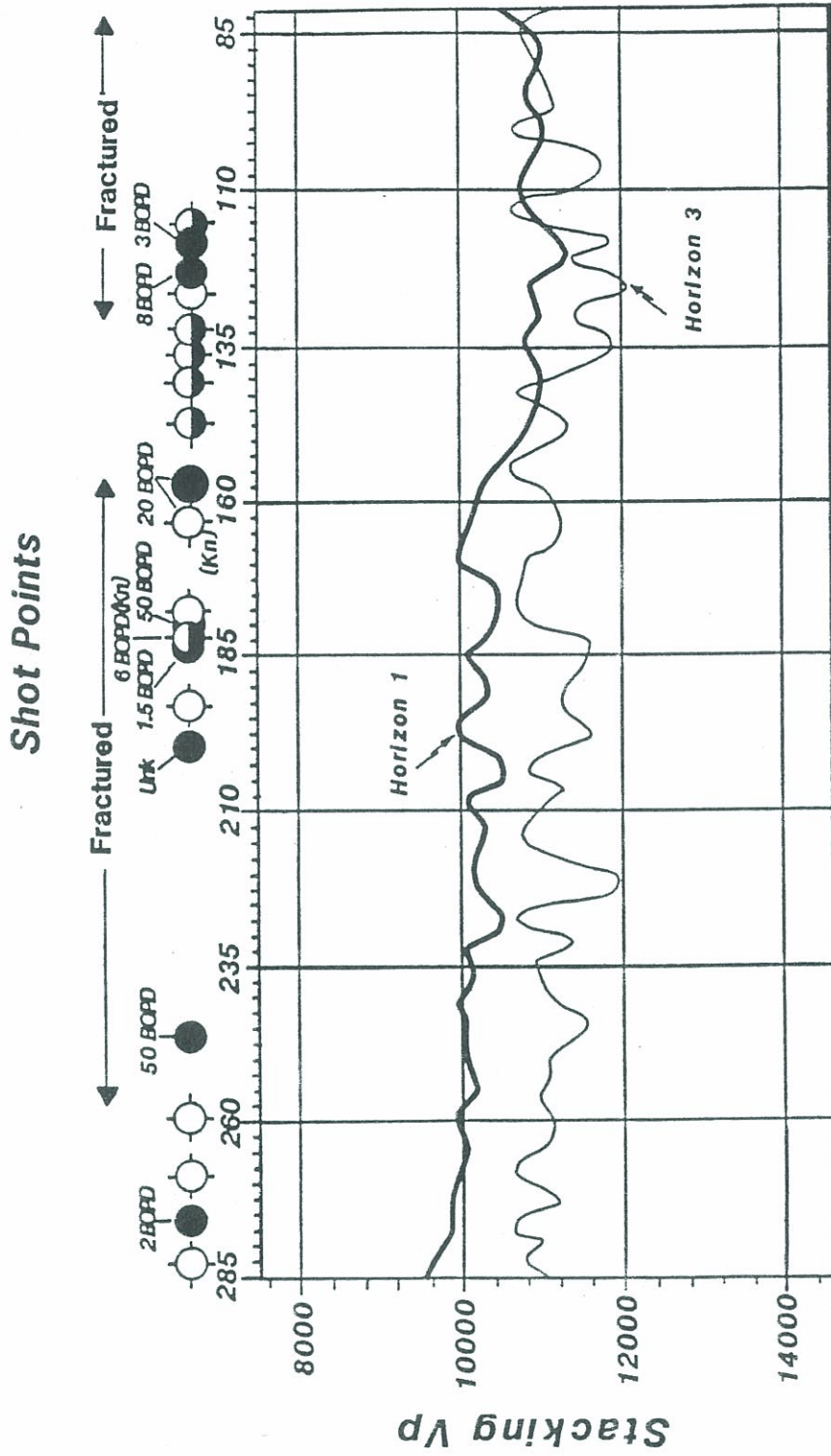


Figure 19: P-wave stacking velocities for horizons 1 and 3 with production information for both Pierre and Niobrara Formations.

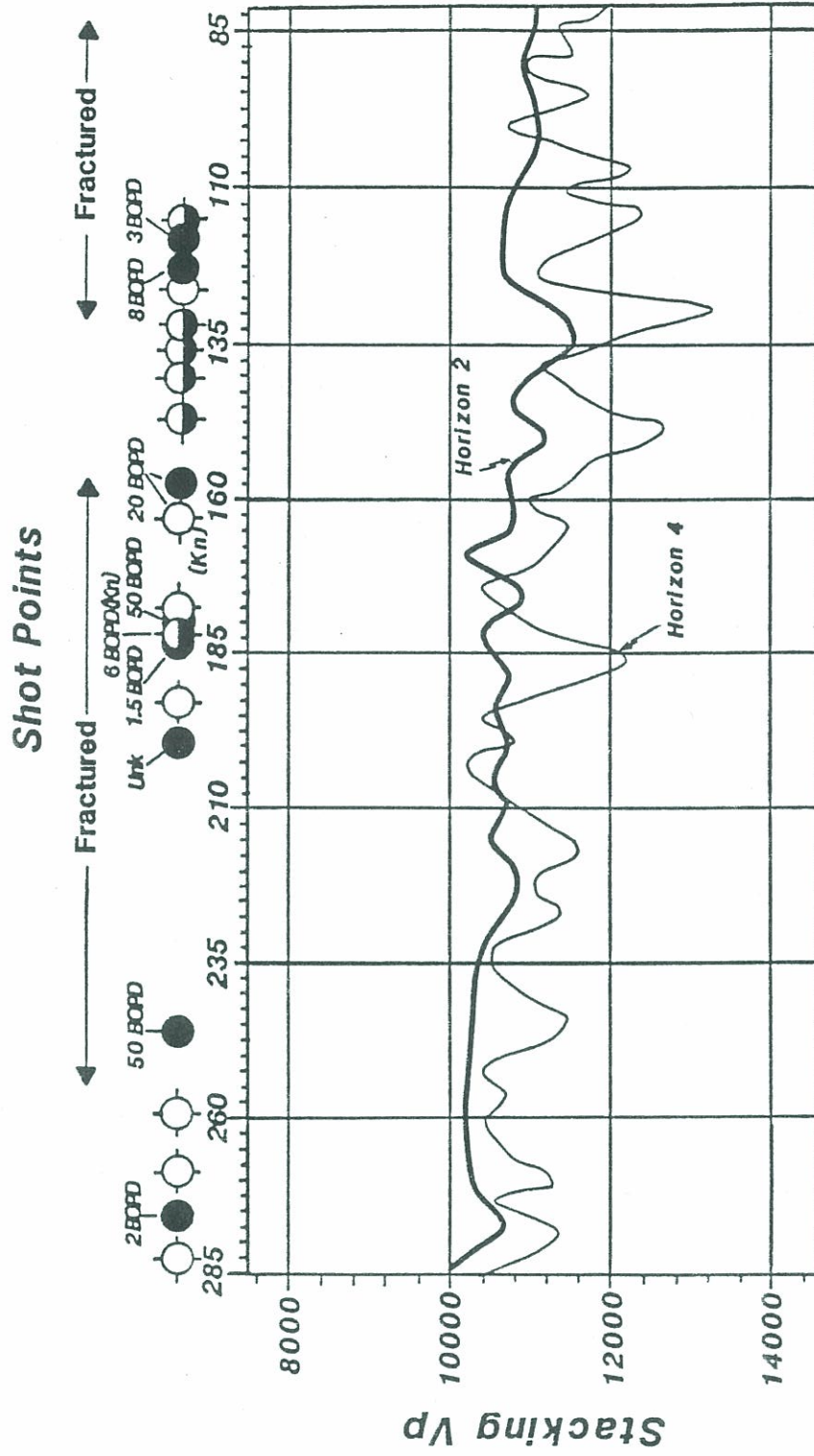


Figure 20: P-wave stacking velocities for horizon 2 and 4 with production information for the Pierre and Niobrara Formations.

Dix's equation was used to calculate interval velocities from the moveout velocities. Given Dix's approximations, each interval velocity is independent of all media in the section except those in the given interval. Therefore, effects of anisotropy in a given interval will be present only in the interval velocities for that interval.

Interval velocities for the SH-waves decrease in two zones along the study area, between SP's 160 to 250 and 110 to 125 (Figure 21). SH-wave interval velocities are variable, causing numerous fluctuations which hinder a detailed study using interval velocities. Unlike SH-wave interval velocities, P-wave interval velocities exhibit no apparent fractured interval results (Figure 22).

For the  $V_s/V_p$  ratio to be a good measure of fractures and/or fluid content, P- and S-wave correlative seismic events must bound the prospective reservoir interval. Since horizons one and two are above the Pierre production interval and horizon three and four are below, the prospective reservoir interval is bound. Results for the Pierre production are conclusive for identifying fractured areas with  $V_s/V_p$  (Figure 23). Because of the

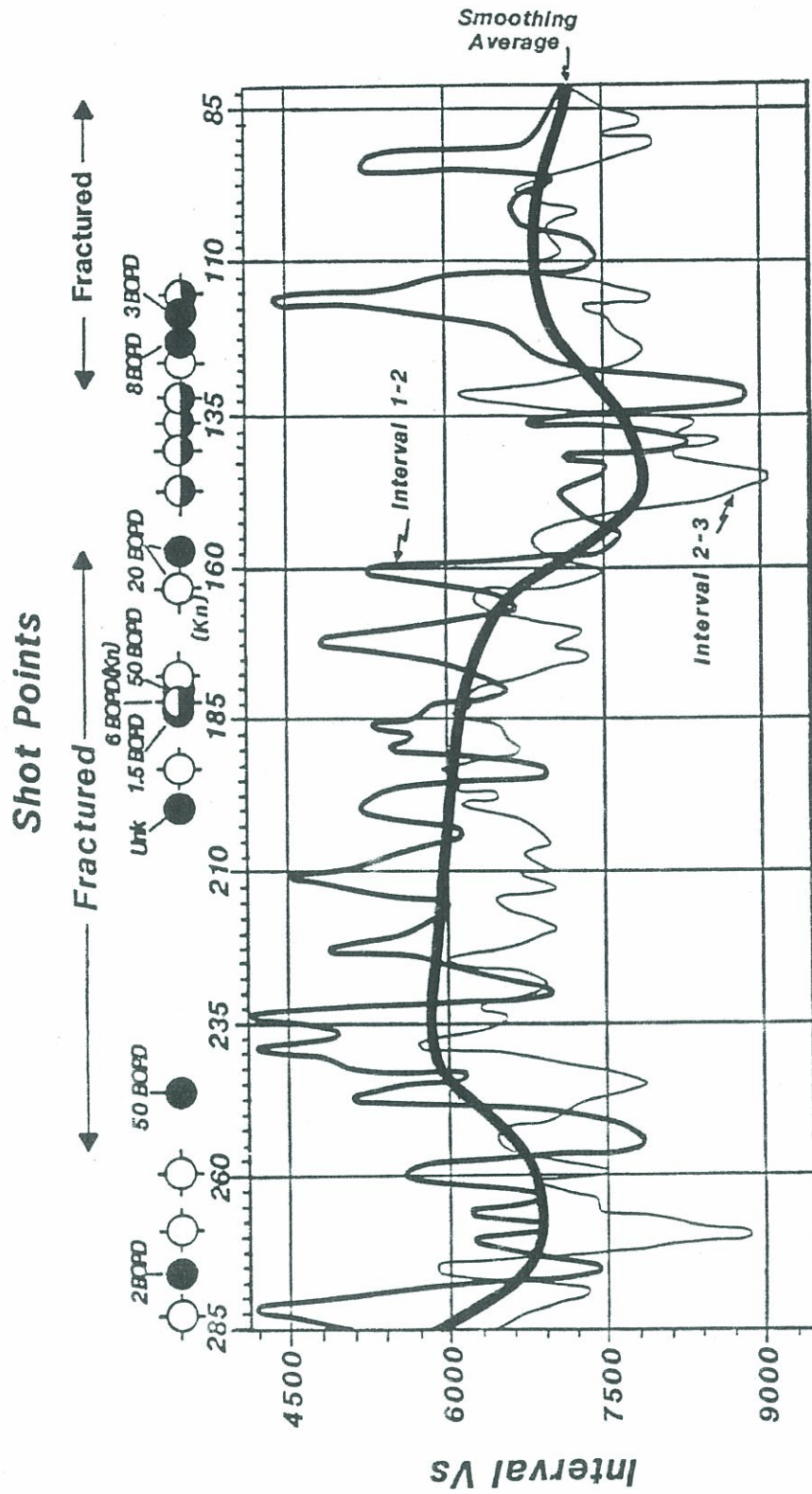


Figure 21: SH-wave interval velocities between horizons 1 to 2 and horizons 2 to 3, with production information for both Pierre and Niobrara Formations.

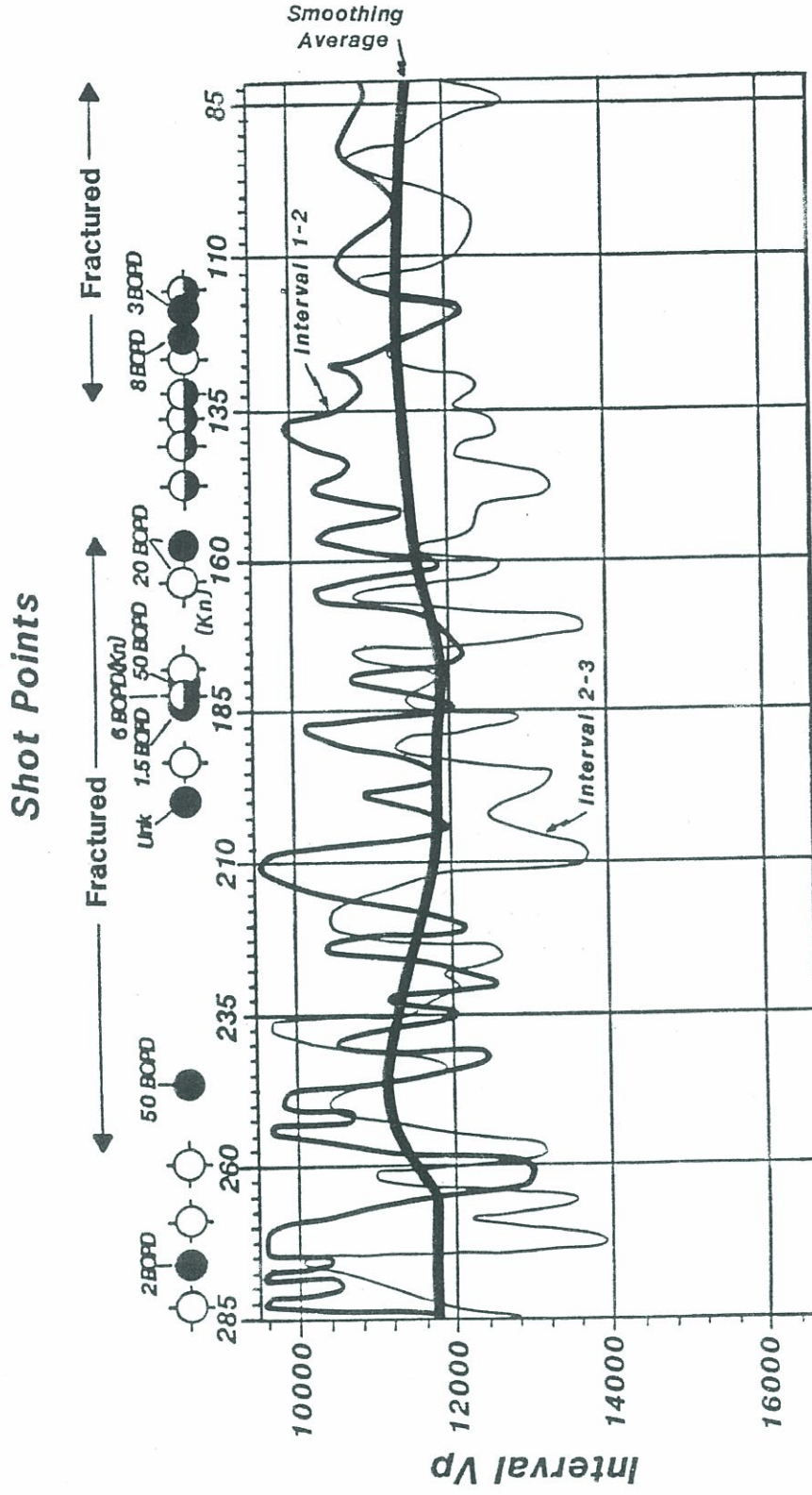


Figure 22: P-wave Interval velocities between horizons 1 to 2 and 2 to 3, with production information for both Pierre and Niobrara Formations.

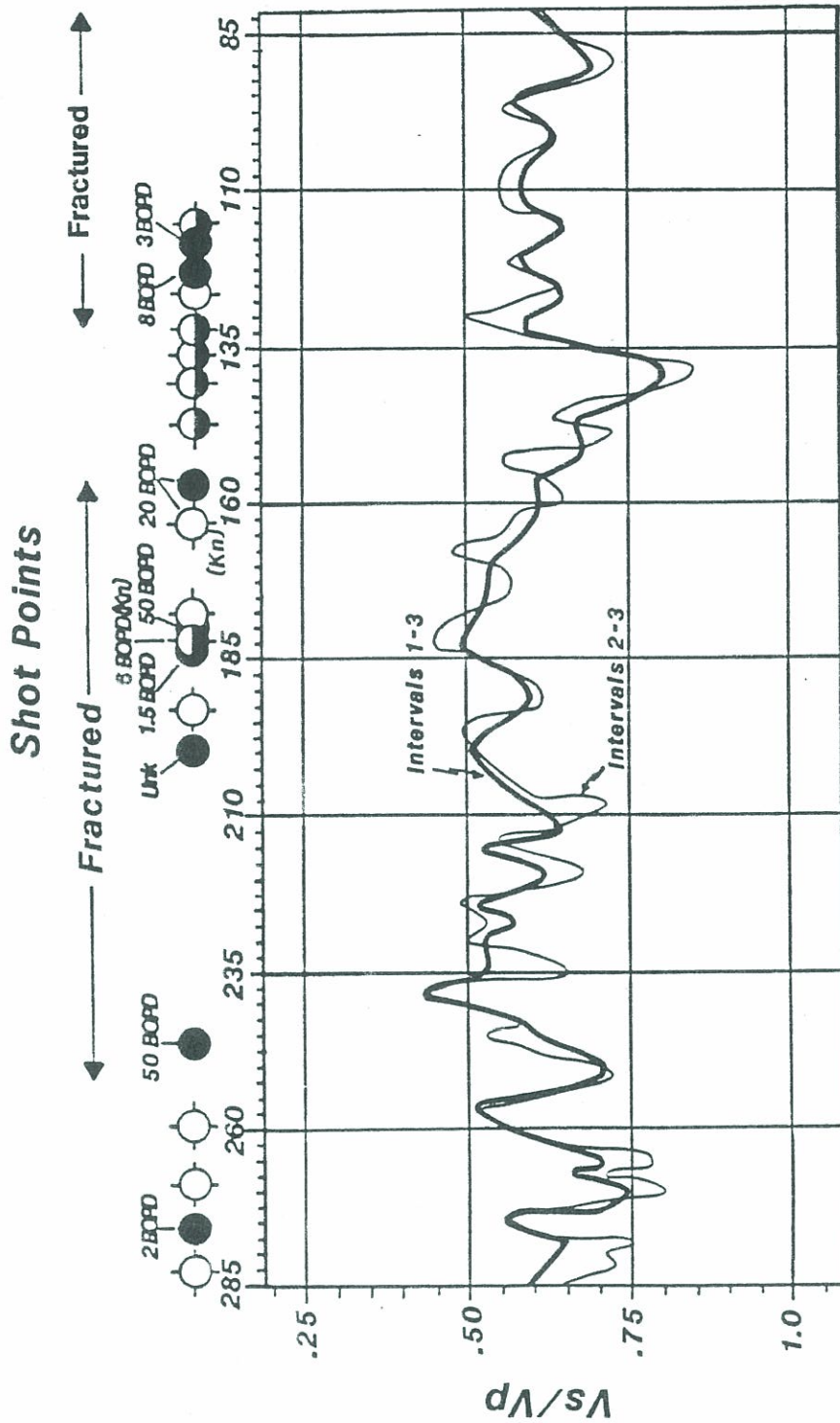


Figure 23:  $V_s/V_p$  ratio for intervals between horizons 1 to 3 and 2 to 3, with production information for both Pierre and Niobrara Formations.

SH-wave velocities Figure 23 shows two zones of lower  $V_s/V_p$  ratios, between SP's 161 to 245 and 90 to 133.

The difference between the  $V_s/V_p$  ratios for horizon interval 2-3 and 2-4 (Figure 24) shows Niobrara fractured areas cause the  $V_s/V_p$  ratio to increase. Niobrara Formation results are different than the Pierre Formation, since the SH-wave stacking velocities actually increase through the Niobrara Formation.

Producing intervals of the Pierre Formation appear to affect the SH-wave velocity to a stronger degree than the P-wave velocity. Lower SH-wave stacking velocities and interval velocities appear to coincide with producing (fractured) intervals, intervals of greatest fracturing.

#### Travel Times

Consideration of the reflection travel times between both the P- and S-wave sections yields a travel time ratio  $T_p/T_s$  ( $T_p$ : P-wave travel time;  $T_s$ : S-wave travel time).  $T_p/T_s$  calculations are based on the correlation of P- and S- common mid-point stack reflections and can be directly related to  $V_s/V_p$  ratios. Since the travel times cover the same depth interval,  $T_s = 2 \cdot \text{depth}/V_s$ , and  $T_p = 2 \cdot \text{depth}/V_p$ , which it then follows that  $T_p/T_s = V_s/V_p$ .

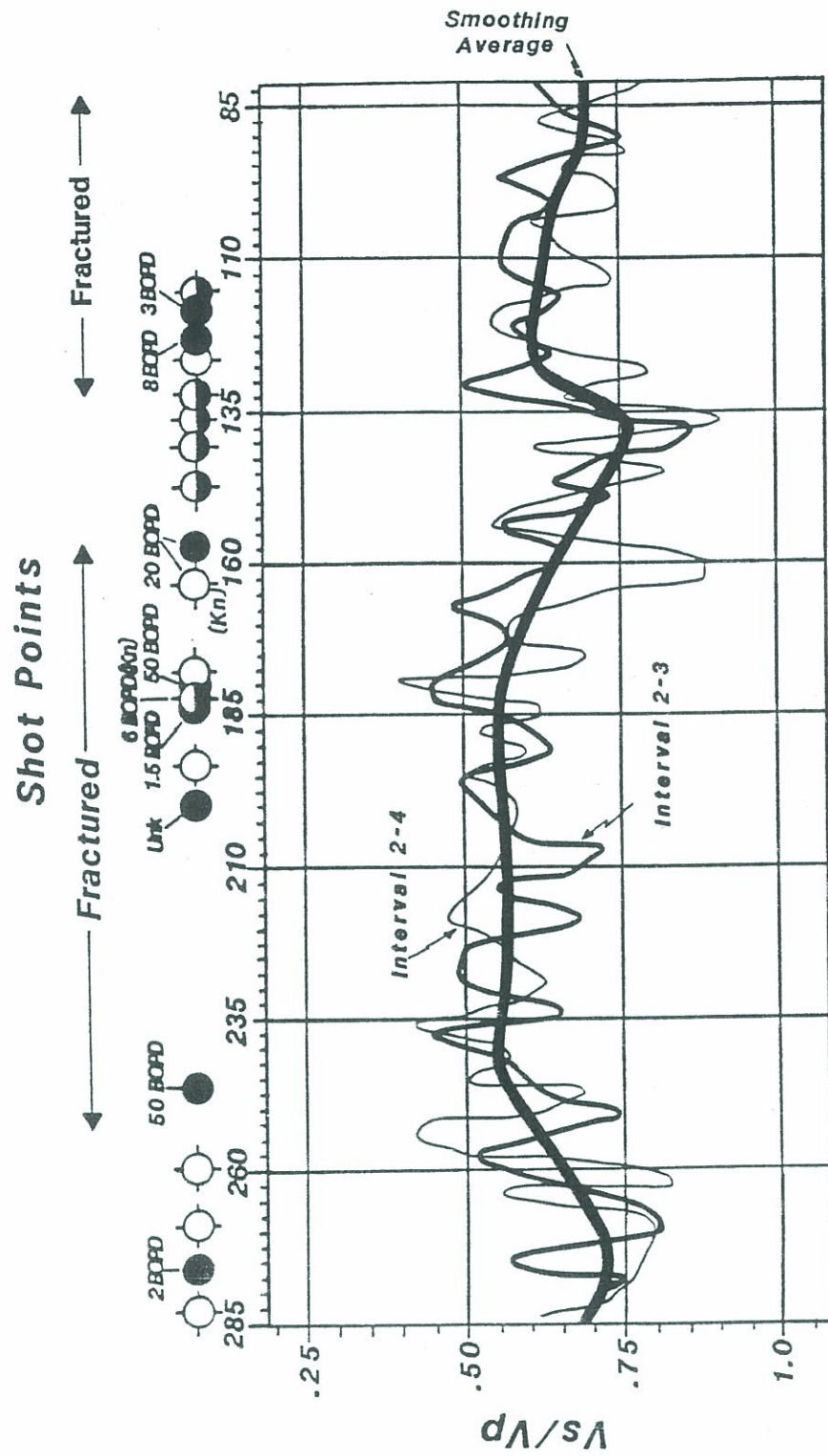


Figure 24: Vs/Vp ratio for Intervals between horizons 2 to 3 and 2 to 4.

Therefore, lateral variations in  $V_s/V_p$  within an interval, must be the result of changes in the rock properties and not an interval thickening or thinning. An independent analysis of the S-wave data or the P-wave data would not allow a discrimination between thickness changes and elastic property variations within a given interval.

Calculated  $V_s/V_p$  ratios are generally higher than  $T_p/T_s$  ratios, because  $V_s/V_p$  ratios correspond to root mean square velocities determined through velocity analyses which reflect the horizontal components of the raypaths (direction parallel to bedding), while  $T_p/T_s$  ratios correspond to vertical raypaths (direction normal to bedding). Therefore an increase in anisotropy (or formation gas) will cause a larger discrepancy between  $V_s/V_p$  and  $T_p/T_s$  ratios (Garotta, 1977). Since shallower beds have a larger degree of anisotropy, larger differences should be observed between  $T_p/T_s$  and  $V_s/V_p$  ratio values at shallower depths.

#### $T_p/T_s$ Calculations

Correlation was not simple, since markers are not continuous across the sections in the Pierre Formation. Removal of the regional effect is important before the

$T_p/T_s$  ratio has significant meaning for fracture detection. Removal of the  $T_p/T_s$  ratio's regional effect is accomplished by considering P- and SH-wave reflectors above and below a zone of interest and comparing the travel times ( $T_p/T_s$ ) ratio between these reflectors. Fractures should increase travel times through the reservoir's interval and by isochroning this fractured interval, increased interval travel times may coincide with fractured zones.

During the velocity analyses based on moveout curves, travel times were extracted for the same four measured horizons. Figure 25 shows two-way travel times increase west of SP 163 and again between SP's 93 to 127. Two-way travel times west of SP 163 are roughly 10ms longer than the times on the northeast side, this might indicate degree of fracturing. A comparison of Figures 25 and 26 indicates an area between SP's 138 to 150 has a slower two-way travel time between horizons 1 to 3 than horizons 2 to 4. This interval travel time increase between SP's 138 to 150 for horizons 2 to 4 may be a result of Niobrara fracturing on the SH-wave sections.

As with P-wave velocities, P-wave interval travel time data is less definitive than the corresponding SH-wave data. An increase in P-wave interval travel times is

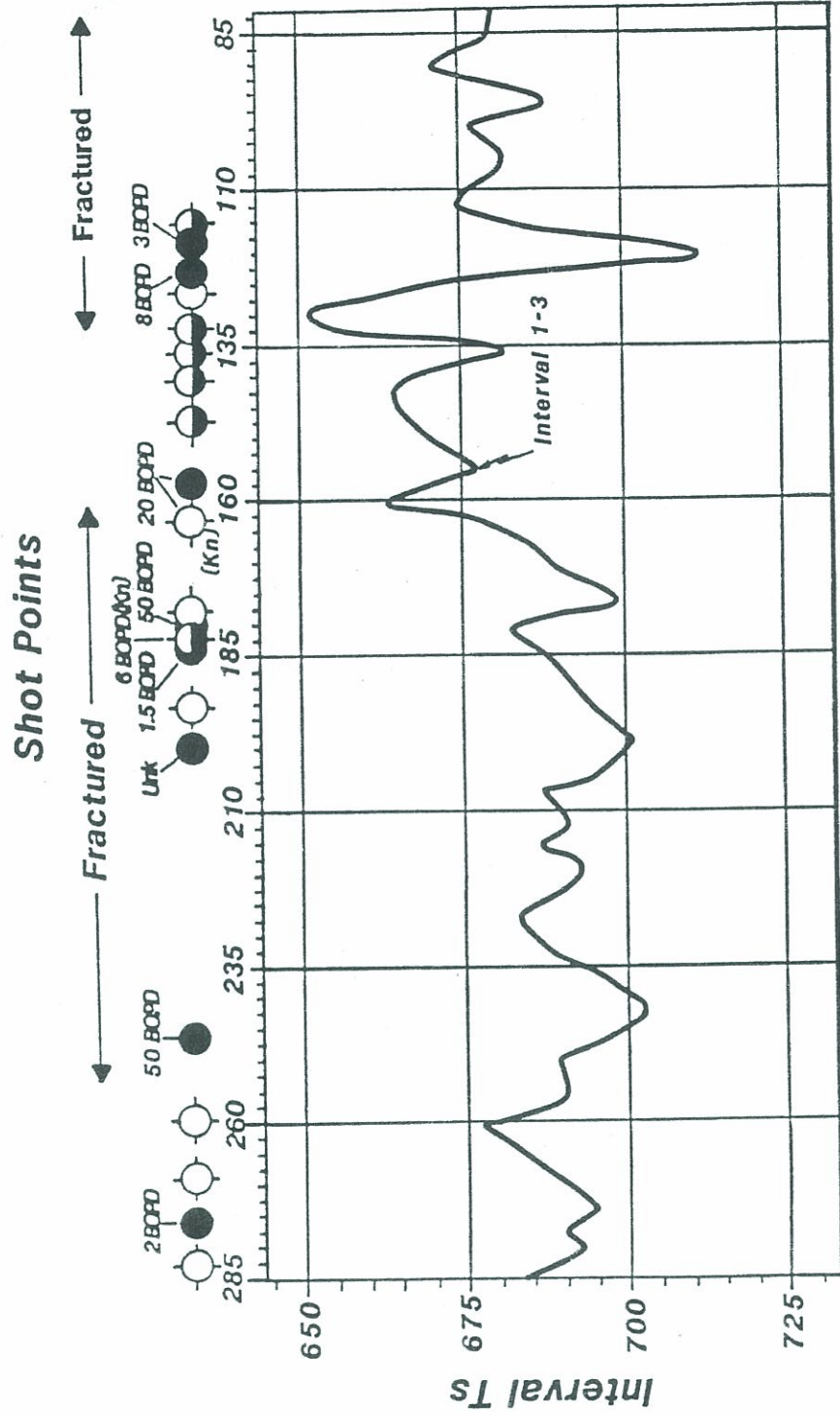


Figure 25: SH-wave two-way interval travel times between horizons 1 and 3, with production information for both Pierre and Niobrara Formations.

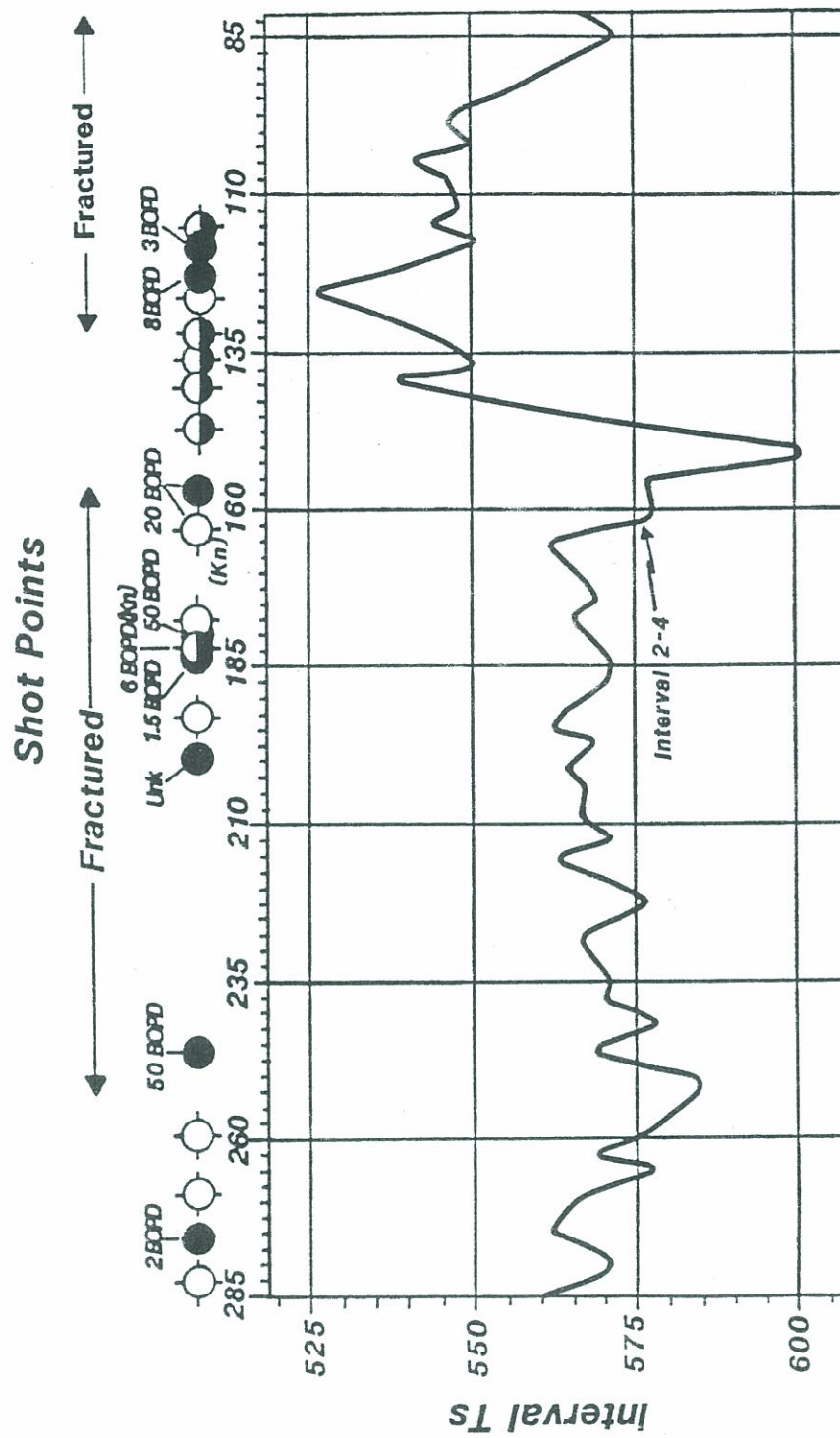


Figure 26: SH-wave Interval two-way travel times between horizons 2 and 4, with production information for both Pierre and Niobrara Formations.

apparent southwest of SP 168, with another increase visible northeast of SP 113 (Figure 27). Between SP's 113 to 168 there is an area of low interval travel times, which is thought to coincide with a zone of reduced fracturing within the Pierre Formation.

Interval above the Pierre and Niobrara Formation production is absent of fracturing effects on  $T_p/T_s$  ratios (Figure 28). Area between SP's 115 to 153 appears to be a transition area between two separated fractured bodies. A complication in processing probably caused the complex results. Pierre Formation fracturing causes  $T_p/T_s$  values to increase on Figure 29. Niobrara fractured zones show a decrease in  $T_p/T_s$  values for interval horizon 2 to 3 and an increase for interval horizon 2 to 4 (Figure 29). Although anisotropy reduces overall resolution of P- and SH-wave travel time differences,  $T_p/T_s$  ratios enhance travel time method for indicating fractured intervals.

#### Amplitudes

Reflection coefficients for P- or S-waves are not the same, therefore additional information can be obtained from the S-wave survey. A good example is the reflection coefficient between shales and sandstones, which can cause

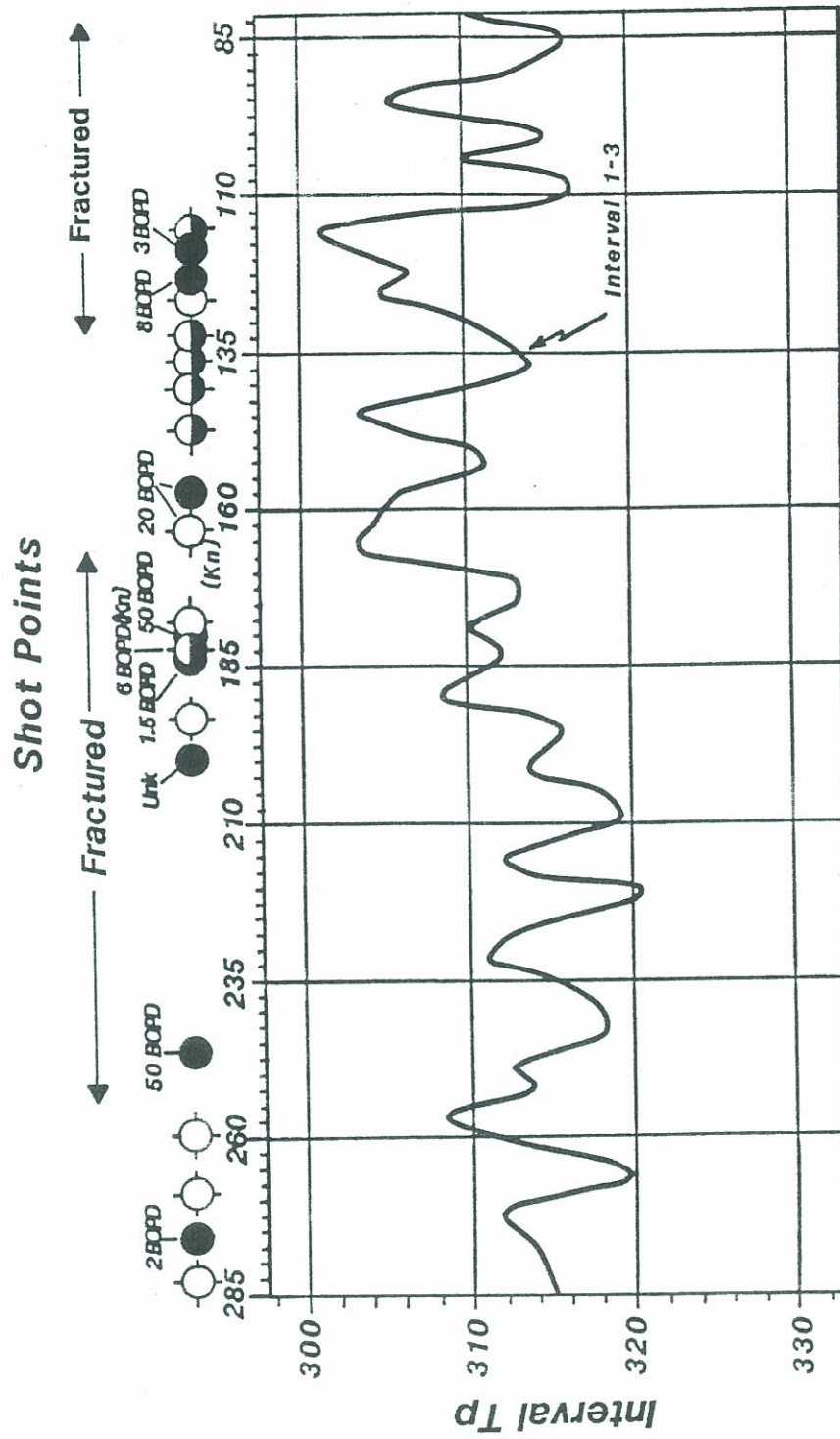


Figure 27: P-wave Interval two-way travel times measured between horizons 1 and 3, with production information for both Pierre and Niobrara Formations.

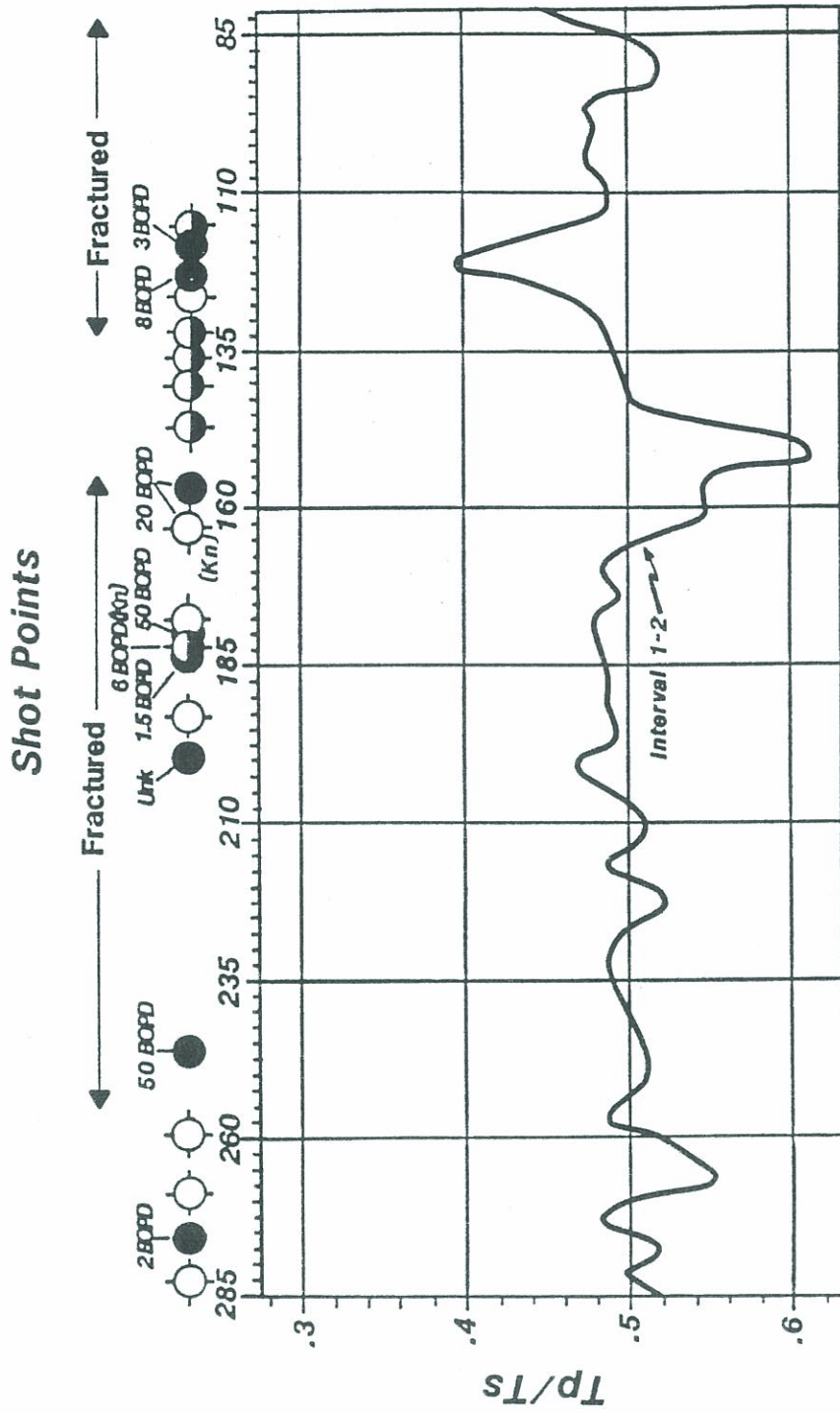


Figure 28:  $T_p/T_s$  ratios for interval times between horizons 1 and 2, with production information for both Pierre and Niobrara Formations.

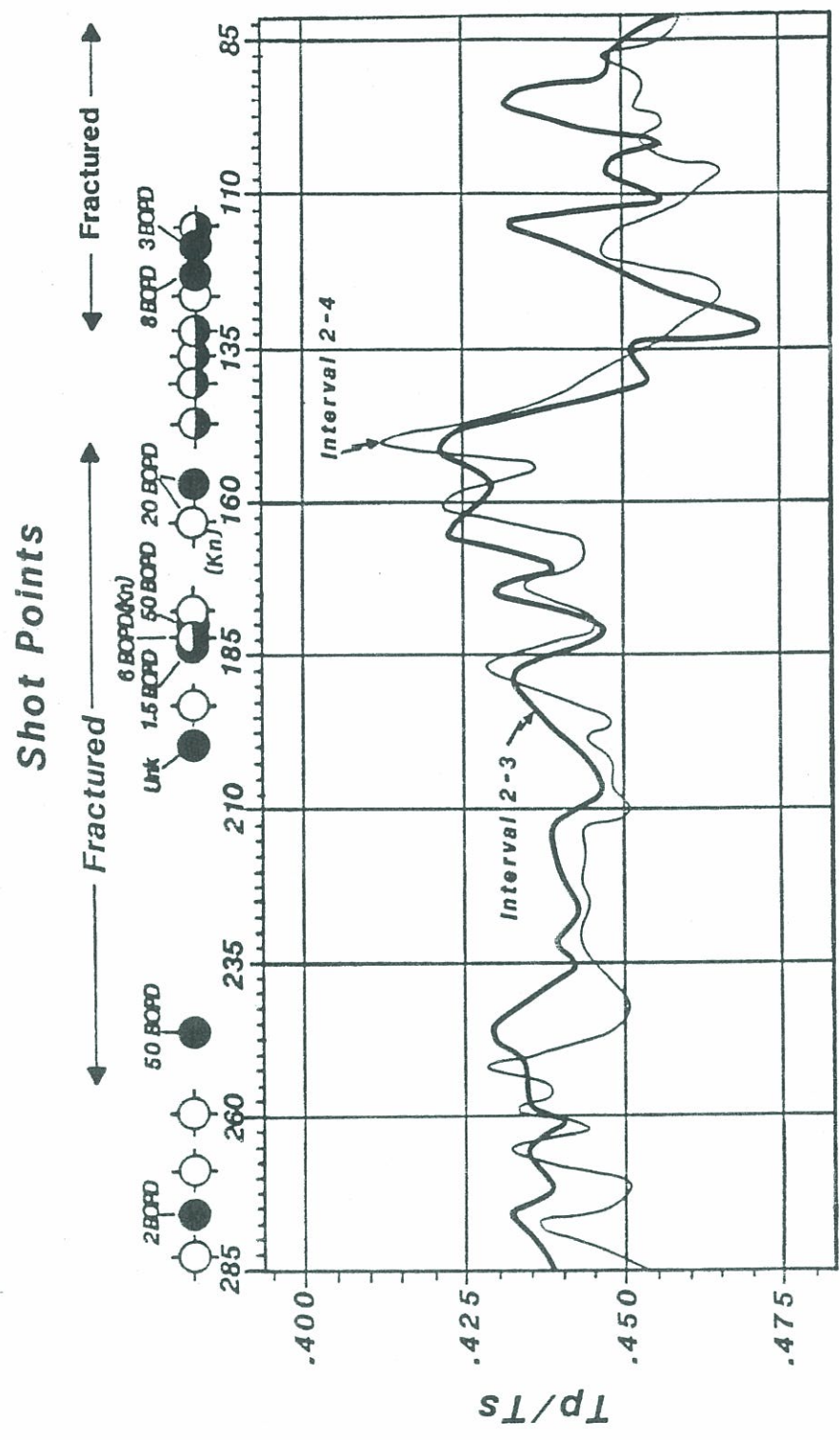


Figure 29:  $T_p/T_s$  ratios for Interval times between horizons 2 to 3 and 2 to 4, with production information for both Pierre and Niobrara Formations.

the reflection coefficient for SH-waves to be higher than those for P-waves. While a P-wave 'bright spot' can be caused by gas, the S-wave 'bright spot' is largely related to the matrix (Omnes, 1976).

Theory predicts that fractured rock amplitudes caused by reflection coefficients should cause a stronger effect on P-wave amplitudes, since for given conditions, fractures should have a stronger effect on P-wave velocities. This may not be the case, since SH-wave velocities were more strongly effected than the corresponding P-wave velocities were by fractured intervals.

SH-wave amplitudes are reported to be more dependent on confining pressure and nature of the saturating fluid. At constant pressure, saturation with hydrocarbons should cause a larger amplitude reduction of SH-waves than P-wave amplitudes under the same conditions. Absorption of energy caused by fractures in a fluid saturated reservoir should cause a stronger effect on SH-wave amplitudes (O'Connell and Budiansky, 1974).

If amplitudes are caused by reflection coefficients alone, then a  $A_s/A_p$  ( $A_s$ : S-wave amplitude;  $A_p$ : P-wave amplitude) ratio would produce an increasingly smaller value for a stronger degree of fractures within the

Pierre Formation. Using P- and SH-wave velocities as an indicator, the author believes the amplitudes will also differ from previous published works. A stronger absorption factor however, should cause the  $A_s/A_p$  ratio to become increasingly smaller. Absorption effects would therefore be indistinguishable on a  $A_s/A_p$  plot and would only become visible as a horizontal dimming effect on a SH-wave section.

Although P-wave 'bright spots' can result from gas reservoirs (Dilay, 1982), apparent bright spots can also result from interference patterns, thin beds, low-velocity rocks, abrupt stratigraphic changes (fractures), and time flat horizons (Ensley, 1984).

SH-wave amplitudes should form a normalizing agent for P-wave amplitudes. Similar P- and SH-wave responses probably are indicative of lithologic interfaces, while differences in P- and SH-wave responses could indicate an addition or change in fluid saturations. On seismic section's included in this study, a 'bright spot' could exhibit the following characteristics for a fractured interval:

Amplitude difference - a change in the reflection coefficient's polarity along the top or bottom of an interval, as long as the nature of the units above and below the fractured interval do not change.

Sag - a reflection time sag, caused by an increase in the travel time through an interval. Because of anisotropy effects, time sag characteristic's interpretative information is minimal.

Shadow zone - a horizon below an interval in which the reflection amplitudes decrease because of lower energy transmission through the interval.

#### Modeling

In order to understand the P- and SH-wave seismic response to the fractured shale reservoir, a general seismic model of the reservoir was made (Figure 30). This model consists of several flat layered horizons with a gentle dip down to the left.

Theory and experimental results show that fractures cause an observable increase in the  $V_s/V_p$  ratio and because the  $V_s/V_p$  ratio is a function of Poisson's ratio,

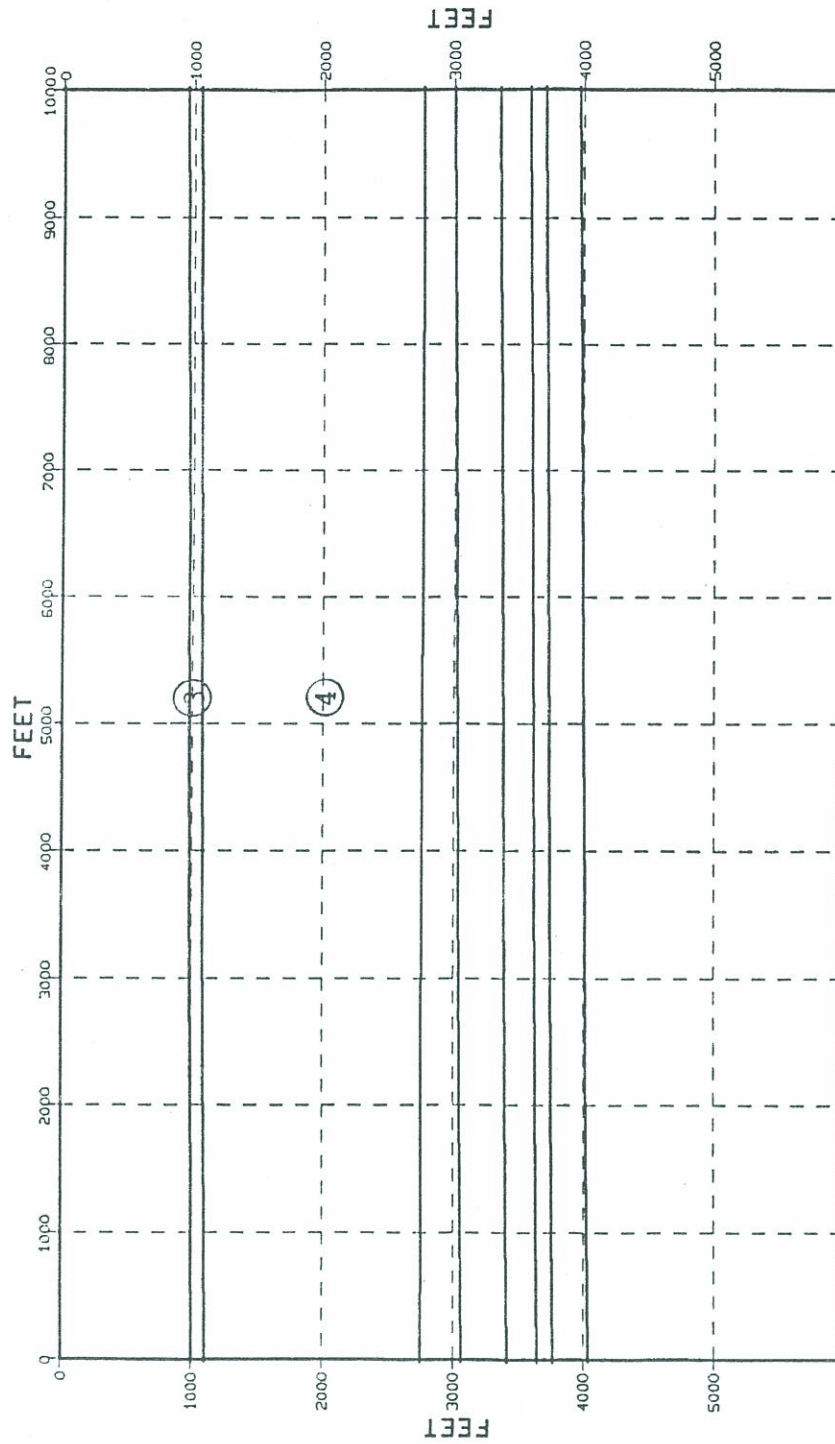


Figure 30: General seismic model for varying Poission's ratio, with 3 being horizon interval three.

$$\frac{V_p}{V_s} = \left( \frac{2(1-\sigma)}{1-2\sigma} \right)^{\frac{1}{2}}$$

where  $\sigma$  is Poisson's ratio, then a change in Poisson's ratio for a given reservoir interval should produce noticeable effects on the generated synthetic traces.

Although shale does not fit theoretical models, since shale is platy and not granular (Hilterman, 1986), the fractured zone's sub-matrix is abundant with sand or possibly the fractured zone could be a clayey sand interval, so theory and experimental results may still hold some significance.

The synthetic trace was generated using a two-dimensional non-zero-offset ray-tracing program, which used Bortfeld's approximation in calculating the reflection and transmission coefficients for the P-wave amplitude synthetic trace. Bortfeld's approximation was used because of the equation's computational simplicity and Hilterman (1986) demonstrates Bortfeld's equations are a good approximation up to the critical angle.

The program generating only P-wave amplitude synthetic traces is a severe modeling limitation. Since the modeling program was not set-up to account for lateral variations

in Poisson's ratio, which is the problem this writer would like to investigate, the general model was iterated several times with different Poisson ratio values for two separate cases.

The initial study involved horizon 3, a relatively thin interval. Lateral Poisson values were varied from almost zero to 0.5, where at  $\sigma = 0.5$  the theoretical S-wave effects are essentially negligible. Synthetic seismograms are displayed for several different Poisson ratios for horizon 3, section includes losses due to transmission effects and reflection coefficients (Figure 31).

Decreasing values of Poisson's ratio cause the P-wave reflector's amplitude to dim-out. However, when Poisson's ratio is between zero and 0.1, the P-wave reflector's amplitude again increases, enough so a P-wave reflector is visible.

Next, the thicker interval horizon 4 is investigated (Figure 32), using the same procedure as with horizon 3. While Poisson's ratio decreases, this reflector's amplitude also decreases, as did the previous thinner interval, but the thicker horizon's amplitude never entirely dim's out, with the same chosen Poisson values. Thickness differences cause these Poisson model amplitude variations,

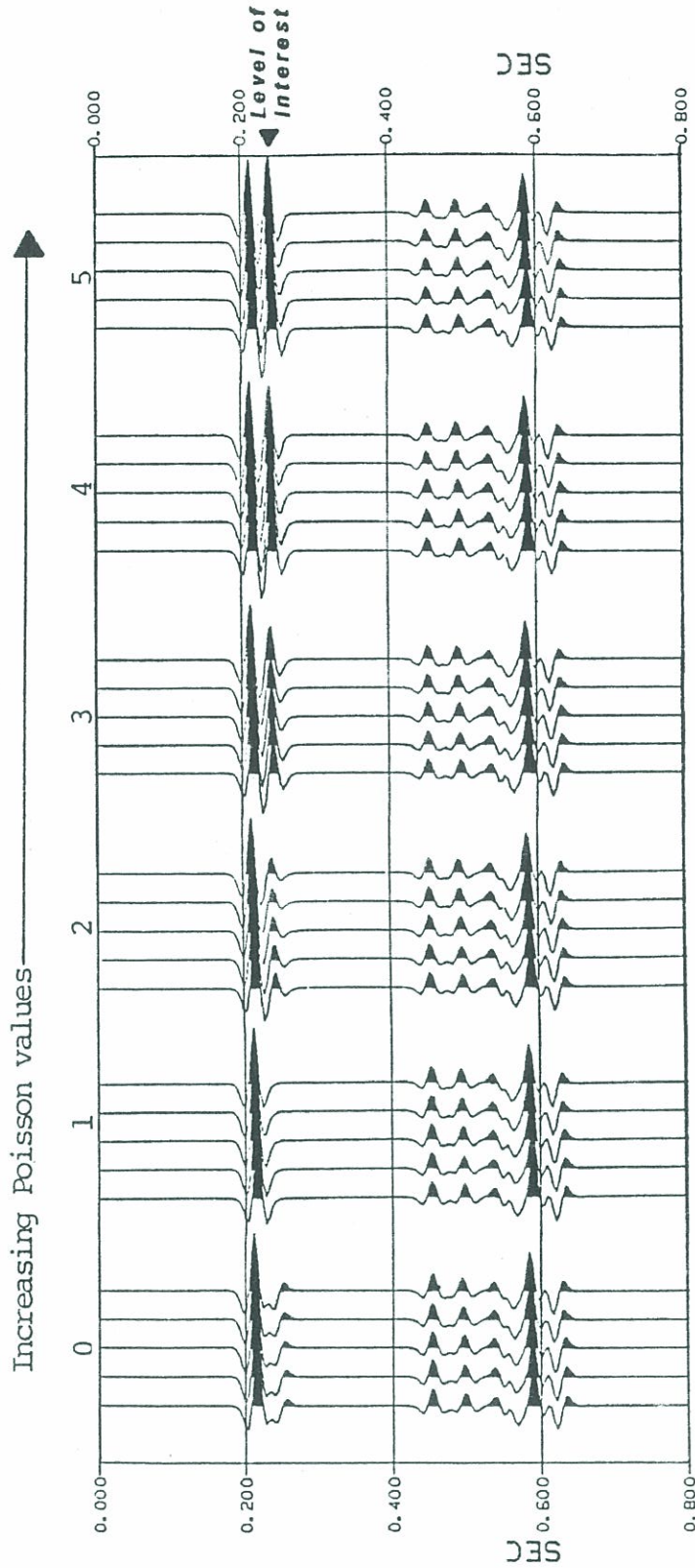


Figure 31: Lateral varying Polsson's ratio for interval horizon 3, accounting for losses due to transmission effects and reflection coefficients.

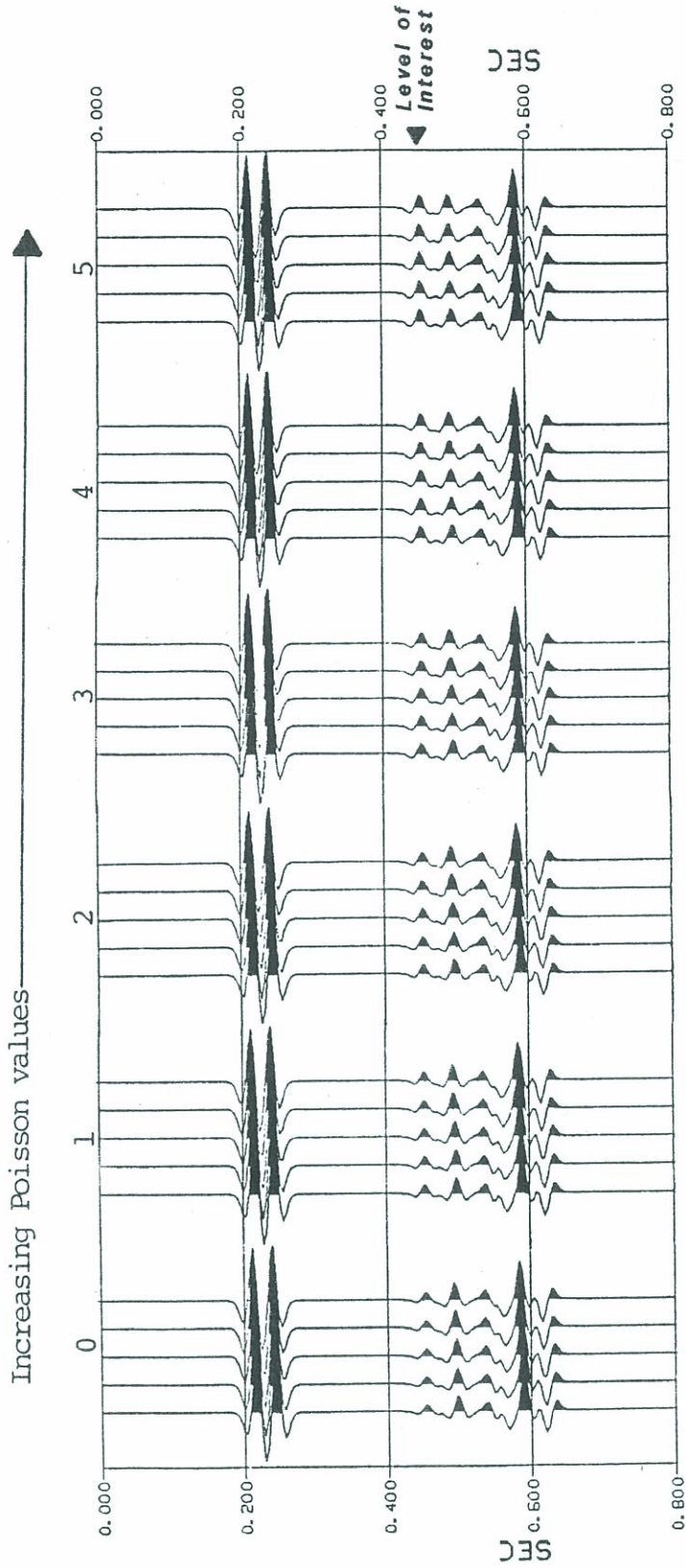


Figure 32: Lateral varying Poisson's ratio for interval horizon 4, accounting for losses due to transmission effects and reflection coefficients.

with the thicker model exhibiting a smaller amplitude reduction.

Theory shows if Poisson's ratio increases, the corresponding  $V_s/V_p$  ratio must decrease. Modeling shows when Poisson's ratio increases the P-wave amplitude also increases. Therefore, the author expects for a decreasing  $V_s/V_p$  ratio, which previously was shown to correspond to fractured intervals, the P-wave amplitude should increase.

Remembering that this program only generates P-wave amplitude information, this writer cannot form any conclusions for S-wave amplitudes from modeling. Since the SH-wave amplitudes shown on the section are larger than the writer expects for a slight increase in S-wave velocity, the writer believes that Poisson's ratio influences SH-wave amplitudes more than P-wave amplitudes.

#### $A_s/A_p$ Calculations

Visual interpretation of the preserved P- and SH-wave amplitude sections does produce a tie between production and amplitude variations along the Niobrara Formation (horizon 3). Amplitudes on the SH-wave preserved amplitude section increase between SP's 70

to 125 and SP's 165 to 280. Unlike SH-wave amplitudes, P-wave preserved amplitude sections appear to decrease from SP's 110 to 140 and SP's 160 to the southwest end of line.

When SH-wave amplitudes for horizons two and three are plotted (Figure 33), both curves show SH-wave amplitudes increase with areas tied to Pierre Formation production. Figure 34 shows SH-wave amplitudes appear to decrease with Niobrara Formation Production. The difference between horizon 4 and horizon 1 curves, exhibit when the horizon 4 curve's amplitude is less than the amplitude for horizon 1, Niobrara Formation production is apparent (Figure 34). SH-wave amplitudes for horizons 2 and 4 show a large increase in amplitudes for horizon 4, when compared to horizon 2's amplitudes, where fracturing occurs in areas of either the Niobrara or Pierre Formation (Figure 35). Even though, P-wave amplitudes on Figure 36 substantiate the fracturing within the Pierre Formation, P-wave amplitude results are less definitive than the corresponding SH-wave amplitudes. An increase in P-wave amplitudes on horizon 3 are tied to fractured zones within the Pierre Formation, which is not evident when looking directly at the sections.

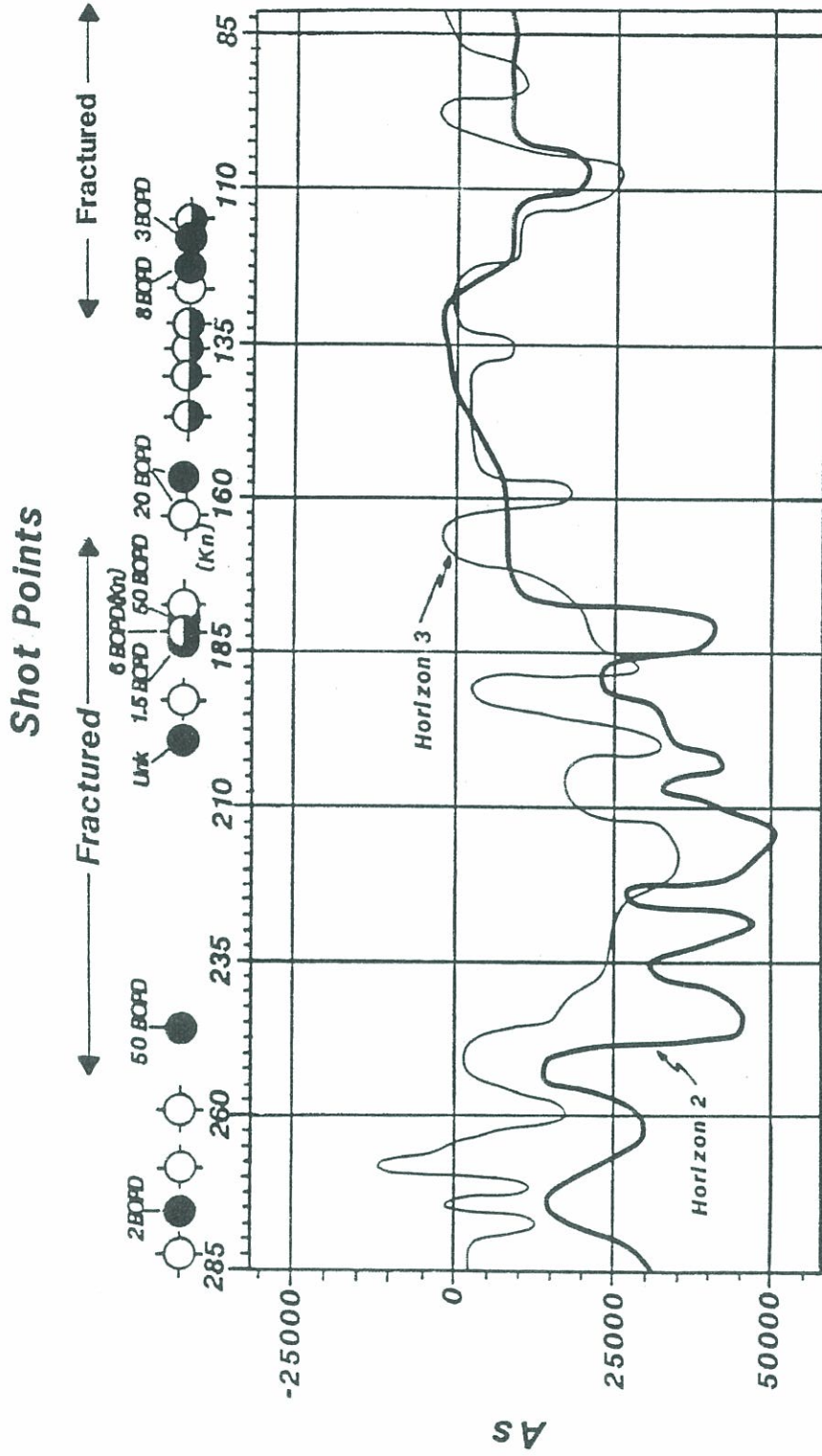


Figure 33: SH-wave amplitudes along horizons 2 and 3, with production information for both Pierre and Niobrara Formations.

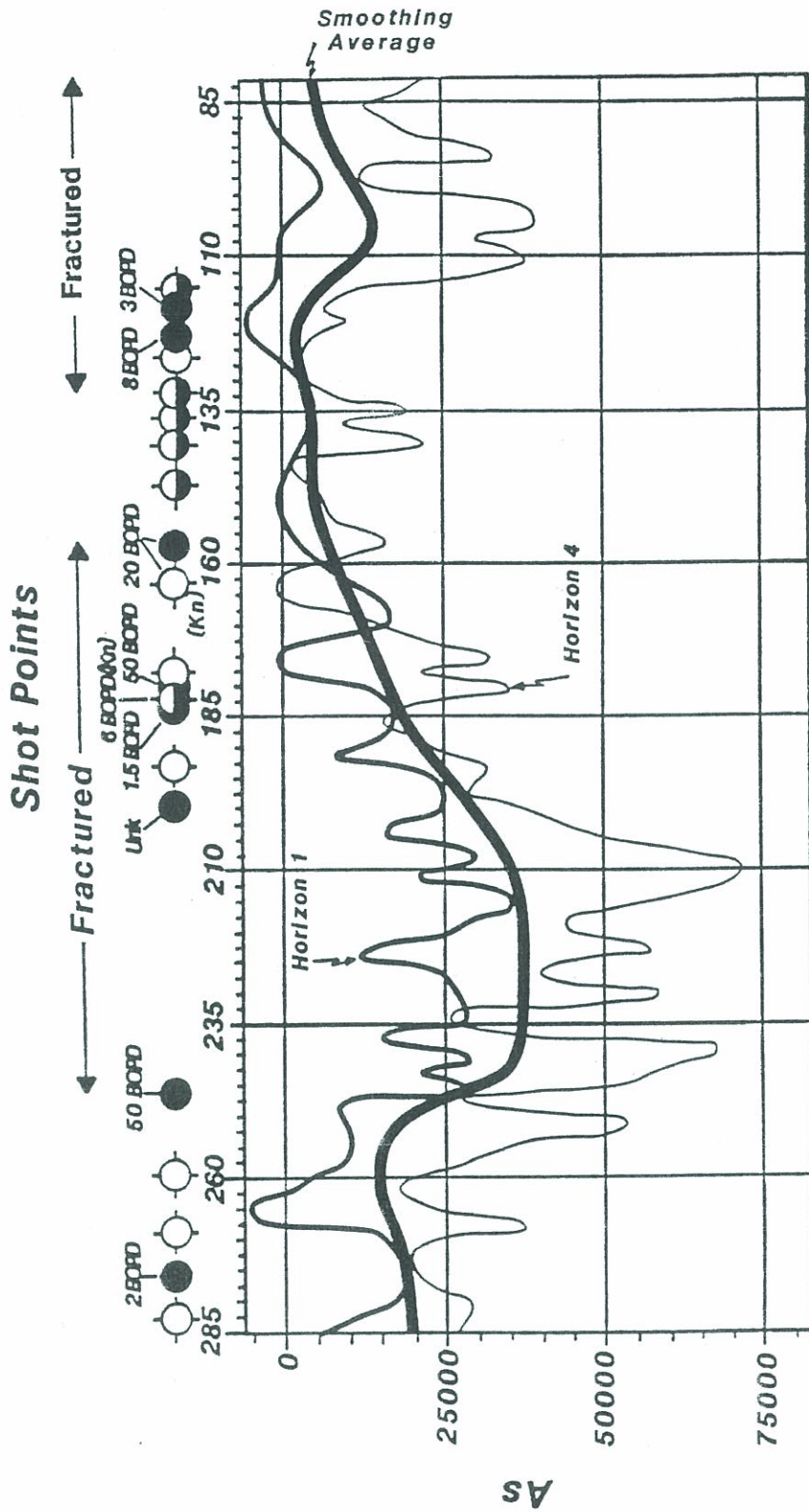


Figure 34: SH-wave amplitudes along horizons 1 and 4, with production information for both Pierre and Niobrara Formations.

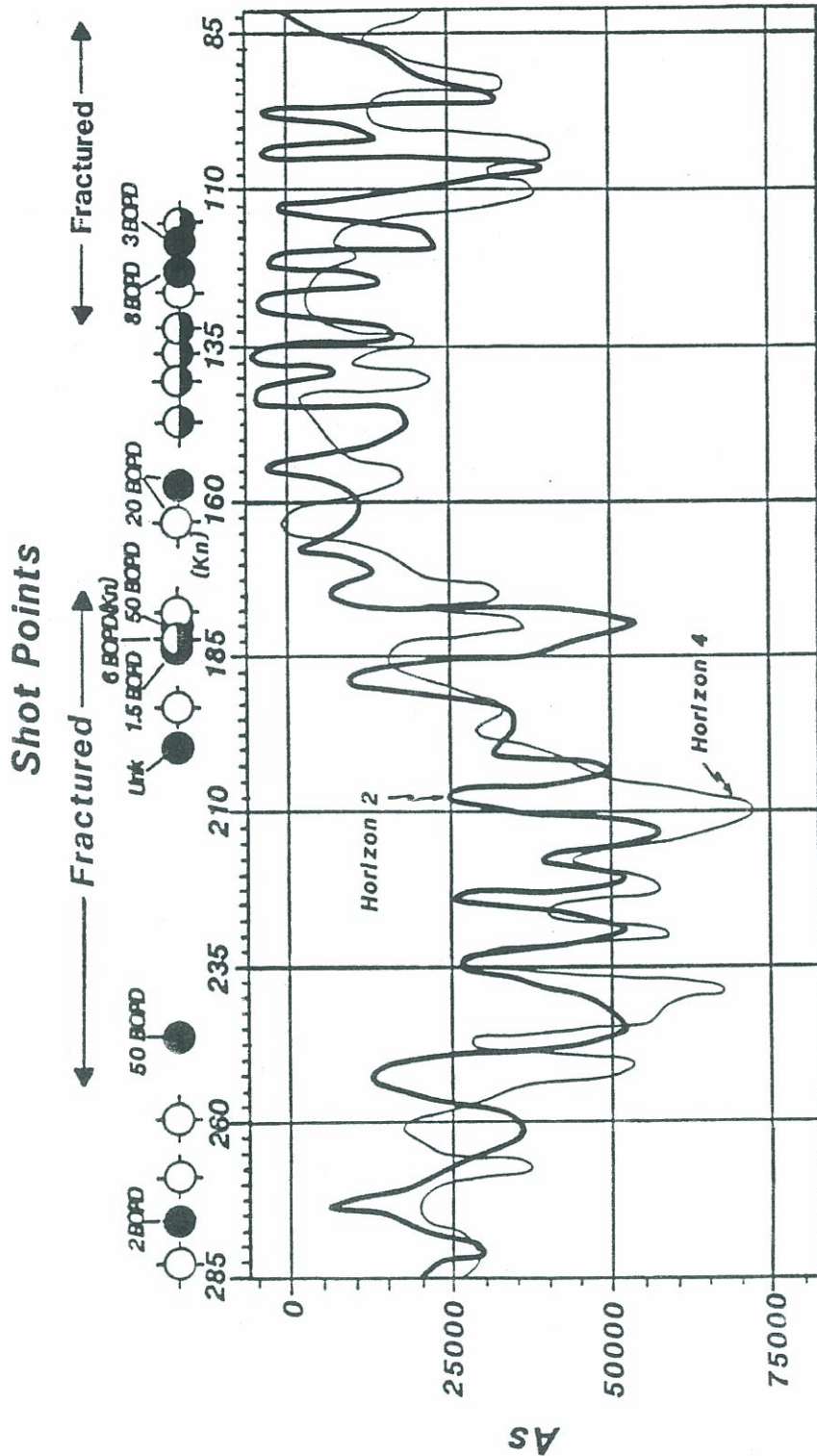


Figure 35: SH-wave amplitudes along horizons 2 and 4, with production information for both Pierre and Niobrara Formations.

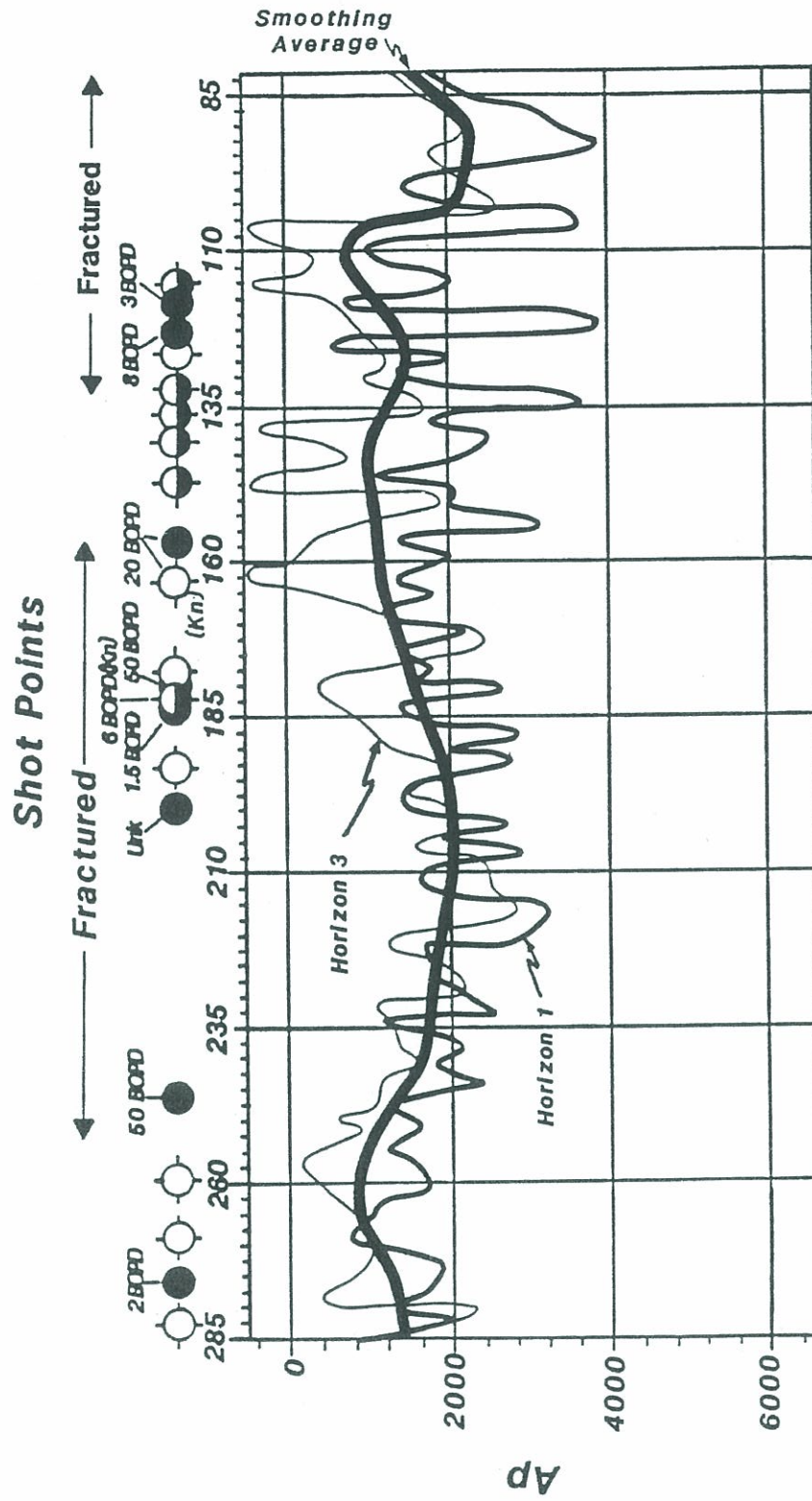


Figure 36: P-wave amplitudes along horizons 1 and 3, with production information for both Pierre and Niobrara Formations.

Zones with an increase in  $A_s/A_p$  ratio for horizon 3 and 4 agree with  $V_s/V_p$  and  $T_p/T_s$  results in identifying fracture zones within the Florence Field (Figures 37 and 38). Although results are not as definitive as with  $V_s/V_p$  and  $T_p/T_s$  ratios,  $A_s/A_p$  ratios appear to increase where fractures are believed to occur.

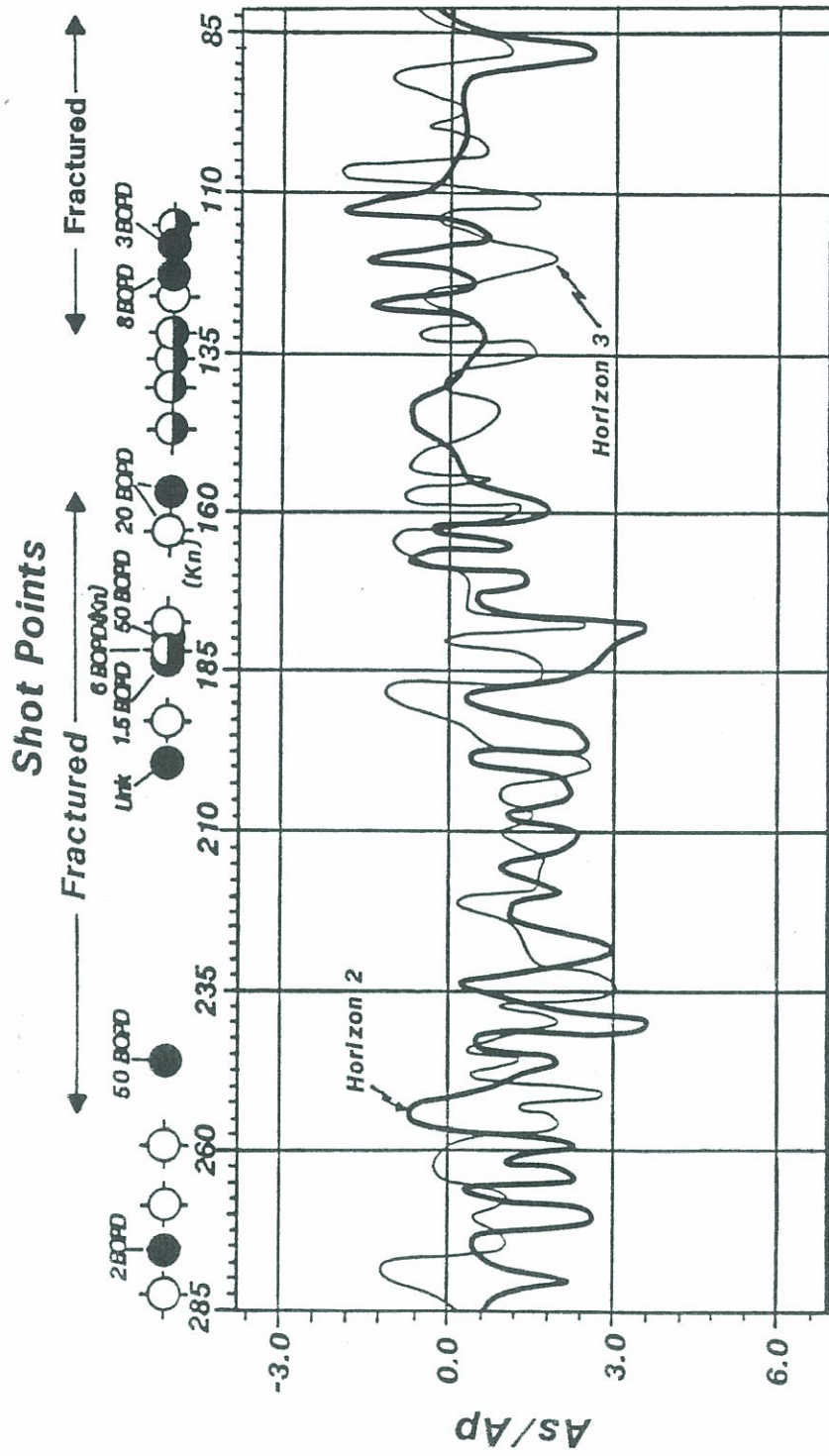


Figure 37: As/Ap ratio for horizons 2 and 3, with production information for both Pierre and Niobrara Formations.

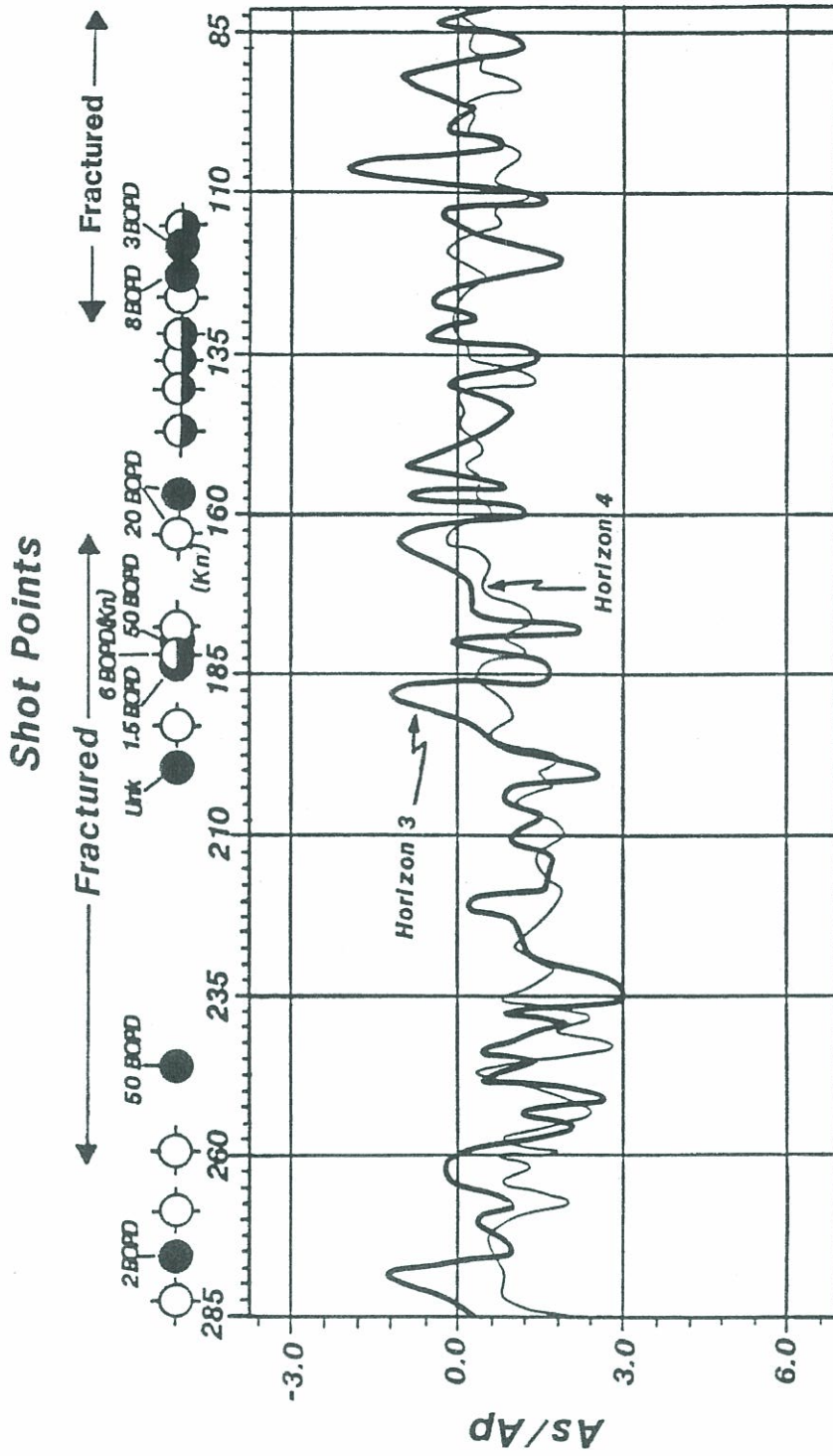


Figure 38: As/Ap ratios for horizons 3 and 4, with production information for both Pierre and Niobrara Formations.

FUTURE WORK

The Syslap method was ineffective in obtaining just the SH-wave amplitude component, probably resulting from the SH-wave minimizing amplitude ratio during the Syslap method's subtraction process. Perhaps a different source and a larger source and receiver spread would generate an overall improvement in the S/N of the SH-wave data, allowing a more reliable and conclusive correlation with the P-wave data.

Given the limitations of P- and SH-wave data acquisition, velocity information does not have adequate resolution for this study.

Bandwidth and phase differences are apparent between the P- and SH-wave seismic sections. A spectral analysis of both P- and SH-wave preserved amplitude sections shows frequency content of the SH-wave section is minimal at best when compared to the P-wave section. Seismic traces are digitized from each preserved amplitude section and the spectrum is computed for each trace (Figure 39). The SH-wave spectrum shows maximum amplitudes have frequencies between 2-20 hz, with a maximum frequency around 45 hz, however dominant frequencies are lower. Higher frequencies are obtained from the P-wave spectrum,

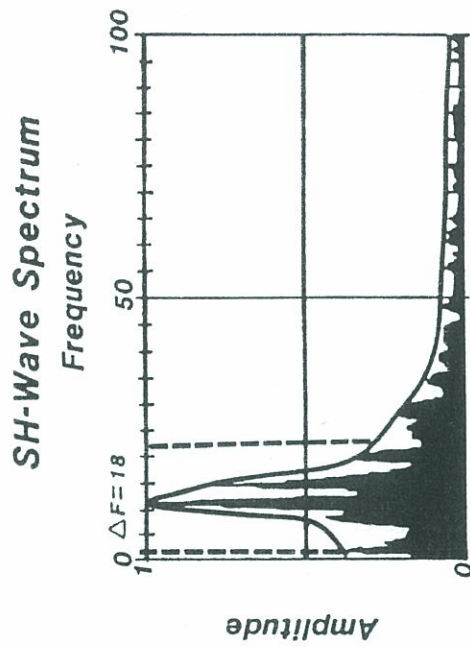
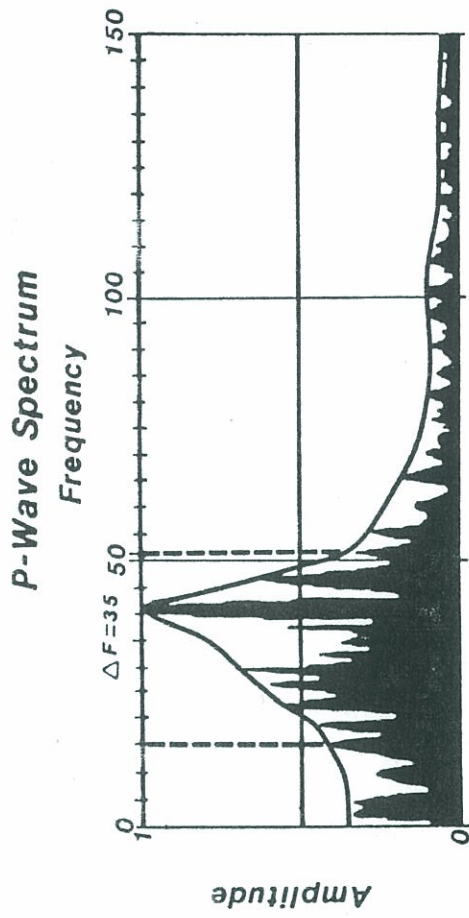


Figure 39: Amplitude spectrum of P- and SH-wave preserved amplitude seismic traces.

which shows maximum P-wave amplitudes have frequencies between 15-50 hz, with a maximum frequency around 70 hz. While the P-wave sections usable bandwidth is approximately 35 hz, a minimal SH-wave bandwidth of 18 hz virtually crippled the SH-wave sections definition.

Inadequacies of velocity acquisition and SH-wave velocity resolution are the limiting factors for defining fracture zones in the Pierre and Niobrara Formations. When designing a seismic survey, several parameters must be considered to assure the required velocity resolution is obtained. A simple equation used to calculate the far offset trace is given;

$$X_{\max} = \left( \frac{T_o V^2}{\Delta F \left( \frac{\Delta V}{V} \right)} \right)^{\frac{1}{2}} \quad (\text{Graul, 1986})$$

where,

$T_o$  = Time of interest.

$V$  = NMO (normal moveout) velocity.

$\Delta F$  = Bandwidth of data.

$\Delta V$  = Change in velocity at  $T_o$ .

When analyzing the P-wave parameters,

$$X_{\max} = 2915 \text{ feet.}$$

$$T_0 = .2 \text{ seconds (one-way).}$$

$$\Delta F = 35 \text{ hz.}$$

$$V = 10,000 \text{ ft/s.}$$

provides a minimum velocity resolution for the P-wave survey of approximately 670 ft/s.

When analyzing the SH-wave parameters,

$$X_{\max} = 2915 \text{ feet.}$$

$$T_0 = .5 \text{ seconds (one-way).}$$

$$\Delta F = 18 \text{ hz.}$$

$$V = 6700 \text{ ft/s.}$$

provides a minimum velocity resolution for the SH-wave survey of approximately 1,000 ft/s, which is not adequate for this study. Bandwidth is a major problem, the bandwidth of the SH-wave section was too narrow for good velocity resolution.

Since SH-wave velocities are roughly half the speed of P-wave velocities, near surface problems will cause serious static problems in SH-wave data. Several refraction shots should be recorded along the seismic line, to aid in interpreting the near surface velocities and changes in velocity along the seismic line. A refraction static

solution program should then be included in the processing sequence. Because near surface data was not available for this study, a refraction static solution was not attempted.

Martin (1986) indicates the importance of knowing the direction of fracturing before laying out a seismic program. Testing is needed in the field, since shear wave amplitude effects are related to direction of seismic acquisition. If seismic acquisition is parallel to fracturing orientation the shear wave velocities will be faster and when acquisition is perpendicular to the fracture orientation the SH-wave velocity will be the slowest. Therefore, recording with two-component geophones will aid processing sequence to minimize directional effects on shear wave amplitudes.

ALTERNATE INTERPRETATION

P-wave and SH-wave sections both have an area in which the processing sequence had ineffective resolution. Both the P- and SH-wave preserved amplitude sections show potential areas between shot points 120 to 150 where basement faulting may continue up to and die out in the Pierre Formation. Three faulted areas can be interpreted, at shot points 125, 137, and 145. Fault zones would help explain loss of data coherency and no production within this zone.

Proper uniform coupling of source to shooting medium is important when studying amplitude variations. With inadequate coupling, amplitude effects may not be fully related to the shooting medium. Therefore, reduction of amplitudes in this study is possible, not a result of fractures, but could result from inadequate coupling of primacord in the buried trenches along portions of the seismic lines.

CONCLUSIONS

1) S/N ratio is the limiting factor in delineating fracture zones. The first part of the Florence field study was to improve the S/N ratio on the P- and SH-wave preserved amplitude sections. Because of insistent SH-wave repeated first breaks, S/N was low on the SH-wave section.

2) P- and SH-wave stacking velocities and interval velocities are lower in fractured intervals. SH-wave velocity information is more definitive of fractured areas.  $V_s/V_p$  ratio's show areas of preferential fracturing in the Pierre Formation.

3) Interval travel times are directly related to velocity, these times do exhibit results that indicate fractures in both Pierre and Niobrara Formations. Both P- and SH-wave interval travel times increase.  $T_p/T_s$  ratios show a definite correlation between fracturing in both the Pierre and Niobrara Formations.

4) Both P- and SH-wave amplitudes increase in fractured zone areas.  $A_s/A_p$  ratio results show a correlation with fracturing. Amplitude reduction caused by both diffractions and attenuation is less than the increasing reflection coefficients effects on the SH-wave amplitudes.

5) Reshooting the area with an effective shear-wave source and receiver program would offer promise for recognizing and estimating fractures as well as anisotropy in the field from combined P- and S-wave studies.

6) Seismic data shows areas of fracturing, but not all these areas will have open fractures. Specific production intervals are a link to the presence of open fractures. Section above Niobrara Formation may also be fractured throughout, not just in the productive intervals.

7) Northeastern interval labeled preferential fracturing along seismic line (Figure 16), between shot points 75 and 130 (Plates 6 and 8), exhibits an area for future exploration.

REFERENCES CITED

- Aguilera, R. and Roberto Aguilera and Assoc., Inc.,  
Calgary Alta, Canada, 1982, Exploring for Naturally  
fractured Reservoirs - A Petroleum Engineer's Point  
of View: American Association of Petroleum Geologists,  
vol. 66, no. 2, p. 242.
- Amstrat, 1963, C.E. Brehm No. 1 Schell (OWDD) F.R.  
Anderson No. 23-27 Schell: NE SW sec. 27 Twp. 19S,  
Rge. 69W, County-Fremont, State-Colorado, Area-  
Florence, log no. D-970 (OWDD).
- Backus, G.E., 1962, Long-wave elastic anisotropy produced  
by horizontal layering: Journal Geophysical Research,  
vol. 67, pp. 4427-4440.
- Berryman, J.G., 1979, Long wave elastic anisotropy in  
transversely isotropic media: Geophysics, vol. 44,  
no. 5, pp. 896-917.
- Biot, M.A., 1956, Theory of propagation of elastic waves  
in a fluid-saturated porous solid; I: Low frequency  
range: Jour. Acoust. Soc. Am., vol. 28, pp. 168-178.
- , 1956, Theory of propagation of elastic waves  
in a fluid-saturated porous solid; II: Higher  
frequency range: Jour. Acoust. Soc. Am., vol. 28,  
pp. 179-191.
- Bortfeld, R., 1961, Approximation to the reflection and  
transmission coefficients of plane longitudinal  
and transverse waves: Geophysical Prospecting,  
vol. 9, no. 4, pp. 485-502.
- , 1962, Exact solution of the reflection and  
refraction of arbitrary spherical compressional  
waves at liquid-liquid interfaces and at solid-  
solid interfaces with equal shear velocities and  
equal densities: Geophysical Prospecting, vol. 10,  
no. 1, pp. 35-67.

- Bostick, N.H. and Pawlewicz, M.J., 1984, Regional variation of vitrinite reflectance of the Pierre Shale (Upper Cretaceous) in mountain basins and along the eastern Rocky Mountain front, Colorado: Rocky Mountain Association of Geologists; Hydrocarbon Source Rocks of the Greater Rocky Mountain Region - 1984, pp. 393-399.
- Brown, D.W., 1978, A reflection seismic study of the Cañon City-Pueblo area, Fremont and Pueblo counties, Colorado: Colorado School of Mines, Golden, Colorado, M.S. thesis, T-2109, unpub.
- Carpenter, L.C., 1961, Florence-Cañon City Field: Rocky Mountain Association of Geologists Oil and Gas Field Volume, Colorado-Nebraska, p. 130.
- Cherry, J.T. and Waters, K.H., 1968, Shear wave recording using continuous signal methods, Part I - Early development: Geophysics, vol. 33, no. 2, pp. 229-239.
- Clayton, J.L. and Swetland, P.J., 1980, Petroleum generation and migration in Denver Basin: American Association of Petroleum Geologists, vol. 64, no. 10, pp. 1613-1633.
- Cobban, W.A., and Scott, G.R., 1975, Geologic and biostratigraphic map of the Pierre Shale in the Cañon City-Florence Basin and the Twelvemile Park area, south-central Colorado: Department of the Interior, United States Geological Survey, Miscellaneous Investigations Series, Map I-937.
- Crampin, S. and Radovich, B.J., 1982, Interpretation of synthetic common-depth-point gathers for a single anisotropic layer: Geophysics, vol. 47, no. 3, pp. 323-325.
- Darton, N.H., 1905, Preliminary report on the geology and underground water resources of the central great plains: United States Geological Survey, Prof. Paper 32, pp. 344, 380-382.
- Deford, R.K., 1929, Surface structure, Florence oil field, Fremont County, Colorado: American Association of Petroleum Geologists, Structure of Typical American Oil Fields, vol. II, pp. 75-92.

- Delaplanche, J., Hagemann, R.F., and Bollard, P.G.C.,  
1963, An example of the use of synthetic seismograms:  
Geophysics, vol. 28, pp. 842-854.
- Dilay, A.J., 1982, Direct hydrocarbon indicators lead to  
a Canadian gas find: World Oil, vol. 195, pp. 149-164.
- Dohr, G. and Janle, H., 1980, Improvements in the observa-  
tion of shear waves: Geophysical Prospecting, vol. 28,  
pp. 208-220.
- Domenico, S.N., 1977, Elastic properties of unconsolidated  
porous sand reservoirs: Geophysics, vol. 42, no. 7,  
pp. 1339-1368.
- , 1984, Rock lithology and porosity determination  
from shear and compressional wave velocity: Geophysics,  
vol. 49, no. 8, pp. 1188-1195.
- Ensley, R.A., 1984, Comparison of P- and S-wave seismic  
data: A new method for detecting gas reservoirs:  
Geophysics, vol. 49, no. 9, pp. 1420-1431.
- Erickson, E.L., Miller, D.E., and Waters, K.H., 1968,  
Shear wave recording using continuous signal methods,  
Part II - Later experimentation: Geophysics, vol. 33,  
no. 2, pp. 240-254.
- Faust, L.Y., 1953, A velocity function including lithologic  
variation: Geophysics, vol. 18, no. 2, pp. 271-288.
- , 1951, Seismic velocity as a function of depth  
and geologic time: Geophysics, vol. 16, no. 2,  
pp. 192-206.
- Ganguli, A.K., 1950, Geology of the area southwest of  
Florence, Fremont County, Colorado: Colorado School  
of Mines, Golden, Colorado, M.S. Thesis, T-694, unpub.
- Gardner, G.H.F., Gardner, L.W., and Gregory, A.R.,  
1974, Formation velocity and density - The diagnostic  
basics for stratigraphic traps: Geophysics, vol. 39,  
no. 6, pp. 770-780.
- Gardner, G.H.F. and Harris, M.H., 1968, Velocity and  
attenuation of elastic waves in sands: 9th Annual  
Logging Symposium, Trans. (SPWLA), pp. M1-M19.

Garotta, R., Michon, D., Coppens, F., Layotte, P.C., Polchkov, M.K., and Brodov, L.Y., 1977, P-wave and S-wave combined interpretation in seismic reflection: 47th Annual International Society of Exploration Geophysicists Meeting, Calgary, Alberta, September 1977.

-----, Land seismic shear waves: Produced by CGG (Technical Series No: 507.78.05).

Gauthier, D.L., Clayton, J.L., Leventhal, J.S., and Reddin, N.S., 1984, Origin and source-rock potential of the Sharon Springs Member of the Pierre Shale, Colorado and Kansas: Rocky Mountain Association of Geologists; Hydrocarbon Source Rocks of the Greater Rocky Mountain Region - 1984, pp. 369-385.

Graul, M., 1986, Seismic lithology: An SEG short course.

Gregory, A.R., 1976, Fluid saturation effects on dynamic elastic properties of sedimentary rocks: Geophysics, vol. 41, no. 5, pp. 895-921.

✓-----, 1977, Aspects of rock physics from laboratory and log data that are important to seismic interpretation: American Association of Petroleum Geologists, Memoir 26, pp. 15-46.

Hazelbroek, P., 1966, Elastic waves from a finite line source: Proceedings of the Royal Society, London, Series A, vol. 294, pp. 38-65.

Herrera, A.O., 1951, Geology of the area southwest of Florence, Fremont County, Colorado: Colorado School of Mines, Golden, Colorado, M.S. Thesis, T-712, unpub.

Hilterman, F., 1986, Seismic lithology: An SEG short course.

Horton, C.W., 1959, A loss mechanism for the Pierre Shale: Geophysics, vol. 24, no. 4, pp. 667-680.

Jolly, R.N., 1956, Investigation of shear waves: Geophysics, vol. 21, no. 4, pp. 905-938.

King, M.S., 1966, Wave velocities in rocks as a function of changes in overburden pressure and pore fluid saturants: Geophysics, vol. 31, no. 1, pp. 50-73.

Kisslinger, C., Mateker, E.J., and McEvilly, T.V., 1961, SH-motion from explosions in soil: *Journal of Geophysical Research*, vol. 66, no. 10, pp. 3487-3496.

Leonard, A., 1986, Special report Florence-Cañon City: New approaches to an old area: *Petroleum Information Corporation, Rocky Mountain Region Report, Section 1*, pp. 3-10.

Levin, F.K., 1978, The reflection, refraction, and diffraction of waves in media with an elliptical velocity dependence: *Geophysics*, vol. 43, no. 3, pp. 528-537.

✓-----, 1979, Seismic velocities in transversely isotropic media: *Geophysics*, vol. 44, no. 5, pp. 918-936.

Love, A.E.H., 1927, *A treatise on the mathematical theory of elasticity*: Cambridge University Press, p. 104.

Ludwig, W.J., Nafe, J.E., and Drake, C.L., 1970, Seismic refraction: *The Sea*, vol. 4, no. 1, p. 84.

Mallory, W.W., 1977, Fractured shale hydrocarbon reservoirs in southern Rocky Mountain Basins: *Rocky Mountain Association of Geologists, Exploration Frontiers of the Central and Southern Rockies*, pp. 89-94.

Mari, J.L., 1984, Estimation of static corrections for shear-wave profiling using the dispersion properties of Love waves: *Geophysics*, vol. 49, no. 8, pp. 1169-1179.

Martin, M., 1986, Personal communication, Ph.D. candidate, Colorado School of Mines, Department of Geophysics.

Mavco, G.M. and Nurr, A., 1979, Wave attenuation in partially saturated rocks: *Geophysics*, vol. 44, no. 2, pp. 161-178.

McDonal, F.J., Angona, F.A., Mills, R.L., Sengbush, R.L., Van Nostand, R.G., and White, J.E., 1958, Attenuation of shear and compressional waves in Pierre Shale: *Geophysics*, vol. 23, no. 3, pp. 421-439.

- Nafe, J.E. and Drake, C.L., 1957, Variation with depth in shales and deep water marine sediments of porosity, density and velocity of compressional and shear waves: Geophysics, vol. 22, no. 3, pp. 523-552.
- Narr, W., Gulf Research and Development Co., Pittsburgh, and Currie, J.B., Univ. of Toronto, Ontario, 1980, Origin of subsurface fracture systems - Example from Altamont Field, Uinta Basin, Utah: American Association of Petroleum Geologists, vol. 64-65, p. 755.
- Neidell, Norman S., 1985, Land applications of shear waves: Geophysics: The Leading Edge of Exploration, vol. 4, no. 11, pp. 32-44.
- , 1986, Amplitude variation with offset: Geophysics: The Leading Edge of Exploration, vol. 5, no. 3, pp. 47-51.
- , 1986, Research elements in amplitude variation with offset: Geophysics: The Leading Edge of Exploration, vol. 5, no. 4, pp. 42-44.
- O'Connell, R.J. and Budiansky, B., 1974, Seismic velocities in dry and saturated cracked solids: Journal of Geophysical Research, vol. 79, pp. 5412-5426.
- Omnes, G., 1976, Exploring with SH-waves: Can. Soc. Expl. Geophys. J., vol. 14, pp. 40-49.
- , 1978, Non-exclusive Syslap shear wave survey, Florence, Colorado: CGG.
- PI (Petroleum Information Corporation), 1985, Oil and gas southern Rockies: Petroleum Information Production Report.
- Radovich, B.J. and Levin, F.K., 1982, Instantaneous velocities and reflection times for transversely isotropic solids: Geophysics, vol. 47, no. 3, pp. 316-322.
- Robertson, J.D. and Pritchett, W.C., 1985, Direct hydrocarbon detection using comparative P-wave and S-wave seismic sections: Geophysics, vol. 50, no. 3, pp. 383-393.

- Sharp, Jr., J.M., Univ. of Texas, Austin, TX and Korten Hof, M.H., Univ. of Missouri, Columbia, MO, Numerical model of shale compaction, aquathermal pressuring, and hydraulic fracturing: American Association of Petroleum Geologists, vol. 66, no. 9, p. 1447.
- Tatham, R.H., 1982,  $V_P/V_S$  and lithology: Geophysics, vol. 47, no. 3, pp. 336-344.
- Tatham, R.H. and Stoffa, P.L., 1976,  $V_P/V_S$  - a potential hydrocarbon indicator: Geophysics, vol. 41, no. 5, pp. 837-849.
- Thigpen, B.B., Dalby, A.E., and Landrum, R., 1975, SEG special report of the subcommittee on polarity standards: Geophysics, vol. 40, no. 4, pp. 694-699.
- Walsh, J.P., 1965, The effect of cracks on the compressibility of rocks: Journal of Geophysical Research, vol. 70, no. 2, pp. 381-389.
- Washburne, C.W., 1908, The Florence oil field, Colorado: United States Geological Survey, Bulletin 381, Contributions to economic geology, Part II, pp. 517-544.
- , 1910, The Cañon City coal field, Colorado: United States Geological Survey Bull. 381, pp. 341-378.
- Weimer, R.J., 1980, Recurrent movement on basement faults, A tectonic style for Colorado and adjacent areas: Rocky Mountain Association of Geologists, 1980 symposium, pp. 23-35.
- Wilkins, R., Simmons, G., and Caruso, L., 1984, The ratio  $V_P/V_S$  as a discriminant of composition for siliceous limestones: Geophysics, vol. 49, no. 11, pp. 1850-1860.
- Winkler, K.W. and Nur, A., 1982, Seismic attenuation: Effects of pore fluids and frictional sliding: Geophysics, vol. 47, no. 1, pp. 1-15.
- Winterstein, D.F., 1986, Anisotropy effects in P-wave and SH-wave stacking velocities contain information on lithology: Geophysics, vol. 51, no. 3, pp. 661-672.

Wyllie, M.R.J., Gregory, A.R., and Gardner, L.W., 1956,  
Elastic wave velocities in heterogeneous and  
porous media: Geophysics, vol. 21, no. 1, pp. 41-70.

APPENDIX

TABLE 1  
P-Wave Recording Parameters

--Shot Point:

One 110 feet strand of 220 grain/foot Primacord buried at 2.7 feet. The Primacord is primed with two caps in the middle.

--Spread:

Symmetrical split; 2195-385-0-385-2195

--Channels:

48.

--Group Interval:

110 feet.

--Fold:

2400%.

--Geophone Array:

8 Hz GSC 20D geophones in line over 140 feet.

--Recorder:

Sample rate - 2 ms.

LC filter - 12.5 hz.

HC filter - 125 hz.

TABLE 2

SH-Wave Recording Parameters

## --Shot Point:

Two 100 feet strands of 220 grain/foot Primacord buried at 2.5 feet, one on each side of middle trench (P-wave). Two records/shot point. Strands primed with two caps in middle.

## --Spread:

Symmetrical split; 3025-495-0-495-3025.

## --Channels:

48.

## --Group Interval:

110 feet.

## --Fold:

2400%.

## --Geophone Array:

36 Sensor, 10 Hz geophones/trace in a parallelogram configuration (two 270 feet rows of 18 geophones each separated by 30 feet and shifted by 160 feet).

## --Recorder:

Sample rate - 4 ms.

LC filter - 8 hz.

HC filter - 62.5 hz.

TABLE 3

CGG Standard Preserved Amplitude P-Wave Processing

- Demultiplexing, editing, gain recovery and an estimate of divergence correction proportional to "t" to the n'th power.
- Correction for residual divergence and absorption, a function of time and depth.
- SIGNET deconvolution (correction for mixed phase source and receiver).
- Account for crooked line.
- Velocity scan and filter tests.
- NMO corrections and mutes.
- Automatic static corrections.
  - Statics to floating datum.
  - Statics based on first breaks.
- Stacking velocities along one horizon.
- Regional master gain curve.
- Preserved amplitude stack with source and receiver compensation.
- Statics to fixed datum.
- Deconvolution.
- Time variant filtering.
- Regional equalization.

TABLE 4

SSC Preserved Amplitude P-Wave Processing

- Edit, SEG Y format to Phoenix format.
- F-K filter.
- Gain curve applied,  $T^{*1.3}$ .
- Geometry and weathering statics applied.
- Deconvolution.
- Filter.
- Velocity analysis, velocities picked from constant velocity stacks. NMO and residual applied.
- Surface consistent statics (1st).
- Velocity analysis, constant velocity stacks for new NMO's. Datum statics applied.
- Bulk shift, 400 ms.
- Surface consistent statics (2nd).
- Stack.
- Time variant filter.
- Constant scale section.

TABLE 5

## PI Completion Record Information (S-Show, P-Pump, A-Abandoned)

Well Name	Township 19 South			Range 69 West			Completion Date
	Location	Well Completion	Drill Depth/ TD Formation	Production Depth	Completion Date		
Geary Evergreen #1	NWSEW sec 20	D/A	3150/Kp	---	(1984)		
Petrocarbon #20-1	NWSENW sec 20	15 MCFGPD	2958/Kp	113-1194	(1983)		
Lear #1-20 Adamic	SWNESE sec 20	16 BOPD	3407/Kp	2665-3195	(1979)		
Lear #2-20 Adamic	CNWESE sec 20	D/A	3690/Kn	---	(1980)		
Lear #3-20 Adamic	W2SESE sec 20	D/A	3656/Kn	---	(1980)		
Energetics 31-20	NWNE sec 20	D/A	4460/Kgh	---	(1978)		
Mizel 22-1 Adamic	NESW sec 22	Oil	---	2999-3368	(---		
Sun #1 Phillips	NWSW sec 23	***	****/Kn	2650-2790	(***		
FR Anderson #25-26	NENWSW sec 26	D/A	975/Kp	---	(1957)		
Standard Oil Colo.	sec 26	unk	1604/--	---	(1930)		
Sun #4 Phillips	SWSW sec 26	***	****/Kn	2650-2790	(***		
Ander-Brehm #1 Sheel	CNESW sec 27	D/A-G	8811/Oh	(projected)	(1963)		
Peak Pet. #1 Hays	SWSWSW sec 27	6 BOPD	2505/Kp	2470-2505	(1959)		
Peak Pet. #2 Hays	NWSW sec 27	210 BOPD	2357/Kp	2350-2357	(1959)		
Peak Pet. #3 Hays	NWSW sec 27	D/A-O	3200/Kp	s-	(1959)		
Peak Pet. #4 Hays	NWSW sec 27	D/A	3400/Kp	1800	(1959)		
Peak Pet. #5 Hays	NWSW sec 27	D/A	2590/--	---	(1959)		
Peak Pet. #6 Hays	SWSW sec 27	D/A-O&G	2645/Kp	---	(1959)		
Peak Pet. #7 Hays	SWSW sec 27	D/A	2594/Kp	---	(1959)		
Peak Pet. #9 Hays	NWSWSW sec 27	60 MCFGPD	2600/Kp	2415-2600	(1959)		
Peak Pet. #10 Hays	NWSW sec 27	23 BOPD	2415/Kp	2300-2415	(1959)		
Peak Pet. #12 Hays	SWSW sec 27	D/A	2807/Kp	---	(1959)		
Peak Pet. #13 Hays	NWSWSW sec 27	D/A-O&G	2600/Kp	s-	(1959)		
Continental #554	NWNWSW sec 28	D/A	4197/--	---	(1944)		
Peak Pet. #1-29	SWSWNE sec 29	D/A-O&G	2500/Kp	sg-	(1958)		
Peak Pet. #1-29A	SESENW sec 29	D/A	2900/Kp	so-	(1959)		
First Expl #29-1	SENESE sec 29	8 BOPD	3004/Kp	108-3004	(1983)		
First Expl #30-1	NWSENE sec 30	D/A	2916/Kp	---	(1983)		

TABLE 5 (continued)

Well Name	Township 19 South		Range 69 West		Completion Date
	Location	Well Completion	Drill Depth/ TD Formation	Production Depth	
Lear Pet. #1-32	NWNE sec 32	D/A-O	3706/Jm	so-2735-3550 sgfr-1800-2700 unk-3010	(1981)
Evergreen Res #23-2	SESEW sec 32	54 BOPD	3010/Kp		(1985)
Lear Pet. #1-33	SESE sec 33	D/A	3386/Kn		(1978)
Lear Pet. Robb 2-33	SESE sec 33	D/A	3386/Kn		(1978)
Peak Pet. Hays 2-33	SESEW sec 33	76 BOPD	2576/Kp	2380-2576	(1959)
Peak Pet. Hays #8	SESEW sec 33	A-76 BOPD	2576/Kp	2380-2576	(1959)
Peak Pet. Hays #11	SESEW sec 33	D/A	2600/Kp		(1959)
unknown	NWWSW sec 33	Oil	2576/--	unknown	(1959)
unknown	SWSWSW sec 33	D/A	3539/--		(1978)
unknown	SESEW sec 33	D/A	3229/--		(1959)
Babitz-Camerlo 34-1	E2SWSW sec 34	8 BOPD	2990/Kp	160-2990	(1985)
Peak Pet. #1 PMHk	SWSW sec 34	D/A	3500/Kn		(1959)
Maloney #264 Slevins Florence Petro Co. 3 wells	SESEW sec 34	P- 3 BOPD	1850/--		(1940)
	sec 34	D/A	1500-1700		(1928)

TABLE 6

## PI Completion Record Information (S-Show, P-Pump, A-Abandoned)

Well Name	Township 20 South			Range 69 West			Completion Date
	Location	Well Completion	Drill Depth/ TD Formation	Production Depth	Completion Date		
Sun #1 Yellico L&C	NESE sec 2	***	****/Kn	2650-2790 (projected)	(****)		
Peak #3 Cont. Oil	SWNW sec 3	D/A-O&G	3004/Kn	sog- 2230 sg- 2551	(1959)		
Mizel 3-1 Yellico	NWNW sec 3	Oil	----/Kc	unknown	(----)		
Mizel 3-2 Yellico	NESW sec 3	Oil	----/Kc	unknown	(----)		
Continental #570	SESW sec 4	P-50 BOPD	2260/---	---	(1926)		
Continental #572	NWNE sec 4	P-20 BOPD	3385/---	---	(1926)		
Continental #574	S2S2S2 sec 4	P-1.5BOPD	1550/---	---	(1926)		
Cont. #1 Templeton	CNWSE sec 4	P-20 BOPD	2630/---	---	(1925)		
Templeton 2 wells	-- sec 4	50 BOPD	3200/---	---	(1925)		
Francis #2 Faricy	SWSE sec 4	D/A	1798/---	---	(1971)		
Lear #1-4	NENENE sec 4	12 BOPD	3761/Kn	sgfr-2780-2980 sgfr-3060-3255 so-2450-2480	(1979)		
K-D #1 Pitzer	SWNWNW sec 4	D/A-O&G	3230/---	sog-1785-1790	(1955)		
Peak #1 Cont. Oil	SWSE sec 4	P- 6 BOPD	3126/Kn	so- 3270 3119-3126	(1959)		
Eboe-Griffith #1	NENWNE sec 5	9 BOPD	1912/Kp	so- 1400	(1962)		
Atwell&Fox #1 Mase	CNENW sec 5	D/A-O	2450/Kp	so- 2139 so- 2551	(1951)		
Atwell&Fox #1 Fee	NWNWNE sec 5	D/A	3620/---	so-2035-2040 (1.5 BOPH bailer)	(1951)		
Folger #1 O-F	NESE sec 5	24 BOPD	1555/---	---	(1969)		
Brammer Camerlo 8-1	NWNE sec 8	7 BOPD	3110/Kp	unknown	(1985)		
K-D #2 Lloyd	CNESE sec 8	D/A-O	3009/Kp	225-3110 so-1993-1997 (bailed oil)	(1961)		

TABLE 6 (continued)  
 PI Completion Record Information (S-Show, P-Pump, A-Abandoned)

Well Name	Township 20 South		Range 69 West		Drill Depth/ TD Formation	Production Depth	Completion Date
	Location	Well Completion	Drill Depth/ TD Formation	Production Depth			
K-D Anderson #1 Lloyd	SESE sec 8	D/A-O	3200/--	sdfr-	-3200 (bailed oil)	(1959)	
Colburn #575 3 wells	NENW sec 9	D/A	4205/--		---	(1927)	
UOC Colburn #576	NENE sec 9	D/A	3420/--		---	(1926)	
unknown	SWNENW sec 9	Oil	-----		---	(-----)	
Peak #4 Cont. Oil	SWSW sec 10	D/A-O	2755/Kp	sdfr-	2415-2755	(1960)	
Sun #1 Morris	SESE sec 11	***	****/Kn		2650-2790 (projected)	(****)	
Continental #571	CW/2 sec 15	D/A	3577/Kn		---	(-----)	
Peak #2 Cont. Oil	SESW sec 15	D/A-O	2708/Kn	so-	2480 (6 BOPD bailed)	(1959)	
Western Oil #1 St.	S2SESW sec 16	D/A-O	3512/--	so-	2322-2330 (3-5 BOPD)	(1950)	
Peak #1 Peaker-St.	NWSW sec 16	D/A-O	3515/Kn	so- sog-	2385 3210 (4 BOPD bailed, gas @ 10 MCFGPD)	(1959)	
ER Good	-- sec 16	Oil	1700/--		-1700	(1927)	
ER Good	-- sec 16	Oil	3250/--		-3250	(1927)	
unknown	CNNW sec 16	50 BOPD	2855/Kn		-2855	(-----)	
Fremont Prod. #1	SWSWSE sec 17	P- 25-100 BOPD	2135/--		-2135	(1925)	
Beltrano&Rocco #1	SWSENE sec 17	D/A-O	2950/--	so-	2400	(1948)	
Gearly #5 Fee	SESENE sec 17	D/A	2500/Kp		---	(1981)	
Gearly #6 Fee	SESENE sec 17	D/A	2500/Kp		---	(1981)	
Gearly #7 Fee	SWNE sec 17	1.5 BOPD	2320/Kp		2150-2200	(1983)	
Gearly #10 Fee	SESENE sec 17	D/A	2500/--		---	(1985)	
Peak #1 Peak	SESW sec 17	D/A	2504/Kp		---	(1959)	
Peak #2 Peak	NESW sec 17	D/A	3076/Kp		---	(1959)	
Peak #3 Peak	NESW sec 17	D/A	2066/Kp		---	(1959)	

TABLE 6 (continued)

PI Completion Record Information (S-Show, P-Pump, A-Abandoned)

Well Name	Township 20 South		Range 69 West		Completion Date
	Location	Well Completion	Drill Depth/ TD Formation	Production Depth	
Peak #4 Fee	CNE sec 17	D/A	2622/Kp	---	(1959)
S #1 Vanwey	NENW sec 21	D/A	2130/--	---	(1981)
Francis #1 Van-Good	NENE sec 21	D/A	1740/--	---	(1978)
Geary #1 Hassler	SESW sec 21	D/A	2705/Kp	---	(1968)
Gibbons-Truesdale #1	NENW sec 22	29 BOPD	2160/--	-2160	(1927)
Cont. Marjo #4	NENW sec 22	71 BOPD	1800/--	-1800	(1928)
Cont. Marjo #5	NENW sec 22	D/A	3010/--	---	(1929)
Sun #1-A Yellico L&C	NWSW sec 23	***	****/Kn	2650-2790 (projected)	(****)

TABLE 7  
 Completion Information After Washborne (1908);  
 USGS, Bulletin 381

Township 19 South		Range 69 West	
Well Name	Location	Well Completion	
United Oil Co	SENESE sec 19	D/A-O	
United Oil Co	S2SENE sec 19	D/A-O	
United Oil Co	CNE sec 19	Oil	
United Oil Co	NENWNE sec 19	D/A	
United Oil Co	CNWNE sec 19	D/A-OG	
United Oil Co	NENWSE sec 19	Oil	
United Oil Co	CNWSE sec 19	D/A-G	
United Oil Co	E2NWSE sec 19	D/A	
United Oil Co	E2NWSE sec 19	Oil	
United Oil Co	E2NWSE sec 19	Oil	
United Oil Co	SEWSE sec 19	Oil	
United Oil Co	S2NWSE sec 19	Oil	
Oak Creek Oil Co	SENESE sec 19	D/A	
United Oil Co	NENESW sec 19	Oil	
United Oil Co	NWNESE sec 19	D/A-O	
United Oil Co	SENESE sec 19	Gas	
United Oil Co	SENESE sec 19	Oil	
United Oil Co	SENESE sec 19	Gas	
United Oil Co	S2NESE sec 19	Oil	
United Oil Co	CNESE sec 19	D/A-O	
United Oil Co	N2NESE sec 19	Oil	
United Oil Co	S2NESE sec 19	D/A-O	
United Oil Co	N2NENE sec 20	Gas	
United Oil Co	NWNESE sec 20	D/A	
United Oil Co	W2NENE sec 20	D/A	
United Oil Co	SENESE sec 20	Gas	
United Oil Co	CNE sec 20	Oil	
United Oil Co	NESESE sec 20	Oil	
United Oil Co	NENESE sec 20	Oil	
United Oil Co	E2NENE sec 20	Oil	
United Oil Co	E2NENE sec 20	Oil	
United Oil Co	E2SENE sec 20	Oil	
United Oil Co	CSENE sec 20	D/A-OG	
United Oil Co	SESENE sec 20	D/A	
United Oil Co	W2NESE sec 20	D/A-G	
United Oil Co	CSW sec 20	D/A-O	

TABLE 7 (continued)

Completion Information After Washborne (1908);  
USGS, Bulletin 381

Township 19 South		Range 69 West	
Well Name	Location	Well Completion	
United Oil Co	N2NWSW sec 20	Gas	
United Oil Co	W2W2SW sec 20	D/A	
United Oil Co	CNWSW sec 20	D/A-G	
United Oil Co	S2SW sec 20	D/A-O	
United Oil Co	SWNWSW sec 20	D/A-O	
United Oil Co	E2SWSW sec 20	D/A-OG	
Stadacona Oil Co	W2SWSW sec 20	Gas	
Stadacona Oil Co	S2SW sec 20	D/A-OG	
Stadacona Oil Co	SESWSW sec 20	D/A-O	
United Oil Co	NENWSE sec 20	D/A-O	
United Oil Co	E2NWSE sec 20	D/A-O	
United Oil Co	NWSWSE sec 20	D/A-OG	
United Oil Co	SWSWSE sec 20	D/A-O	
United Oil Co	SESWSE sec 20	Oil	
United Oil Co	W2SESE sec 20	D/A-O	
United Oil Co	SESESE sec 20	Gas	
United Oil Co	NESESE sec 20	D/A	
United Oil Co	NESESE sec 20	Oil	
United Oil Co	CNESE sec 20	Oil	
United Oil Co	SENESE sec 20	Oil	
United Oil Co	SENESE sec 20	Oil	
United Oil Co	SWSWNE sec 20	D/A	
United Oil Co	CW2NE sec 20	D/A	
United Oil Co	NWSENE sec 20	D/A-O	
United Oil Co	SWSENE sec 20	D/A-O	
United Oil Co	CSENE sec 20	Oil	
United Oil Co	CSENE sec 20	Oil	
United Oil Co	N2SENE sec 20	Gas	
United Oil Co	N2SENE sec 20	Oil	
United Oil Co	SWNESE sec 20	D/A	
United Oil Co	SENESE sec 20	Gas	
United Oil Co	NWNWNW sec 21	Oil	
United Oil Co	NWNWNW sec 21	D/A	
United Oil Co	NWNWNW sec 21	Gas	
United Oil Co	NENWNW sec 21	Oil	
United Oil Co	E2NWNW sec 21	D/A-O	

TABLE 7 (continued)

Completion Information After Washborne (1908);  
USGS, Bulletin 381

Township 19 South		Range 69 West		
Well Name	Location		Well Completion	
United Oil Co	SENWNW	sec 21	D/A-O	
United Oil Co	SWNWNW	sec 21	Oil	
United Oil Co	NWSWNW	sec 21	Oil	
United Oil Co	NESWNW	sec 21	D/A	
United Oil Co	CSWNW	sec 21	Oil	
United Oil Co	CSWNW	sec 21	Gas	
United Oil Co	NENWSW	sec 21	D/A-O	
United Oil Co	SWSWSW	sec 21	D/A	
United Oil Co	NESWSW	sec 21	D/A-O	
United Oil Do	CS2SW	sec 21	Oil	
United Oil Co	SESESW	sec 21	Oil	
United Oil Co	NWSESW	sec 21	D/A	
United Oil Co	NENESW	sec 21	D/A	
United Oil Co	CW2	sec 21	Oil	
United Oil Co	CE2NW	sec 21	Oil	
Florence O&R Co	N2N2N2	sec 21	D/A-OG	
United Oil Co	S2SESE	sec 21	D/A-OG	
United Oil Co	N2SWSE	sec 21	D/A	
United Oil Co	SWNWSE	sec 21	D/A	
United Oil Co	SWNWSE	sec 21	Oil	
United Oil Co	E2NWSE	sec 21	D/A	
United Oil Co	NENWSE	sec 21	Gas	
United Oil Co	N2N2SE	sec 21	Gas	
United Oil Co	SENESE	sec 21	D/A	
United Oil Co	CNESE	sec 21	D/A	
United Oil Co	NWNESE	sec 21	D/A-O	
United Oil Co	N2N2SE	sec 21	D/A	
United Oil Co	SESENE	sec 21	Gas	
United Oil Co	SESENE	sec 21	Gas	
United Oil Co	SWSENE	sec 21	D/A-G	
United Oil Co	CSWNE	sec 21	Gas	
United Oil Co	NESWNE	sec 21	Oil	
United Oil Co	CNE	sec 21	Gas	
United Oil Co	CNE	sec 21	Gas	
United Oil Co	SENWNE	sec 21	D/A-O	
United Oil Co	S2NWNE	sec 21	Oil	
United Oil Co	SWNWME	sec 21	D/A-O	

TABLE 7 (continued)

Completion Information After Washborne (1908);  
USGS, Bulletin 381

Township 19 South		Range 69 West	
Well Name	Location	Well Completion	
United Oil Co	SWNWNE sec 21	D/A	
United Oil Co	SWNWNE sec 21	Oil	
United Oil Co	S2NWNE sec 21	Oil	
United Oil Co	NWNWNE sec 21	Oil	
United Oil Co	N2NWNE sec 21	Oil	
United Oil Co	CNE sec 21	Gas	
United Oil Co	NWNENE sec 21	Oil	
United Oil Co	CNENE sec 21	Oil	
United Oil Co	SWNWSW sec 22	D/A	
United Oil Co	NWNWSW sec 22	Gas	
United Oil Co	NWNWSW sec 22	D/A-O	
United Oil Co	CSWNW sec 22	D/A-G	
Florence O&R Co	NWNENW sec 22	D/A-O	
Florence O&R Co	CNENW sec 22	Oil	
United Oil Co	NWNENW sec 27	D/A-OG	
United Oil Co	NENENW sec 27	D/A-O	
United Oil Co	E2E2NW sec 27	D/A	
United Oil Co	W2SWNW sec 27	D/A-OG	
United Oil Co	NWNWSW sec 27	D/A	
United Oil Co	NWNWSW sec 27	Oil	
United Oil Co	NWNWSW sec 27	Gas	
United Oil Co	W2NWSW sec 27	D/A	
United Oil Co	E2W2 sec 27	Oil	
United Oil Co	N2NWSW sec 27	Oil	
United Oil Co	CNWSW sec 27	Gas	
United Oil Co	SWSWSW sec 27	Oil	
United Oil Co	SESWSW sec 27	D/A-OG	
United Oil Co	SWSWNE sec 27	D/A-O	
United Oil Co	SESENE sec 27	D/A	
United Oil Co	NWNWNW sec 28	D/A	
United Oil Co	NENWNW sec 28	D/A-O	
United Oil Co	SWNWNW sec 28	D/A-O	
United Oil Co	SENWNW sec 28	Oil	
United Oil Co	NWNENW sec 28	Oil	
United Oil Co	E2NW sec 28	Oil	
United Oil Co	NWSWNW sec 28	D/A-O	

TABLE 7 (continued)

Completion Information After Washborne (1908);  
USGS, Bulletin 381

Township 19 South		Range 69 West	
Well Name	Location	Well Completion	
United Oil Co	SWSWNW sec 28	D/A-O	
United Oil Co	SWSENW sec 28	Gas	
Rocky Mtn Oil Co	NWNWSW sec 28	D/A	
Rocky Mtn Oil Co	W2W2 sec 28	D/A	
Rocky Mtn Oil Co	NENWSW sec 28	Oil	
Rocky Mtn Oil Co	W2NWSW sec 28	Oil	
Rocky Mtn Oil Co	W2NWSW sec 28	Oil	
Rocky Mtn Oil Co	CNWSW sec 28	Oil	
Rocky Mtn Oil Co	SWNWSW sec 28	Oil	
United Oil Co	E2NWSW sec 28	D/A	
Rocky Mtn Oil Co	CSWSW sec 28	Oil	
Rocky Mtn Oil Co	W2SWSW sec 28	Oil	
Rocky Mtn Oil Co	SWSWSE sec 28	D/A	
Rocky Mtn Oil Co	N2SWSE sec 28	Oil	
United Oil Co	S2SESE sec 28	Gas	
Rocky Mtn Oil Co	W2SE sec 28	D/A	
Rocky Mtn Oil Co	S2NWSE sec 28	D/A	
Rocky Mtn Oil Co	S2NWSE sec 28	D/A	
Rocky Mtn Oil Co	S2NWSE sec 28	D/A	
Rocky Mtn Oil Co	E2NWSE sec 28	D/A-O	
United Oil Co	CNWE sec 28	D/A	
Rocky Mtn Oil Co	N2NWSE sec 28	Oil	
Rocky Mtn Oil Co	E2E2 sec 28	D/A	
United Oil Co	S2SENE sec 28	D/A-O	
United Oil Co	E2SENE sec 28	D/A	
United Oil Co	W2SWNE sec 28	D/A	
United Oil Co	W2SWNE sec 28	D/A-O	
United Oil Co	NWNWNE sec 28	D/A-OG	
United Oil Co	S2NWNE sec 28	Oil	
United Oil Co	S2NENE sec 28	D/A-OG	
United Oil Co	NENENE sec 28	D/A	
United Oil Co	CNWNW sec 29	D/A-O	
United Oil Co	CNENW sec 29	D/A-OG	
United Oil Co	SWSWNW sec 29	D/A-OG	
United Oil Co	S2SWNW sec 29	D/A-O	
United Oil Co	NENWSW sec 29	Oil	

TABLE 7 (continued)

Completion Information After Washborne (1908);  
USGS, Bulletin 381

Township 19 South		Range 69 West	
Well Name	Location	Well Completion	
United Oil Co	CNWSW sec 29	Gas	
United Oil Co	CSW sec 29	D/A-OG	
Union Oil M&D Co	N2S2SW sec 29	D/A-OG	
Union Oil M&D Co	E2SESW sec 29	Gas	
Union Oil M&D Co	E2SESW sec 29	Oil	
United Oil Co	CNESW sec 29	D/A-OG	
United Oil Co	NWNESW sec 29	Oil	
United Oil Co	CNESW sec 29	Oil	
United Oil Co	E2E2SW sec 29	D/A-OG	
United Oil Co	N2N2 sec 29	Gas	
McComas Oil Co	W2NE sec 29	D/A-OG	
United Oil Co	W2SWNE sec 29	Oil	
United Oil Co	CSWNE sec 29	D/A-OG	
United Oil Co	N2S2N2 sec 29	D/A-OG	
United Oil Co	N2NWSE sec 29	Gas	
United Oil Co	NENWSE sec 29	Oil	
United Oil Co	CNWSE sec 29	Gas	
United Oil Co	CNWSE sec 29	Oil	
United Oil Co	SENWSE sec 29	Gas	
United Oil Co	S2NWSE sec 29	Oil	
United Oil Co	NWSWSE sec 29	Oil	
United Oil Co	SWSWSE sec 29	D/A-O	
United Oil Co	SWNESE sec 29	D/A	
United Oil Co	SENESE sec 29	D/A-O	
United Oil Co	N2SENE sec 29	D/A-O	
United Oil Co	E2SENE sec 29	D/A-O	
United Oil Co	CS2NE sec 29	Gas	
United Oil Co	SWNESE sec 29	Gas	
United Oil Co	SENESE sec 29	Oil	
United Oil Co	NENENE sec 29	Oil	
United Oil Co	S2NWNW sec 30	D/A-O	
United Oil Co	CN2NW sec 30	D/A-O	
United Oil Co	N2NENW sec 30	Oil	
United Oil Co	NWNWNE sec 30	D/A-O	
United Oil Co	NENWNE sec 30	D/A	

TABLE 7 (continued)

Completion Information After Washborne (1908);  
USGS, Bulletin 381

Tonwship 19 South		Range 69 West	
Well Name	Location	Well Completion	
United Oil Co	S2NWNE sec 30	D/A-O	
United Oil Co	SWSWNE sec 30	D/A	
United Oil Co	NWNWSE sec 30	D/A-O	
United Oil Co	E2NWSE sec 30	D/A-O	
Empire Oil Co	NWNESE sec 30	D/A-O	
United Oil Co	W2NESE sec 30	Gas	
United Oil Co	S2NESE sec 30	Gas	
United Oil Co	NWNENW sec 31	D/A	
United Oil Co	CS2NE sec 31	D/A-O	
United Oil Co	S2SWNE sec 31	D/A-O	
United Oil Co	SENESE sec 31	Oil	
United Oil Co	SESWSE sec 31	Oil	
United Oil Co	S2SESE sec 31	Oil	
Rocky Mtn Oil Co	NWNESE sec 32	D/A	
Rocky Mtn Oil Co	NWSENE sec 32	D/A	
Rocky Mtn Oil Co	SWSENE sec 32	Oil	
Union Oil M&D Co	E2W2NE sec 32	D/A-O	
Rocky Mtn Oil Co	NENESE sec 32	D/A	
United Oil Co	CNESE sec 32	Gas	
Rocky Mtn Oil Co	CNESE sec 32	Oil	
Birmingham Oil Co	SWSWSE sec 32	D/A	
Rocky Mtn Oil Co	CSE sec 32	Oil	
United Oil Co	S2N2SE sec 32	Oil	
Rocky Mtn Oil Co	CSESE sec 32	Oil	
Rocky Mtn Oil Co	SESESE sec 32	D/A	
Rocky Mtn Oil Co	S2SESE sec 32	Oil	
United Oil Co	SWSESE sec 32	D/A	
United Oil Co	SESWSE sec 32	D/A-O	
Rocky Mtn Oil	SESWSE sec 32	Oil	
United Oil Co	E2SWSE sec 32	Gas	
Rocky Mtn Oil Co	CSWSE sec 32	Gas	
Rocky Mtn Oil Co	CSWSE sec 32	Oil	
United Oil Co	SWSWSE sec 32	Gas	
Rocky Mtn Oil Co	NENWSE sec 32	Oil	
Rocky Mtn Oil Co	NWNWSE sec 32	Oil	
Rocky Mtn Oil Co	W2NWSE sec 32	D/A-O	

TABLE 7 (continued)

Completion Information After Washborne (1908);  
USGS, Bulletin 381

Township 19 South		Range 69 West	
Well Name	Location	Well Completion	
Rocky Mtn Oil Co	SWNWSE sec 32	D/A	
United Oil Co	SESESW sec 32	Oil	
United Oil Co	S2SESW sec 32	D/A-OG	
United Oil Co	SWSESW sec 32	Oil	
United Oil Co	CSESW sec 32	Oil	
United Oil Co	CSESW sec 32	Oil	
United Oil Co	N2SESW sec 32	D/A-OG	
W. Lebanon Oil Co	E2E2SW sec 32	Gas	
W. Lebanon Oil Co	CNESW sec 32	D/A	
United Oil Co	SESENEW sec 32	D/A-O	
United Oil Co	S2N2N2 sec 32	D/A-O	
United Oil Co	N2NENW sec 32	Oil	
United Oil Co	NWNENW sec 32	D/A-O	
United Oil Co	NENWNW sec 32	Gas	
United Oil Co	CNWNW sec 32	Oil	
United Oil Co	NWSWNW sec 32	D/A-O	
United Oil Co	CSWNW sec 32	D/A-O	
United Oil Co	W2SWNW sec 32	D/A	
United Oil Co	SESWNW sec 32	D/A-OG	
Isaac Canfield	NENWSW sec 32	D/A-O	
United Oil Co	NWNWSW sec 32	D/A-O	
National Oil Co	E2NWSW sec 32	D/A-OG	
National Oil Co	SENWSW sec 32	D/A-OG	
United Oil Co	SWNWSW sec 32	Oil	
United Oil Co	CS2SW sec 32	D/A-O	
United Oil Co	SESWSW sec 32	Oil	
Stadacona Oil Co	S2SWSW sec 32	Oil	
Fremont O&G Co	NENESE sec 33	Gas	
Fremont O&G Co	E2NESE sec 33	Oil	
Fremont O&G Co	W2E2SE sec 33	Gas	
Fremont O&G Co	CSWSE sec 33	D/A-O	
Fremont O&G Co	CSWSE sec 33	Oil	
Fremont O&G Co	NWNWSE sec 33	Oil	
Central Oil Co	SENWNE sec 33	D/A	
Central Oil Co	NWNWNE sec 33	D/A	
Rocky Mtn Oil Co	CNENW sec 33	Oil	

TABLE 7 (continued)

Completion Information After Washborne (1908);  
USGS, Bulletin 381

Township 19 South		Range 69 West	
Well Name	Location	Well Completion	
W. Lebanon Oil Co	NWNWNW sec 33	D/A-OG	
United Oil Co	W2NWNW sec 33	Oil	
W. Lebanon Oil Co	NESWNW sec 33	D/A	
United Oil Co	N2NWSW sec 33	Gas	
United Oil Co	NWNWSW sec 33	D/A	
United Oil Co	W2NWSW sec 33	Oil	
Sterling Oil Co	NENWSW sec 33	D/A	
United Oil Co	SENWSW sec 33	Oil	
United Oil Co	S2NWSW sec 33	D/A-O	
United Oil Co	N2NWSW sec 33	Oil	
United Oil Co	N2SWSW sec 33	Gas	
United Oil Co	NESWSW sec 33	D/A-O	
N.P. Hill	CSWSW sec 33	D/A	
United Oil Co	W2SWSW sec 33	D/A	
Arkansas Valley Oil	S2SWSW sec 33	Oil	
N.P. Hill	SESWSW sec 33	D/A	
United Oil Co	NENWNW sec 34	D/A-O	
United Oil Co	S2NWNW sec 34	D/A-OG	
United Oil Co	W2NWNW sec 34	Oil	
United Oil Co	NESWNW sec 34	Gas	
United Oil Co	CSWNW sec 34	D/A-OG	
United Oil Co	NENWSW sec 34	Oil	
United Oil Co	CNWSW sec 34	Gas	
United Oil Co	W2NESW sec 34	D/A-OG	
United Oil Co	CE2SW sec 34	D/A-O	
United Oil Co	E2W2SW sec 34	Oil	
United Oil Co	NESWSW sec 34	Oil	
United Oil Co	W2SWSW sec 34	D/A-OG	
United Oil Co	S2SWSW sec 34	Oil	
United Oil Co	E2SWSW sec 34	Oil	
United Oil Co	SESWSW sec 34	D/A	
United Oil Co	W2SESW sec 34	Oil	

TABLE 8

Completion Information After Washborne (1908);  
USGS, Bulletin 381

Township 20 South		Range 69 West		
Well Name	Location		Well Completion	
Florence O&R Co	NENWNW	sec 3	D/A-O	
Florence O&R Co	NENWNW	sec 3	D/A-O	
Florence O&R Co	CN2NW	sec 3	D/A-O	
Florence O&R Co	NWNWNW	sec 3	Oil	
Florence O&R Co	SENWNW	sec 3	D/A-OG	
Florence O&R Co	E2W2NW	sec 3	D/A-OG	
Florence O&R Co	NENENE	sec 4	Oil	
Florence O&R Co	N2NENE	sec 4	D/A	
Florence O&R Co	CNENE	sec 4	D/A-O	
Florence O&R Co	E2NENE	sec 4	D/A-O	
Florence O&R Co	N2SWNE	sec 4	Oil	
Florence O&R Co	E2SWNE	sec 4	D/A	
Florence O&R Co	S2NWSE	sec 4	D/A	
Unknown	E2NESW	sec 4	D/A-O	
Victor Oil Co	N2NWSW	sec 4	D/A	
Florence O&R Co	CNENW	sec 4	D/A-O	
Keystone Oil Co	E2NWNW	sec 4	Oil	
Keystone Oil Co	NENWNW	sec 4	Gas	
Keystone Oil Co	NWNWNW	sec 4	Oil	
Keystone Oil Co	SWNWNW	sec 4	Oil	
Keystone Oil Co	SWNWNW	sec 4	Oil	
Columbia Crude Oil	NENENE	sec 5	D/A-OG	
Columbia Crude Oil	CNENE	sec 5	Oil	
Columbia Crude Oil	SENENE	sec 5	D/A-O	
Columbia Crude Oil	SENENE	sec 5	Oil	
Columbia Crude Oil	NWNENE	sec 5	Oil	
Columbia Crude Oil	E2SENE	sec 5	D/A	
Victor Oil Co	NENESE	sec 5	D/A	
Victor Oil Co	N2NESE	sec 5	D/A	
Victor Oil Co	N2NESE	sec 5	D/A	
Victor Oil Co	NENESE	sec 5	D/A	
Victor Oil Co	SWNESE	sec 5	D/A	
Philip Griffith	NENWNE	sec 5	Oil	
Philip Griffith	NENWNE	sec 5	D/A	

TABLE 8 (continued)

Completion Information After Washborne (1908);  
USGS, Bulletin 381

Township 20 South		Range 69 West		
Well Name	Location			Well Completion
Philip Griffith	NWNWNE	sec	5	D/A
Philip Griffith	N2NWNE	sec	5	Oil
Philip Griffith	CNWNE	sec	5	Gas
Philip Griffith	S2NWNE	sec	5	D/A
Philip Griffith	W2NWNE	sec	5	D/A
Philip Griffith	S2N2N2	sec	5	Gas
Philip Griffith	S2N2N2	sec	5	Gas
Philip Griffith	NWSWNE	sec	5	Oil
Philip Griffith	W2SWNW	sec	5	D/A
Philip Griffith	NWSENW	sec	5	Oil
Philip Griffith	E2SWNW	sec	5	Oil
Philip Griffith	NWSWNW	sec	5	D/A
Philip Griffith	N2SWNW	sec	5	D/A
Philip Griffith	S2NENW	sec	5	Oil
Philip Griffith	CNENW	sec	5	D/A
Philip Griffith	CNENW	sec	5	Oil
Philip Griffith	CNENW	sec	5	Oil
Philip Griffith	E2NWNW	sec	5	D/A
Philip Griffith	NWNWNW	sec	5	D/A-O
Philip Griffith	NWNWNW	sec	5	D/A-O
United Oil Co	NENWNE	sec	6	Oil
United Oil Co	NENWNE	sec	6	D/A-O
United Oil Co	SEWNE	sec	6	D/A-OG
United Oil Co	NWNENE	sec	6	D/A-O
United Oil Co	CSEW	sec	6	D/A
United Oil Co	SESWNW	sec	6	D/A-O
United Oil Co	E2E2W2	sec	6	D/A
United Oil Co	E2E2W2	Sec	6	D/A
United Oil Co	N2NESW	sec	6	Oil
Hiawatha Oil Co	N2NENE	sec	8	D/A-O
Florence O&R Co	SENE	sec	8	Oil
Hiawatha Oil Co	NWSENE	sec	8	Gas
Florence O&R Co	NWSENE	sec	8	Oil
Florence O&R Co	E2SENE	sec	8	D/A-O
Florence O&R Co	S2SENE	sec	8	Oil
Columbia Crude Oil	W2SWNW	sec	9	D/A-O

TABLE 8 (continued)

Completion Information After Washborne (1908);  
USGS, Bulletin 381

Township 20 South		Range 69 West	
Well Name	Location	Well Completion	
Keystone Oil Co	W2NWSW sec 10	D/A	
Keystone Oil Co	W2NWSW sec 10	D/A	
Florence O&R Co	W2SENW sec 16	D/A-O	
Florence O&R Co	CSEnw sec 16	Oil	
Florence O&R Co	N2S2N2 sec 16	D/A-OG	
Florence O&R Co	CSEnw sec 16	Gas	
Wilkes-Barre Colo.	NWSWNE sec 16	D/A	
Florence O&R Co	NENENE sec 16	D/A	
Independent Oil Co	SWSWNW sec 17	D/A	
Simon Smith	SWNWNE sec 17	D/A-OG	
Simon Smith	S2NWNE sec 17	Gas	

TABLE 9"A" Parameters Used for Smoothing Faust's Formula

--Pierre - 3032.6615.  
--Niobrara - 2426.9103.  
--Ft. Hays - 2568.7676.  
--Carlile:Codell - 2518.065.  
--Greenhorn - 2376.5225.  
--Graneros - 2311.232.  
--Dakota - 2207.933.  
--Morrison - 2533.9425.  
--Ralston Cr.:Lykins:Lyons - 2662.0233.  
--Fountain - 2579.804.  
--Glen Eyrie - 1685.8927.  
--Hardscrabble - 2109.7009.  
--Williams Canyon - 2432.4513.  
--Fremont - 1812.2606.  
--Harding - 1876.65.  
--Granite Wash:Manitou - 1863.596.  
--Precambrian - 1806.4865.